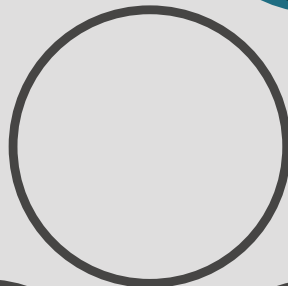




# The effect of timber bands and columns on the seismic behaviour of rubble stone masonry

A numerical study on Nepal's proposition for reconstruction of residential buildings





1 February 2021

“Does the confinement of timber bands and columns increase the resistance of rubble stone masonry shear walls against earthquake loads?”

### Master’s thesis research

Carlijn A. van Hoogdalem

Specialisation: Hydraulic Structures  
Department of Structural Engineering  
Faculty of Civil Engineering and Geosciences  
Delft University of Technology

### Committee

Chairman: Prof. dr. ir. J.G. Rots, *Delft University of Technology*  
Dr. ir. H.R. Schipper, *Delft University of Technology*  
Dr. ir. G.J.P. Ravenshorst, *Delft University of Technology*  
Dr. ir. F. Messali, *Delft University of Technology*

### Cover picture

Surroundings Kathmandu Valley, Nepal (source: own pictures)





# PREFACE

---

A year after the 2015 earthquakes in Nepal, I have attended the multidisciplinary project “Shock Safe Nepal” - a program that allows engineering students of any specialty to apply and expand TU Delft’s research on earthquakes and earthquake safe constructions through field work in disaster areas. During this project, the damage of the earthquakes of 2015 is investigated together with the Nepali building methods, and it became clear that there are many uncertainties and contradictions along different parties (government, construction companies, non-profit organisations) concerning the implementation of earthquake safe construction in Nepal.

Building on these findings I perform this research to obtain a master’s degree in Civil Engineering.

The goal of this research is to investigate the effect of strengthening a traditional Nepali house with seismic bands and columns, as stated in the Nepal Design Catalogue. To reach this goal, I have performed an analytical and numerical study to investigate the behaviour of a shear wall. Ultimately I will use the findings of the numerical analyses to compose an advise on how to implement earthquake resistant measures efficiently in a rubble stone masonry building.

I would like to thank my committee for providing guidance, advise and depth for my master’s thesis research:

Prof. dr. ir. J.G. Rots, *Delft University of Technology*  
Dr. ir. H.R. Schipper, *Delft University of Technology*  
Dr. ir. G.J.P. Ravenshorst, *Delft University of Technology*  
Dr. ir. F. Messali, *Delft University of Technology*

I hope you enjoy your reading.

Carlijn van Hoogdalem

Delft, 1 February 2021

# ABSTRACT

---

This research investigates if confining rubble stone masonry by timber bands and columns increases resistance against earthquake loads, by performing a number of numerical analyses in the finite element software program DIANA. In order to establish a reliable model, the input parameters are investigated by means of a literature study and sensitivity study. Additionally, the numerical model is validated by comparing the results to an analytical study. From the analytical study it is determined that the failure mechanisms are correctly estimated by the numerical analysis. However, differences between the values of ultimate strength and ductility were observed.

The effect of the confinement is investigated by a pushover analysis on a shear wall with two different masonry tensile strengths:  $f_t = 0.01 \text{ N/mm}^2$  and  $f_t = 0.03 \text{ N/mm}^2$ . These values are selected to show how such a small difference in tensile strength results in a different failure mechanism of the wall, and therefore results in a vastly different displacement capacity and ultimate strength. Additionally, a shear wall with and without a window opening is studied.

If the building is constructed with extremely low-strength masonry ( $f_t = 0.01 \text{ N/mm}^2$ ), the timber frame confinement will increase the resistance of the wall (with or without window opening) against the pushover load. If the building is constructed with masonry having a tensile strength of  $0.03 \text{ N/mm}^2$  or higher, the confinement has a negative impact on the ductility of the closed wall. For the wall with window opening the confinement triples its ultimate strength. Whether a strong or a ductile structure is more desirable, depends on the demand with respect to the seismic spectrum. If the ground motion demands a strong structure, it is advised to confine the masonry with a timber frame consisting of four timber bands, and columns at each wall junction.

The design of the timber frame as recommended by the Nepali building codes is determined to not be sufficient and must be altered in order to provide this positive impact on the structure's resistance. Firstly, the columns must be placed at both sides of the band, instead of on the inner side only, to avoid eccentric loads on the bands. Secondly, the cross-sectional dimensions of the bands and columns

must be increased avoid failure of the connections and splitting of the timber. Taking these aspects into account, a new design for the confinement method is presented in this study.

The limitations of the conclusions of this research follow from the investigation of a single, in-plane wall only. One of the goals of the use of bands is to improve the box behaviour, for which the out-of-plane performance must be investigated. Moreover, an analysis on a three-dimensional structure is needed to fully answer the research question. In a three-dimensional study, the closed walls and walls with opening give a combined response to the load, therefore, the advantages and disadvantages of the confinement are combined as well.



# TABLE OF CONTENT

---

Preface. . . . .	v
Abstract. . . . .	vi
List of figures. . . . .	xii
List of tables. . . . .	xv
<b>1. Introduction. . . . .</b>	<b>1</b>
1.1 Relevance of this research. . . . .	1
1.2 Damage in masonry. . . . .	2
1.2.1 <i>In-plane damage</i> . . . . .	3
1.2.2 <i>Out-of-plane damage</i> . . . . .	3
1.3 Design guidelines. . . . .	4
1.4 Uncertainties that follow from the DUDBC guidelines. . . . .	5
<b>2. Research setup. . . . .</b>	<b>7</b>
2.1 Scope of the research. . . . .	7
2.1.1 <i>Rubble stone masonry</i> . . . . .	7
2.1.2 <i>Shear wall</i> . . . . .	7
2.2 Problem statement. . . . .	9
2.3 Methodology. . . . .	10
<b>3. Analytical study on the timber confinement. . . . .</b>	<b>13</b>
3.1 Boundary conditions. . . . .	13
3.2 Calculation method. . . . .	14
3.2.1 <i>Calculations as recommended in the NPR 9998</i> . . . . .	15
3.2.2 <i>Strut and tie models by P. Roca</i> . . . . .	18
3.3 Estimated resistance. . . . .	19
3.4 Conclusions Chapter 3. . . . .	22
3.4.1 <i>Applicability of strut and tie models</i> . . . . .	22
3.4.2 <i>Applicability of NPR calculations</i> . . . . .	22
3.4.3 <i>Timber frame</i> . . . . .	22
3.4.4 <i>Estimated ultimate strength</i> . . . . .	23
3.4.5 <i>Failure modes</i> . . . . .	23

<b>4. Discretisation of the masonry structure.</b> . . . . .	<b>25</b>
4.1 Basic routine FEA. . . . .	25
4.2 Scale level. . . . .	26
4.3 Modelling of masonry. . . . .	27
4.3.1 <i>Element model.</i> . . . .	27
4.3.2 <i>Material model.</i> . . . .	28
4.3.3 <i>Material properties.</i> . . . .	29
4.4 Modelling of bands and columns. . . . .	30
4.4.1 <i>Element model.</i> . . . .	30
4.4.2 <i>Material model.</i> . . . .	30
4.4.3 <i>Material properties.</i> . . . .	31
4.5 Modelling of band-to-masonry connection. . . . .	31
4.5.1 <i>Element model.</i> . . . .	31
4.5.2 <i>Material model.</i> . . . .	32
4.5.3 <i>Material properties.</i> . . . .	34
4.6 Modelling of band-to-column connection. . . . .	36
4.7 Force model. . . . .	36
4.8 Conclusions of Chapter 4. . . . .	38
<b>5. Parameter study of the numerical model.</b> . . . . .	<b>41</b>
5.1 General. . . . .	41
5.2 Tensile behaviour. . . . .	43
5.2.1 <i>Numerical results of varying parameters in tension.</i> . . . .	43
5.2.2 <i>Comparison with the analytical results.</i> . . . .	45
5.2.3 <i>Chosen values tensile behaviour.</i> . . . .	46
5.3 Compressive behaviour. . . . .	46
5.3.1 <i>Numerical results of varying parameters in compression.</i> . . . .	46
5.3.2 <i>Chosen values compressive behaviour.</i> . . . .	47
5.4 Young's modulus. . . . .	48
5.4.1 <i>Numerical results of varying Young's modulus.</i> . . . .	48
5.4.2 <i>Chosen value Young's modulus.</i> . . . .	48
5.5 Mass density. . . . .	50
5.5.1 <i>Numerical results of varying mass density.</i> . . . .	50
5.5.2 <i>Chosen value mass density.</i> . . . .	52
5.6 Poisson's ratio. . . . .	52
5.6.1 <i>Numerical results of varying Poisson's ratio.</i> . . . .	52
5.6.2 <i>Chosen value Poisson's ratio.</i> . . . .	52
5.7 Conclusions Chapter 5. . . . .	53
<b>6. Numerical study on the timber confinement.</b> . . . . .	<b>55</b>
6.1 General. . . . .	55
6.2 Closed walls. . . . .	55
6.2.1 <i>Numerical model.</i> . . . .	55
6.2.2 <i>Results for <math>f_t = 0.01 \text{ N/mm}^2</math>.</i> . . . .	57
6.2.3 <i>Results for <math>f_t = 0.03 \text{ N/mm}^2</math>.</i> . . . .	61

6.3 Walls with window opening. ....	63
6.3.1 Numerical model. ....	63
6.3.2 Results for $f_t = 0.01 \text{ N/mm}^2$ . ....	66
6.3.3 Results for $f_t = 0.03 \text{ N/mm}^2$ . ....	68
6.4 Redesign timber joint. ....	71
6.4.1 Case 1: Confinement consists of two bands. ....	71
6.4.2 Case 2: Confinement consists of four bands. ....	72
6.5 Validation numerical models. ....	73
6.5.1 Unconfined closed wall. ....	73
6.5.2 Confined closed wall. ....	74
6.5.3 Wall with window opening. ....	76
6.5 Conclusions Chapter 6. ....	78
6.5.1 Validation of the numerical model. ....	78
6.5.2 The effect of the confinement on masonry with $f_t = 0.01 \text{ N/mm}^2$ . ....	79
6.5.3 The effect of the confinement on masonry with $f_t = 0.03 \text{ N/mm}^2$ . ....	81
<b>7. Conclusions. ....</b>	<b>83</b>
7.1 Answer to the research question. ....	83
7.2 Parameter study. ....	85
7.3 Validation of the numerical results. ....	85
7.4 Design of the timber frame. ....	85
<b>8. Discussion of the limitations of the study. ....</b>	<b>87</b>
8.1 Answer to the research question. ....	87
8.2 Parameter study. ....	88
8.3 Validation of the numerical results. ....	88
8.4 Design of the timber frame. ....	88
<b>9. Recommendations for further research. ....</b>	<b>91</b>
<b>References. ....</b>	<b>93</b>
<b>Appendix. ....</b>	<b>I</b>
A. Parameters used for the calculations as recommended by NEN NPR 9998. ....	II
B. Load carrying capacity timber connection. ....	IV
C. DIANA report closed shear wall. ....	VIII
D. Redesign timber joint. ....	XXIV

# LIST OF FIGURES

---

## Chapter 1

1.1	World map tectonic plates. ....	1
1.2	Severity of the damage. ....	1
1.3	In-plane and out-of-plane mechanisms. ....	2
1.4	Diagonal cracks and rocking in masonry piers. ....	3
1.5	Total collapse of an out-of-plane loaded wall. ....	4
1.6	Typical overturning of the top of the wall. ....	4
1.7	Box action by implementation of ductile elements. ....	4
1.8	Seismic bands as recommended by the DUDBC. ....	4
1.9	Earthquake resistant elements in building. ....	5
1.10	(a) Reinforced concrete, (b) wood, (c) bamboo for the construction of seismic bands and columns. ....	5
1.11	Different band and column placements. ....	6

## Chapter 2

2.1	Different types of rubble stone masonry as referred to in this research. ...	8
2.2	Dimensions of a small Nepali house: one storey and two rooms. ....	8
2.3	Configuration seismic bands and columns. ....	9
2.4	Flow chart representing the structure of this research. ....	10

## Chapter 3

3.1	Cross-section foundation. ....	13
3.2	Boundary conditions shear wall for analytical calculations. ....	14
3.3	Force equilibrium when the bending moment due to the initial shear strength is excluded. ....	15
3.4	Horizontal ( $\Delta u$ ) and vertical ( $\Delta w$ ) displacement of the confined wall. ....	17
3.5	Deviation of compression stress fields by horizontal tensile forces. ....	18
3.6	Model proposed by Roca for walls subjected to uniform vertical load. ...	19
3.7	Model proposed by Roca for walls with opening. ....	19
3.8	Diagonal compressive struts expected to develop in the masonry. ....	22
3.9	Bar diagram of the estimated ultimate resistance of the shear wall configurations. ....	24

## Chapter 4

4.1	Basic routine one FEA iteration in DIANA. ....	26
4.2	Micro-, macro-, and meso-scale discretisation. ....	27
4.3	Characteristics of plane stress elements. ....	28
4.4	Predefined tensile (left) and compressive (right) behaviour of the total strain based crack elements. ....	29



4.5	Beam elements, characteristics.....	30
4.6	Predefined behaviour of the class-III beam elements.....	31
4.7	Example of a timber-to-masonry connection in Nepali structure.....	32
4.8	Interlock between band and masonry.....	32
4.9	Two dimensional line interface element characteristics.....	32
4.10	Angle of friction between masonry and bottom side timber band.....	34
4.11	Dilatation angle between masonry and top side timber band.....	35
4.12	Mohr-Coulomb model for line interface properties.....	35
4.13	Force-displacement analysis domain.....	37

## Chapter 5

5.1	Overview of the numerical model of the masonry wall.....	42
5.2	Force-displacement diagram for varying values of $f_t$ , with crack width contours at peak load.....	44
5.3	Force-displacement diagram for varying values of $f_t$ , with crack width contours of the first cracks at the end of the elastic stage.....	45
5.4	Force-displacement diagram for $G_{fc} = 5.0$ N/mm.....	47
5.5	Force-displacement diagram for $G_{fc} = 0.1$ N/mm.....	47
5.6	Stress-strain curve in compression for $f_c = 3.0$ N/mm <sup>2</sup> and $G_{fc} = 0.1$ N/mm	47
5.7	Force-displacement diagram for varying values of $E$ , with stresses and crack strains for the three models at failure.....	49
5.8	First part of the force-displacement diagram for varying values of $E$ , with stresses for the three models at yield strength.....	50
5.9	Force-displacement diagram for varying values of $\rho$ , with crack strains for the three models at failure.....	51
5.10	Strain contours in X-direction for the upper bound model at failure.....	51
5.11	Force-displacement diagram for varying values of $v$ , with crack width contours for the three models at failure.....	53

## Chapter 6

6.1	Impression of the position of the columns.....	56
6.2	Overview of the numerical model of the masonry wall confined by a roof and floor band and two columns.....	56
6.3	Overview of the numerical models of the confined masonry walls.....	57
6.4	Force-displacement diagram as a response to the pushover load on the unconfined wall and confined walls, for $f_{tmasonry} = 0.01$ N/mm <sup>2</sup> .....	58
6.5	Relative displacement of the interface elements of the three band model during the hardening phase at $u = 0.36$ mm (left) and $u = 0.75$ mm (right)	58
6.6	Crack strains at failure of the unconfined and confined models, for $f_{tmasonry} = 0.01$ N/mm <sup>2</sup> .....	59
6.7	Load transfer of the joints in the timber frame, with (a) column-to-roof band connection; (b) column-to-lintel band connection; (c) column-to-floor band connection.....	60
6.8	Principal stresses in the timber elements at global failure of the structure with $f_{tmasonry} = 0.01$ N/mm <sup>2</sup> , for the confined models.....	60

- 6.9 Force-displacement diagram as a response to the pushover load on the unconfined wall and confined walls, for  $f_{t,masonry} = 0.03 \text{ N/mm}^2$ . . . . . 61
- 6.10 First part of the force-displacement diagram of the unconfined wall and confined walls, for  $f_{t,masonry} = 0.03 \text{ N/mm}^2$ . . . . . 61
- 6.11 Vertical stresses over the length of the wall at the support, for different values of the horizontal displacement of the wall. . . . . 62
- 6.12 Crack strains at failure for  $f_{t,masonry} = 0.03 \text{ N/mm}^2$ , of the unconfined and confined walls. . . . . 62
- 6.13 Principal stresses in the timber elements at global failure of the structure with  $f_{t,masonry} = 0.03 \text{ N/mm}^2$ , for the confined models. . . . . 63
- 6.14 Typical Nepali window: timber frame connected to the masonry by interlock. . . . . 64
- 6.15 Overview of the numerical model of the unconfined masonry wall with window opening. . . . . 64
- 6.16 Overview of the numerical models of the confined masonry walls with window opening. . . . . 65
- 6.17 Force-displacement diagram of the unconfined and confined walls with window opening, with crack strain contour plots at failure. . . . . 66
- 6.18 Principal stresses in the timber elements at global failure of the structure with  $f_{t,masonry} = 0.01 \text{ N/mm}^2$ , for the confined models with window opening. . . . . 67
- 6.19 Force-displacement diagram of the unconfined and confined walls with window opening, with  $f_{t,masonry} = 0.03 \text{ N/mm}^2$ . . . . . 68
- 6.20 Crack strain contour plots at failure of the unconfined and confined wall with window opening, with  $f_{t,masonry} = 0.03 \text{ N/mm}^2$ . . . . . 69
- 6.21 Principal stresses in the timber elements at global failure of the structure with  $f_{t,masonry} = 0.03 \text{ N/mm}^2$ , for the confined models with window opening. . . . . 70
- 6.22 Redesign timber joint for Case 1. . . . . 71
- 6.23 Redesign timber joint for Case 2. . . . . 72
- 6.24 Applied load for NPR calculations (left) and pushover analysis (right). . . . . 74
- 6.25 Ultimate strength and failure mechanisms of the closed shear wall configurations, for the lower (top) and higher (bottom) values of the masonry tensile strength. . . . . 75
- 6.26 Ultimate strength and failure mechanisms of the shear wall configurations with opening, for the lower (top) and higher (bottom) values of the masonry tensile strength. . . . . 77
- 6.26 Force-displacement curves of the unconfined and confined walls with and without window opening, for  $f_{t,masonry} = 0.01 \text{ N/mm}^2$ . . . . . 79
- 6.27 Force-displacement curves of the unconfined and confined walls with and without window opening, for  $f_{t,masonry} = 0.03 \text{ N/mm}^2$ . . . . . 81

**Chapter 7**

- 7.1 Design of the confinement method as recommended by the Nepali building code (top) and by this research (bottom). . . . . 84

# LIST OF TABLES

---

## Chapter 1

1.1	Typology of Nepali households.....	2
-----	------------------------------------	---

## Chapter 2

2.1	Overview shear wall configurations.....	11
-----	---	----

## Chapter 3

3.1	Calculations as recommended in the NPR 9998 for in-plane failure mechanisms of masonry.....	16
3.2	Estimated resistance using calculations of NEN NPR 9998.....	20

## Chapter 4

4.1	Overview material properties masonry.....	30
4.2	Overview material properties timber.....	31
4.3	Advantages and disadvantages of the interface material models.....	33
4.4	Overview material properties band-to-masonry connection.....	35
4.5	Characteristics pushover analysis and time-history analysis.....	38
4.6	Overview modelling choices.....	39

## Chapter 5

5.1	Varying values for the masonry material properties.....	42
5.2	Chosen values for the masonry material properties.....	54

## Chapter 6

6.1	Estimated resistance and failure mechanism found by the analytical and numerical studies, for different values for the masonry tensile strength..	73
6.2	The benefit of confinement for a masonry tensile strength of 0.01 N/mm <sup>2</sup> .....	80
6.3	The benefit of confinement for a masonry tensile strength of 0.03 N/mm <sup>2</sup> .....	82

## Appendix

A.1	Fixed parameters NPR calculations.....	II
A.2	Variable parameters NPR calculations.....	III

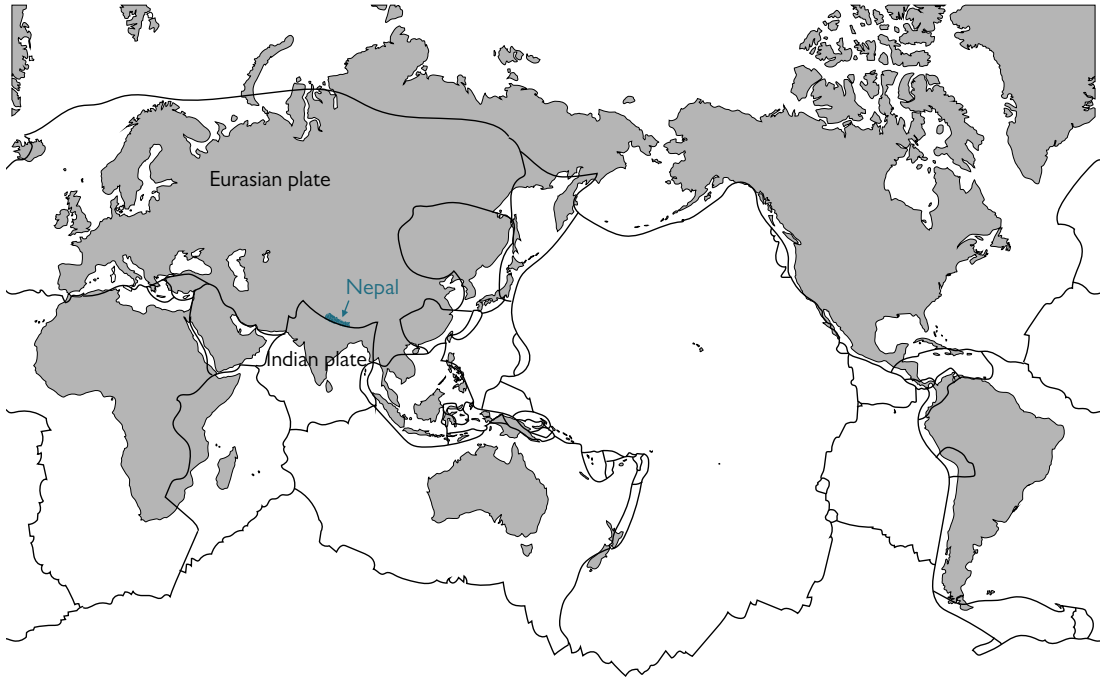


Figure 11: World map tectonic plates, Nepal lies on the fault of the Eurasian and Indian plates (adapted based on Worldatlas, 2016)



Figure 12: Severity of the damage (source map: adapted from Maps of World, 2015; source photos: SSN 3, 2016)

# CHAPTER 1

---

## Introduction

*Seismic disasters in Pakistan (2005), Haiti (2010) and Nepal (2015) have led to an increase in research on construction methods that result in affordable, safe housing that can be built, maintained and adapted by local people. The solution to this problem has been proven to be difficult, and has been studied by many different parties. Design rules and guidelines on how to increase the strength of a building are worldwide known and different views on their implementation have led to this master's thesis research. This introduction to the research shows the characteristics of rubble stone masonry buildings and their failure mechanisms under seismic loading, followed by a few examples on how to strengthen stone masonry buildings.*

### 1.1 RELEVANCE OF THIS RESEARCH

On April 25, 2015, Nepal experienced one of the heaviest earthquakes of the past century, named the Gorkha earthquake, approximately 80 km to the Northwest of the capital Kathmandu. It was caused by the collision of the Eurasian plate and the Indian plate and had a magnitude of 7.8 on Richter's scale (USGS, 2015). It destroyed half a million houses and partially damaged another quarter million (NRA, 2016). Figure 1.1 shows the world map with the tectonic plates, Nepal is one of many countries that lies on a fault of these plates.

Figure 1.2 shows the severity of the damage: 90% of the houses in rural Nepal had fully collapsed. The pictures show damage observed in the Kathmandu valley, the region most severely hit by the earthquake (located in the Gandaki zone). When visiting this region the severity of the damage sank in: all that was left of people's houses were the stones still intact, collected and neatly stacked in the corner of the lot, waiting to be used for reconstruction.

Table 1.1 gives an overview of a typology of Nepali households, based on the National Population and Housing Census 2011 (NPHC 2011) brought out by Central Bureau of Statistics (CBS). It shows that most houses in Nepal are constructed with (rubble) stone masonry, which are the houses that suffered the most damage. Part of this master’s thesis research is to understand the relation between the damage shown in Figure 1.2 and the materials discussed in Table 1.1. Subsequently, it can be understood how to increase the strength of these buildings.

**Table 1.1:** Typology of Nepali households

Typology house	Percentage of households
<b>Foundation</b>	
Mud-bonded bricks	44 %
Wooden pillar	25 %
Cement-bonded bricks	18 %
RCC pillar	10 %
Other	2 %
<b>Outer wall</b>	
Mud-bonded bricks or stones	41 %
Cement-bonded bricks or stones	29 %
Bamboo	20 %
Wooden planks	5 %
<b>Roof</b>	
CGI sheets	28 %
Tile/slate	27 %
RCC	22 %
Thatched/straw	19 %

## 1.2 DAMAGE IN MASONRY

Masonry consists of stacked blocks bonded with mortar. This structure is brittle, meaning it will deform very little when loaded beyond its capacity, resulting in crack propagation eventually followed by collapse. Masonry knows typical crack diagrams and failure mechanisms, which distinguishes between in-plane damage and out-of-plane damage (Figure 1.3).

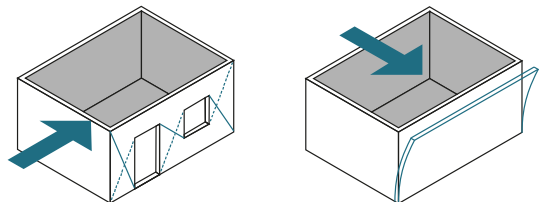


Figure 1.3: *In-plane and out-of-plane mechanisms, left and right respectively (source: Giaretton et al., 2016)*

### 1.2.1 In-plane damage

In-plane damage is caused by forces acting parallel to the wall, resulting in cracks associated with shear. The direction of the crack development depends on the compressive stress, the dimensions of the wall, and the quality of the mortar. In-plane damage generally does not result in total collapse of the structure and is therefore a stable failure mode (Van Wijnbergen, 2015). In-plane loaded walls (i.e. shear walls) know three types of failure mechanisms: rocking, sliding, and diagonal tensile failure (NPR 9998, 2020).

Rocking occurs in structures with low axial stresses, slender walls or piers, and a relatively high mortar strength. Masonry elements exhibiting rocking behaviour have substantial deformation capacity after the formation of cracks, but also show a low energy loss within the element itself which makes this a more ductile failure mode than the diagonal tensile failure mode (Javed et al., 2016). The diagonal tensile failure mode is more common where axial stresses are high, piers are squatter, and the tensile strength of masonry is low. It causes a rapid degradation in strength and stiffness past initial cracking, ultimately leading to loss of load path and therefore brittle failure. Figure 14 shows a picture of diagonal cracks in a pier and of a pier that experienced rocking.



Figure 14: *Diagonal cracks and rocking in masonry piers, left and right respectively (source: Javed et al., 2006)*

### 1.2.2 Out-of-plane damage

Out-of-plane damage is caused by forces acting perpendicular to the wall, resulting in (partially) overturning of the wall, thus immediate collapse. Figure 15 shows total collapse of an out-of-plane loaded wall. Since the roof structure is relatively light and not sufficiently connected to the walls it could not restrain the wall, the so called “box action” could not be developed. The flexural bending of the wall also causes shear forces between the top of the wall and the roof. Insufficient roof-to-wall connections can cause failure of the top of the wall, shown in Figure 1.6.





Figure 1.5: Total collapse of an out-of-plane loaded wall (source: Javed et al., 2006)



Figure 1.6: Typical overturning of the top of the wall (source: Javed et al., 2006)

### 1.3 DESIGN GUIDELINES

To advance to safe reconstruction, the Department Urban Development & Building Construction (DUDBC) of the government of Nepal, has published a new building code in October 2015, as well as a catalogue with designs for houses using approved building methods. The building code describes rules of thumb for Nepali buildings and is based on other codes of similar building methods (like the Indian building code), and on worldwide known design guidelines that can be found in literature (DUDBC, 2015a). Two of these guidelines are discussed here since they form the base of this research:

- When subjected to seismic loads, a structure experiences tensile forces. A building consisting of brittle materials, like masonry, needs to be reinforced to encounter these forces. Horizontal and vertical ductile elements will tie the building together, making it move as a rigid box, shown in Figure 1.7. (SSN 3, 2016).
- The government of Nepal describes these horizontal and vertical ductile elements as “seismic bands and columns”. The DUDBC Design Catalogue states that a minimum of four bands needs to be incorporated in housing reconstruction, shown in Figure 1.8. The floor and roof band are to tie the walls together. The sill and lintel band tie the openings in the walls together.

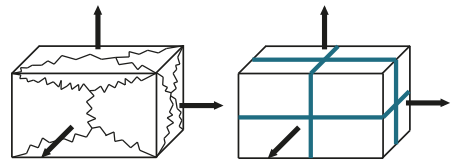


Figure 1.7: Box action by implementation of ductile elements

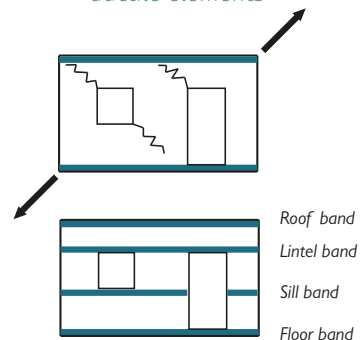


Figure 1.8: Seismic bands as recommended by the DUDBC



The design catalogue represents a schematic overview of good practise of different rural housing types, based on the design guidelines. The goal of the design catalogue is to provide Nepali rural households with examples regarding earthquake resistant construction techniques (DUDBC, 2015b). One of these designs is shown in Figure 1.9. It shows the presence of the seismic bands and columns, constructed in timber.

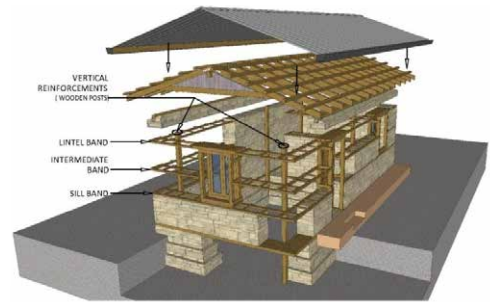


Figure 1.9: Earthquake resistant elements in building (source: DUDBC, 2015b, p. 141)

## 1.4 UNCERTAINTIES THAT FOLLOW FROM THE DUDBC GUIDELINES

General design rules for earthquake resistant buildings can be found in several papers and books and have been applied for many different cases worldwide, but thorough structural justification is lacking. When talking with different engineers in Nepal during the Shock Safe Nepal project, it became clear that the current knowledge in this field of construction is based on best practise. There is too much discussion based on empirical results rather than scientific research. It is uncertain for example how many horizontal bands is needed to give sufficient lateral support, and if this will be different when using different materials, e.g. will timber bands be as efficient as reinforced concrete bands? Figure 1.10 shows examples taken from the DUDBC Design Catalogue of seismic bands with different materials, where they appear interchangeable.

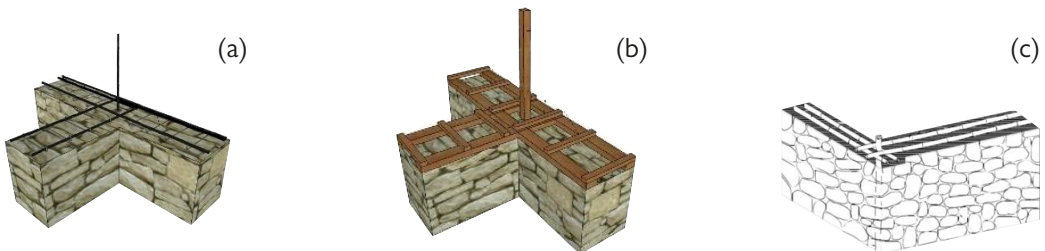


Figure 1.10: (a) Reinforced concrete, (b) wood, (c) bamboo for the construction of seismic bands and columns (source: DUDBC, 2015b)

The Nepali building codes state that vertical tensile elements are needed for earthquake safety. However, the DUDBC Design Catalogue shows inconsistencies in their application as well. Different materials and positions of the vertical elements are suggested, but the difference between them is unclear as well as their contribution to the earthquake resistance. Figure 1.11 shows the different positions of the vertical elements, as presented in the DUDBC Design Catalogue.

In addition, there are unanswered questions that were stumbled upon during the Shock Safe Nepal project concerning the foundation and critical details, like: What are the benefits of anchoring the frame to the foundation? What are the effects of poorly prepared, loose timber connections? What is the behaviour of nailed timber joints in comparison to joints without mechanical fasteners? In short, in order to use structural materials efficiently to obtain earthquake safe buildings, many questions still need to be answered. This research will focus on some of these uncertainties, further explained in Chapter 2.

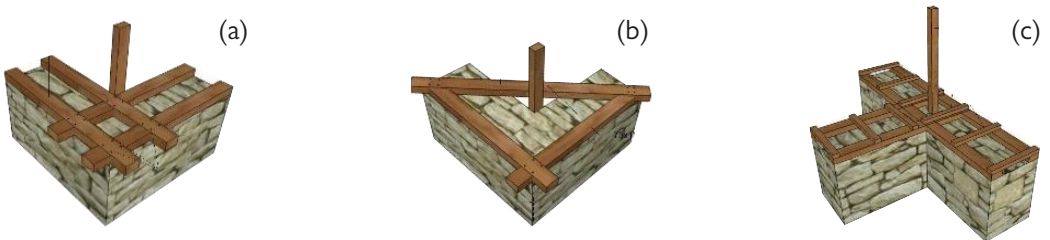


Figure 1.11: Different band and column placement: (a) band consists of two parallel beams and the column is connected to the inner beam, (b) band consists of one beam and the column is connected with a diagonal beam, (c) band consists of two parallel beams with traverse batten and the column is placed inside the wall (source: DUDBC, 2015b)

# CHAPTER 2

---

## Research setup

*The goal of this mater's thesis research is to investigate the effect of strengthening a traditional Nepali house with seismic bands and columns and, ultimately, to compose an advise on how to implement these measures efficiently in a rubble stone masonry building. This chapter explains how this research will be conducted to reach this goal. It covers the scope of the research, the problem statement, and the methodology.*

### 2.1 SCOPE OF THE RESEARCH

#### 2.1.1 Rubble stone masonry

This research concerns Nepali masonry houses subjected to earthquake loads. Depending on the region, these houses are build in brick masonry or rubble stone masonry. This research focusses on rubble stone masonry, which generally has a lower strength than brick masonry. Additionally, a distinction in the strength of mortar can be made: high strength mortar consists of cement, whereas low strength mortar consist mostly of mud. Rural Nepal is known to build with mud mortar since the remote locations of the villages prohibit the availability of qualitative building materials. Figure 2.1 shows examples of the different types of rubble stone masonry. This research will study the behaviour of unconfined rubble stone masonry constructed with mud mortar, and the behaviour of stone masonry confined by timber bands and columns.

#### 2.1.2 Shear wall

This research will focus on the behaviour of a shear wall only, since modelling of a full three-dimensional building is very complex and time consuming. This would not allow the performance of an in-depth investigation within the time of a thesis, and for this reason, the scope of the study is restricted to a single shear wall only. By investigating the behaviour of a shear wall, already a lot can be said about

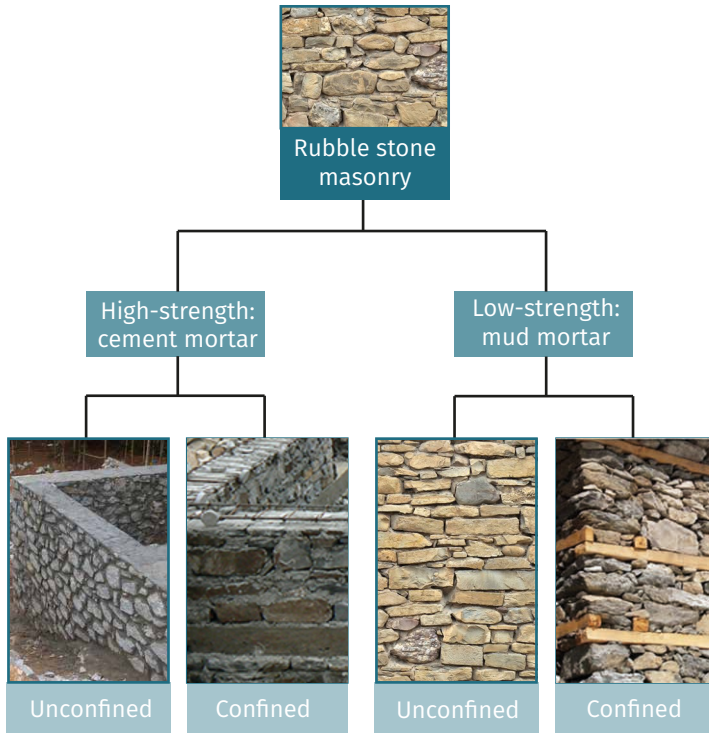


Figure 2.1: Different types of rubble stone masonry as referred to in this research (pictures obtained from Schildkamp & Araki, 2019; Carabbio et al., 2018)

the structural contribution of the seismic system to the masonry’s resistance to earthquakes: it provides an insight in vulnerabilities of the structure and identifies weak links of the structure’s load transfer mechanisms.

Typically, Nepali houses in rural areas are relatively small due to the costs of the building materials. Such buildings will consist of one or sometimes two stories with a height not more than 2.7 metres. A floor plan of 3 by 6 metres, divided by a transverse wall into two rooms of 3 by 3 metres, is not uncommon. Assuming that the transverse wall is connected to the long wall such that it provides a fixed lateral resistance, a typical wall element will have a length of 3 metres (Figure 2.2).

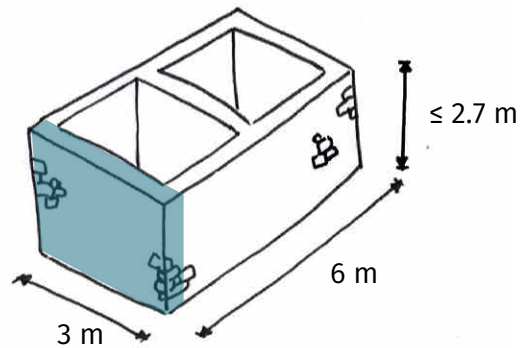


Figure 2.2: Dimensions of a small Nepali house: one storey and two rooms.

The masonry wall will be strengthened by a system of timber bands and columns. As stated in Chapter 1, this system should tie the masonry together and is therefore expected to increase its ultimate strength. The columns are placed at each wall junction and at window openings. The bands consist of two timber beams connected by transverse batten and are placed at critical levels of the masonry structure (Figure 2.3):

- A floor band at the base of the wall;
- A sill band at the bottom of the window openings;
- A lintel band at the top of the window openings;
- A roof band at the top of the wall.

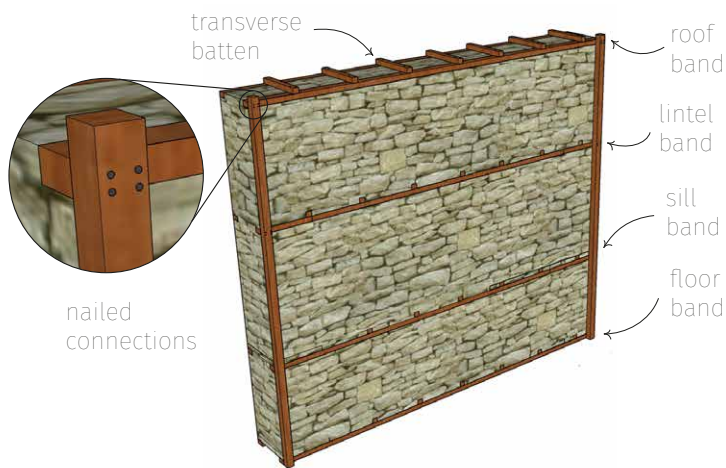


Figure 2.3: Configuration seismic bands and columns as recommended by the Government of Nepal.

## 2.2 PROBLEM STATEMENT

The central phenomenon of this research will be the implementation of seismic bands with low-strength stone masonry buildings, resulting in the following research question:

**“Does the confinement of timber bands and columns increase the resistance of rubble stone masonry shear walls against earthquake loads?”**

The sub-questions leading to answering the research question are:

- Is there a difference in the response of the shear wall, when confined by zero, two, three, or four seismic bands?
- What is the effect on the response of the shear wall of increasing the amount of columns?
- How do the band-to-column connections contribute to the response of the shear wall?

## 2.3 METHODOLOGY

Figure 2.4 shows the structure of this report by means of a flow chart. The effect of the confinement method on the structural behaviour of the masonry will be investigated by performing a numerical analysis in the finite element software programme DIANA (Chapter 6). In order to establish a reliable model, the input parameters must be investigated by means of a literature study and sensitivity study (Chapters 4 and 5). Additionally, the numerical model must be validated by results of another type of study. This will be done by performing an analytical study on the effect of the confinement method (Chapter 3).

A total of nine configurations will be investigated to analyse the effect of the confinement (i.e. the timber bands and columns) on a wall element with and without a window opening, gradually increasing the amount of bands and columns. An overview of the different configurations is given in Table 2.1.

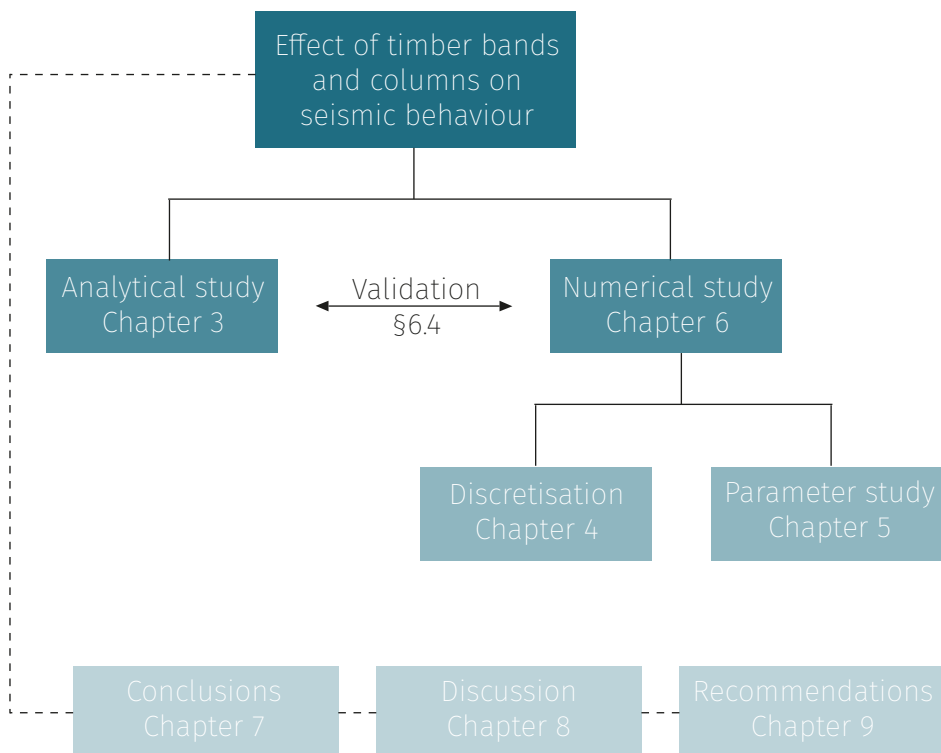
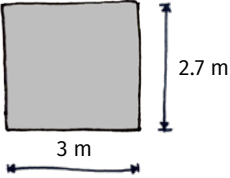
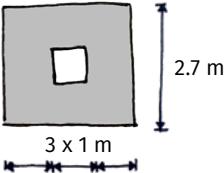
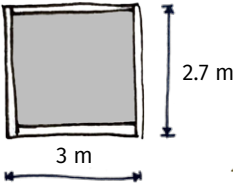
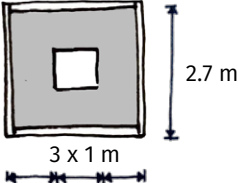
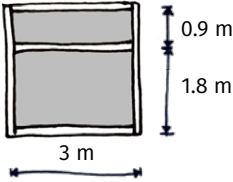
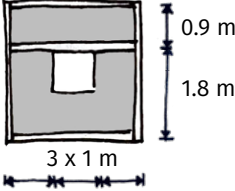
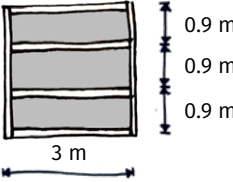
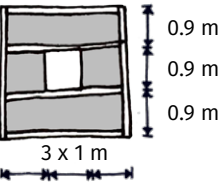
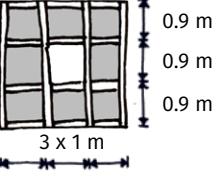


Figure 2.4: Flow chart representing the structure of this research

Table 2.1: Overview shear wall configurations

Closed shear walls	Shear walls with window opening	Confinement
		No confinement
		Roof and floor band
		Roof, floor and lintel band
		Roof, floor, lintel and sill band
		Roof, floor, lintel and sill band, and two extra columns at the window opening





# CHAPTER 3

## Analytical study on the effect of confinement

*The implementation of the seismic bands and columns will be assessed using an analytical study based on simplified models by the NEN NPR9998 and by P. Roca. This analytical study is performed to provide a first indication of the ultimate strength of the masonry, which can function as a first validation of the numerical models later on in this research. As stated in Chapter 2, a total of nine in-plane walls will be studied, gradually increasing the amount of the timber confinement. This chapter starts with a description of the boundary conditions of the walls, followed by a description of the calculation methods. Subsequently, the resistance of the models is observed and conclusions of the analytical study are given.*

### 3.1 BOUNDARY CONDITIONS

The boundary conditions of the wall element are determined by its connections to the surrounding elements such as the foundation and the roof structure. The connections to the transverse walls influence the structural behaviour of the wall element as well, but only when applying out-of-plane loading, which, as stated in Chapter 2, will not be discussed in this research.

The stiffer the connection of the wall to the foundation and roof, the less the wall will be able to rotate when loaded. Theoretically, if the elements would be rigidly connected, even the tiniest rotations would be restricted, but this would mean that the connection itself should be able to resist great stresses. In practise, this is never the case, especially for buildings that follow simple structural principles. This means that the structural scheme used for the calculations will not contain fully rigid connections, but only hinged connections.

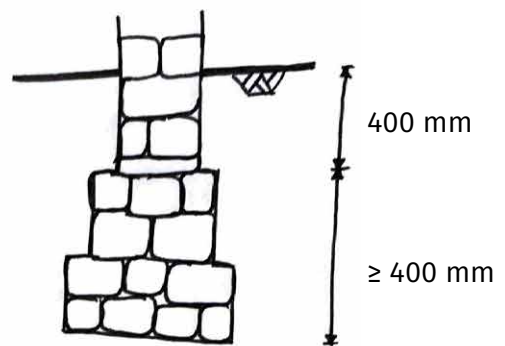


Figure 31: Cross-section foundation

Figure 3.1 shows what the foundation of rural Nepali houses could look like: stones are stacked with mud mortar into a hole of approximately 1 metre. The tapered width of the foundation restricts vertical displacements of the wall when loaded in tension. In practise, these displacements are not fully restricted, meaning that the wall will actually be lifted up from the ground when loaded heavily (for example during an earthquake). The calculation methods used for this analytical study are based on equilibrium, allowing the wall element to lift up and to rotate around its toe. The toe itself is fixed in translational directions (Figure 3.2).

The top of the wall will be able to move freely, since the roof structure of these type of houses should be very light. The roof could collapse during an earthquake and if it were to be heavy this could have deadly consequences. A light-weight roof is therefore much safer, but will not restrict the movements of the walls whatsoever, it will follow the movements of the walls.

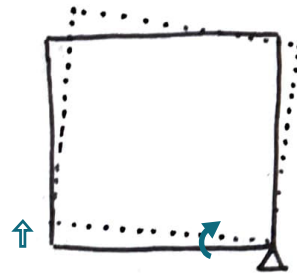


Figure 3.2: Boundary conditions shear wall for analytical calculations.

## 3.2 CALCULATION METHOD

Seismic loads generated by earthquakes are dynamic ground accelerations, i.e. the amplitude and period of the vibrations change of time. These vibrations cause a dynamic response of the building. Dynamic responses of structures can be calculated by means of differential equations that include, amongst others, values for damping, eigenfrequencies and stiffness. The result is the resisting force of the building plotted against its displacement, which is obtained by numerical calculation programs.

However, for simple structures such as a shear wall, or a single-storey building with a symmetric floor plan, where the response is dominated by the sway mechanism, it is not necessary to apply complex calculation methods to obtain a reliable representation of the resistance of the building to earthquakes (NPR 9998, 2020a).

In this paragraph, two linear-static calculation methods from literature are used to obtain the strength and displacement capacities of the wall element:

- 1) NEN NPR 9998, adopted from international best practise; and
- 2) P. Roca, based on equilibrium using strut and tie models.

By using two different approaches to estimate the ultimate capacity of masonry shear-walls, it is expected to obtain a range of results that represent the actual strength of Nepali masonry more accurately.

### 3.2.1 Calculations as recommended by the NPR 9998

Annex G.9 of the NPR 9998+C1 (NPR 9998, 2020b) validates the shear strength of masonry piers by means of simplified methods that are developed for unreinforced masonry structures and extended to the Dutch masonry by means of dedicated experimental tests (Groningen region). These piers are considered the weakest link of a masonry building and are therefore likely to form the plastic mechanism and collapse mode of the global structure.

According to the NPR 9998+C1, the in-plane resistance of a masonry wall or pier is governed by its shear resistance or its flexural resistance, with bed-joint sliding and rocking as corresponding failure modes respectively (both stable failure modes since they provide substantial deformation capacity). Since the rubble stone masonry, investigated in this study, consists of mud mortar (which has a low resistance to tensile forces) and by definition has a random stone configuration, this masonry is susceptible to diagonal tensile failure as well. This brittle failure mode is not considered in the NPR 9998+C1 since it has been established that this mechanism is not of concern for Dutch masonry.

However, diagonal tensile failure was included in the calculations of the previous version of the NPR 9998 (NPR 9998, 2017), based on the New Zealand standard NZSEE. This formula is used for this analytical study additionally to the formulas provided by the NPR 9998+C1 concerning bed-joint sliding and rocking. Table 3.1 shows the formulas belonging to the three failure modes considered in this analytical study.

The formula for bed-joint sliding is simplified by assuming an initial shear strength of zero. This is justified by the reasoning that this type of masonry consists of mud mortar which has a very low tensile strength. Therefore, the shear strength of the masonry degrades to zero at early stages of loading. This allows for excluding the use of  $L_c$  since the force equilibrium now only exists of the normal stresses in the masonry instead of also a bending moment due to the shear strength. This is shown in Figure 3.3, where  $\sigma_0$  is the initial compressive stress in the masonry and  $\sigma_N$  is the compressive stress in the compressive area of the cross section during loading.

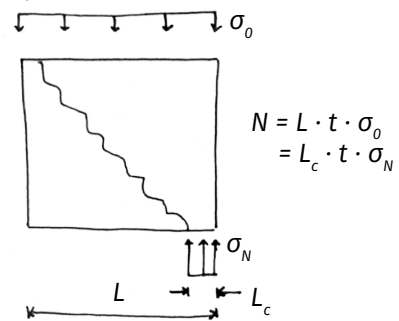
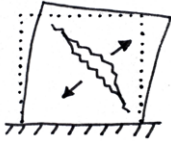
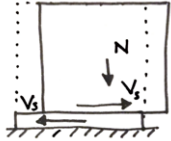
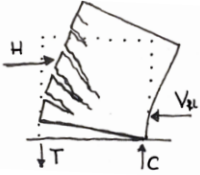


Figure 3.3: Force equilibrium when the bending moment due to the initial shear strength is excluded.

The parameters used for the calculations are defined in Appendix A. Some of these parameters depend on the dimensions of the wall or pier that form the governing mechanism of the structure. Adding bands and columns to the masonry wall

**Table 3.1:** Calculations as recommended in the NPR 9998 for in-plane failure mechanisms of masonry

Mechanism		Resistance
Shear mechanism: diagonal tensile failure (brittle)		$V_{dt} = f_{dt} \cdot L \cdot t \cdot \beta \sqrt{1 + \frac{\sigma_n}{f_{dt}}}$
Shear mechanism: bed-joint sliding (ductile)		$V_s = L \cdot t \cdot \mu_f \cdot \sigma_n$
Flexural mechanism: rocking (ductile)		$V_{fl} = P_{tot} \cdot \frac{L}{2h} \cdot \left(1 - 1.15 \frac{\sigma_n}{f_{c,m}}\right)$

Note. Formulas from NPR 9998+C1, 2020, p. 200-201; and NPR 9998, 2017, p. 170. Figures adapted from NPR 9998, 2017, p. 187.

changes the dimensions of the governing mechanism and therefore changes these parameters. Other parameters are fixed, like the density of the masonry. These values are obtained from literature. The NPR 9998 provides a relation between the diagonal tensile strength and the friction behaviour of brick masonry, which is based on sliding along the mortar. However, for rubble stone masonry this relation is not as accurate. Therefore, the value of the diagonal tensile strength of rubble stone masonry is based on diagonal compressive tests found in literature.

The calculations as recommended by the NPR 9998 predict the behaviour of unreinforced shear walls. However, this research investigates masonry walls confined by timber frames. The contribution of the timber frame is taken into account by increasing the superimposed load by an additional load  $P_{add}$ , and therefore increasing the normal stress in the masonry. The magnitude of  $P_{add}$  is determined by the normal force developed in the timber column(s). The timber columns are activated by vertical displacement of the masonry due to dilatancy of the stones:

$$\tan(\varphi) = \frac{\Delta w}{\Delta u}$$

where  $\varphi$  is the dilatancy angle, assumed to be  $27.5^\circ$  (Angiolilli & Gregori, 2020);  
 $\Delta w$  is the vertical displacement of the wall or pier;  
 $\Delta u$  is the horizontal displacement of the wall or pier.

The horizontal displacement of the wall or pier is determined by the formulas for drift as stated in the NPR 9998:

$$\Delta u = \theta \cdot h$$

where  $h$  is the height of the wall or pier;  
 $\theta$  is the drift limit when the “near collapse” limit state is reached:

$$\theta = \begin{cases} \theta_R = 0.0135 \left( 1 - 2.6 \frac{\sigma_n}{f_{c,m}} \right) \frac{h_{\text{wall}}}{h} \sqrt{\frac{h}{L}} & \text{for a rocking mechanism} \\ \theta_S = 0.0075 & \text{for a shear mechanism} \end{cases}$$

By using Hooke’s Law, the internal load of the column(s) ( $P_{\text{add}}$ ) is determined:

$$P_{\text{add}} = \frac{\Delta h_{\text{column}}}{h_{\text{column}}} EA \leq 74 \text{ kN}$$

where  $\Delta h_{\text{column}}$  is the extension of the column, equal to the vertical displacement of the wall:

$\Delta h_{\text{column}}$  is the deformation of the column =  $\Delta w = \tan(\varphi) \cdot \Delta u$ ;  
 $h_{\text{column}}$  is the length of the column;  
 $E$  is the modulus of elasticity of the timber;  
 $A$  is the cross-sectional area of the column;

The internal load of the column is limited by the load carrying capacity of the band-to-column connection, which is 74 kN. For the calculations of the load carrying capacity is referred to Appendix B. Since columns are placed at both sides of the band,  $P_{\text{add,max}} = 2 \cdot 74 = 14.8 \text{ kN}$ . Figure 3.4 shows the (exaggerated and simplified) displacement of the confined wall which leads to the extension of the columns.

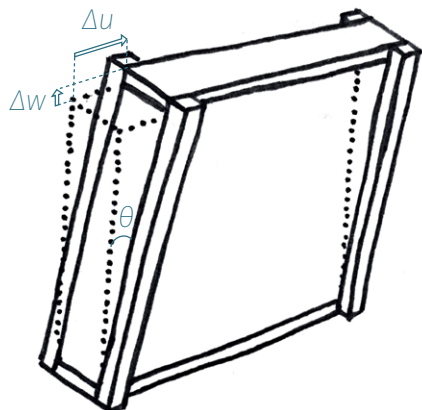


Figure 3.4: Horizontal ( $\Delta u$ ) and vertical ( $\Delta w$ ) displacement of the confined wall.

### 3.1.2 Strut and tie models by P. Roca

To study the ultimate strength of masonry walls, Roca adopted the possibility of using strut and tie models from modern concrete codes. Since masonry has a very limited tensile strength, the ultimate capacity of shear walls is formed by diagonal fields of compression stresses in equilibrium with the external loads. Due to the geometry of the wall and the particular loading case, these diagonal compression fields will deviate within the wall, causing internal tensile and compressive forces. Therefore, the deviation of a compression stress field is only possible if a horizontal tensile force can be developed within the masonry, shown in Figure 3.5.

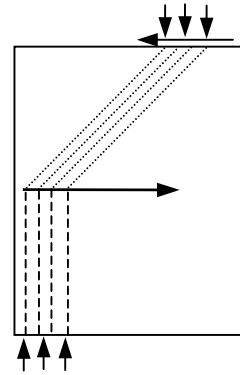


Figure 3.5: Deviation of compression stress fields by horizontal tensile forces (source: Roca, 2004)

From these considerations, Roca has established a list of rules that the strut and tie models should meet. These rules include requirements on the positions and amount of struts and ties. Since this research studies masonry with a low-strength mortar, two rules in particular are of importance:

- The maximum slope ( $\alpha$ ) of the compressive struts is limited by the frictional response of the mortar:

$$\tan(\alpha) = \tan(\phi) + c/\sigma_n$$

where  $\phi$  is the friction angle of the mortar,  $c$  is the cohesion, and  $\sigma_n$  is the average vertical compression.

- Due to the low tensile strength of the masonry, ties can only exist in horizontal direction. The maximum tensile force ( $T$ ) carried out by a tie is determined by the friction between the stones and the tensile strength of the masonry:

$$T \leq V_i \cdot \tan(\alpha)$$

$$T \leq A_n \cdot f_t$$

where  $V_i$  is the vertical force carried by the struts,  $A_n$  is the area contributing to resist the tensional force (which is for this study assumed to be the entire horizontal cross section of the wall:  $A_n = L \cdot t$ ), and  $f_t$  is the tensile strength of the masonry.

Based on these rules, Roca proposes several strut and tie models, applicable for different types of walls. Figures 3.6 and 3.7 show two of them that could be applicable for this study: smeared struts arranged according to a parallel or fan distribution for walls resisting vertical uniformly distributed loads; and for walls with an opening a mechanism describing the internal forces, where almost no vertical compression exists close to the top and bottom edges of the opening, meaning that such a mechanism is only possible if the ties can be mobilised. The strut and tie models introduced by Roca assume the vertical and the horizontal load to be applied at the upper edge of the wall, while the self-weight is considered negligible. For this

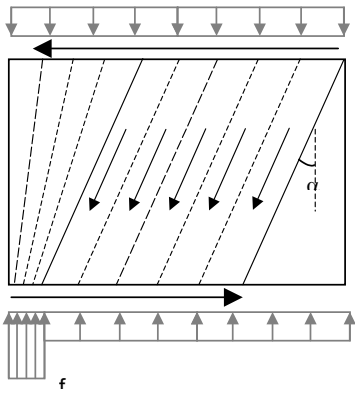


Figure 3.6: Model proposed by Roca for walls subjected to uniform vertical load. (source: Roca, 2004)

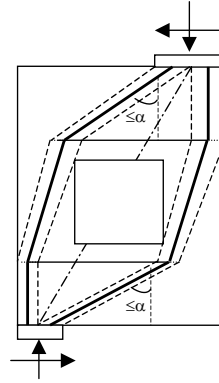


Figure 3.7: Model proposed by Roca for walls with opening. (source: Roca, 2004)

research on Nepali masonry, the self-weight of the wall is actually not negligible, since it is much larger than the superimposed load on the top of the wall that follows from the self-weight of the roof structure.

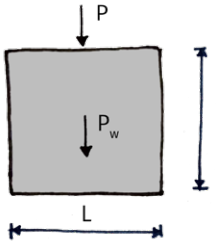
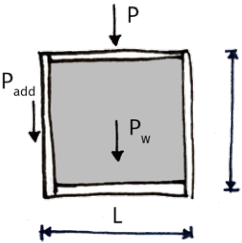
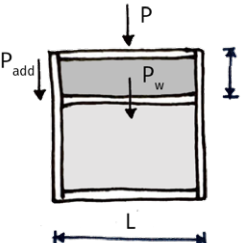
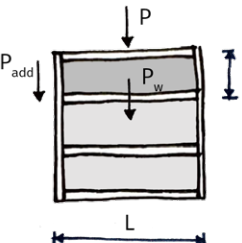
Due to the low average vertical compression stress in the in-plane walls of this research, it has proven to be impossible to implement the method of strut and tie models for this particular type of structure. The slopes of the struts cannot be determined in a way that would lead to reliable results. It is therefore decided to disregard the use of strut and tie models to study the ultimate strength of these masonry walls.

### 3.3 ESTIMATED RESISTANCE

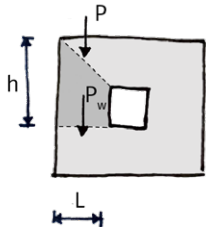
A total of nine configurations of in-plane loaded walls have been analytically analysed; four closed walls with zero to four bands, and five walls with a window opening with zero to four bands and columns. Unfortunately, the results obtained by the strut and tie models have been disregarded due to the fact that this particular masonry does not have sufficient compressive loads acting on the top of the wall to establish reliable strut and tie models.

The ultimate strength of the in-plane walls are estimated only by means of using the calculations as recommended by the NPR 9998. This method states that the weakest link of the structure is likely to form the plastic mechanism and collapse mode of the global structure. Table 3.2 shows the different wall configurations and their governing pier (highlighted in a darker shade of grey) together with the corresponding parameters, estimated resistance, and governing failure mode. A schematic representation of the diagonal compressive struts that are expected to develop in the masonry, is given in Figure 3.8.

Table 3.2: Estimated resistance using calculations of NEN NPR9998

Type of shear wall	Variable parameters	Resistance	Failure mechanism
	$P = 1000 \text{ N}$ $P_{w,h} = 85818 \text{ N}$ $P_{w,h/2} = 42909 \text{ N}$ $h = 2700 \text{ mm}$ $L = 3000 \text{ mm}$	$\sigma_{n,h} = 0.064 \text{ N/mm}^2$ $\sigma_{n,h/2} = 0.032 \text{ N/mm}^2$ $\mu_f = 0.70$ $\beta = 0.84$ $V_s = 60.5 \text{ kN}$ $V_{fl} = 47.0 \text{ kN}$ $V_{dt} = 36.6 \text{ kN}$	Diagonal tensile failure
	$P = 1000 \text{ N}$ $P_{w,h} = 85818 \text{ N}$ $P_{w,h/2} = 42909 \text{ N}$ $h = 2700 \text{ mm}$ $L = 3000 \text{ mm}$ $\theta_s = 0.0075 \text{ rad}$	$\Delta h_{\text{column}} = 10.5 \text{ mm}$ $P_{\text{add}} = P_{\text{max}} = 14800 \text{ N}$ $\sigma_{n,h} = 0.075 \text{ N/mm}^2$ $\sigma_{n,h/2} = 0.043 \text{ N/mm}^2$ $\mu_f = 0.80$ $\beta = 0.84$ $V_s = 81.0 \text{ kN}$ $V_{fl} = 54.8 \text{ kN}$ $V_{dt} = 40.3 \text{ kN}$	Diagonal tensile failure
	$P = 1000 \text{ N}$ $P_{w,h} = 28606 \text{ N}$ $P_{w,h/2} = 14303 \text{ N}$ $h = 900 \text{ mm}$ $L = 3000 \text{ mm}$ $\theta_s = 0.0075 \text{ rad}$	$\Delta h_{\text{column}} = 3.5 \text{ mm}$ $P_{\text{add}} = P_{\text{max}} = 14800 \text{ N}$ $\sigma_{n,h} = 0.033 \text{ N/mm}^2$ $\sigma_{n,h/2} = 0.022 \text{ N/mm}^2$ $\mu_f = 0.80$ $\beta = 1.00$ $V_s = 35.6 \text{ kN}$ $V_{fl} = 71.9 \text{ kN}$ $V_{dt} = 39.1 \text{ kN}$	Bed-joint sliding
	$P = 1000 \text{ N}$ $P_{w,h} = 28606 \text{ N}$ $P_{w,h/2} = 14303 \text{ N}$ $h = 900 \text{ mm}$ $L = 3000 \text{ mm}$ $\theta_s = 0.0075 \text{ rad}$	$\Delta h_{\text{column}} = 3.5 \text{ mm}$ $P_{\text{add}} = P_{\text{max}} = 14800 \text{ N}$ $\sigma_{n,h} = 0.033 \text{ N/mm}^2$ $\sigma_{n,h/2} = 0.022 \text{ N/mm}^2$ $\mu_f = 0.80$ $\beta = 1.00$ $V_s = 35.6 \text{ kN}$ $V_{fl} = 71.9 \text{ kN}$ $V_{dt} = 39.1 \text{ kN}$	Bed-joint sliding



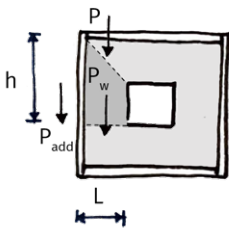


$$\begin{aligned}
 P &= 333 \text{ N} \\
 P_{w,h} &= 14303 \text{ N} \\
 P_{w,h/2} &= 7151 \text{ N} \\
 h &= 1800 \text{ mm} \\
 L &= 1000 \text{ mm}
 \end{aligned}$$

$$\begin{aligned}
 \sigma_{n,h} &= 0.033 \text{ N/mm}^2 \\
 \sigma_{n,h/2} &= 0.017 \text{ N/mm}^2 \\
 \mu_f &= 0.70 \\
 \beta &= 0.67
 \end{aligned}$$

$$\begin{aligned}
 V_s &= 10.4 \text{ kN} \\
 V_{fl} &= 4.0 \text{ kN} \\
 V_{dt} &= 8.2 \text{ kN}
 \end{aligned}$$

Rocking

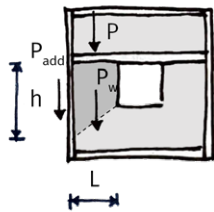


$$\begin{aligned}
 P &= 333 \text{ N} \\
 P_{w,h} &= 14303 \text{ N} \\
 P_{w,h/2} &= 7151 \text{ N} \\
 h &= 1800 \text{ mm} \\
 L &= 1000 \text{ mm} \\
 \theta_{fl} &= 0.027 \text{ rad}
 \end{aligned}$$

$$\begin{aligned}
 \Delta h_{\text{column}} &= 25.4 \text{ mm} \\
 P_{\text{add}} = P_{\text{max}} &= 14800 \text{ N} \\
 \sigma_{n,h} &= 0.065 \text{ N/mm}^2 \\
 \sigma_{n,h/2} &= 0.050 \text{ N/mm}^2 \\
 \mu_f &= 0.70 \\
 \beta &= 0.67
 \end{aligned}$$

$$\begin{aligned}
 V_s &= 20.5 \text{ kN} \\
 V_{fl} &= 8.0 \text{ kN} \\
 V_{dt} &= 11.3 \text{ kN}
 \end{aligned}$$

Rocking

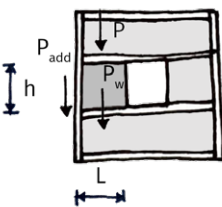


$$\begin{aligned}
 P &= 9869 \text{ N} \\
 P_{w,h} &= 14303 \text{ N} \\
 P_{w,h/2} &= 7151 \text{ N} \\
 h &= 1800 \text{ mm} \\
 L &= 1000 \text{ mm} \\
 \theta_{fl} &= 0.027 \text{ rad}
 \end{aligned}$$

$$\begin{aligned}
 \Delta h_{\text{column}} &= 25.4 \text{ mm} \\
 P_{\text{add}} = P_{\text{max}} &= 14800 \text{ N} \\
 \sigma_{n,h} &= 0.087 \text{ N/mm}^2 \\
 \sigma_{n,h/2} &= 0.070 \text{ N/mm}^2 \\
 \mu_f &= 0.70 \\
 \beta &= 0.67
 \end{aligned}$$

$$\begin{aligned}
 V_s &= 27.4 \text{ kN} \\
 V_{fl} &= 10.5 \text{ kN} \\
 V_{dt} &= 12.8 \text{ kN}
 \end{aligned}$$

Rocking

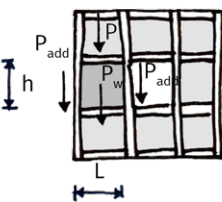


$$\begin{aligned}
 P &= 9869 \text{ N} \\
 P_{w,h} &= 9535 \text{ N} \\
 P_{w,h/2} &= 4768 \text{ N} \\
 h &= 900 \text{ mm} \\
 L &= 1000 \text{ mm} \\
 \theta_{fl} &= 0.038 \text{ rad}
 \end{aligned}$$

$$\begin{aligned}
 \Delta h_{\text{column}} &= 17.9 \text{ mm} \\
 P_{\text{add}} = P_{\text{max}} &= 14800 \text{ N} \\
 \sigma_{n,h} &= 0.076 \text{ N/mm}^2 \\
 \sigma_{n,h/2} &= 0.065 \text{ N/mm}^2 \\
 \mu_f &= 0.80 \\
 \beta &= 0.84
 \end{aligned}$$

$$\begin{aligned}
 V_s &= 27.4 \text{ kN} \\
 V_{fl} &= 18.4 \text{ kN} \\
 V_{dt} &= 15.6 \text{ kN}
 \end{aligned}$$

Diagonal tensile failure



$$\begin{aligned}
 P &= 9869 \text{ N} \\
 P_{w,h} &= 9535 \text{ N} \\
 P_{w,h/2} &= 4768 \text{ N} \\
 h &= 900 \text{ mm} \\
 L &= 1000 \text{ mm} \\
 \theta_{fl} &= 0.038 \text{ rad}
 \end{aligned}$$

$$\begin{aligned}
 \Delta h_{\text{column}} &= 17.9 \text{ mm} \\
 P_{\text{add}} = P_{\text{max}} &= 14800 \text{ N} \\
 \sigma_{n,h} &= 0.109 \text{ N/mm}^2 \\
 \sigma_{n,h/2} &= 0.098 \text{ N/mm}^2 \\
 \mu_f &= 0.80 \\
 \beta &= 0.84
 \end{aligned}$$

$$\begin{aligned}
 V_s &= 39.2 \text{ kN} \\
 V_{fl} &= 26.1 \text{ kN} \\
 V_{dt} &= 18.4 \text{ kN}
 \end{aligned}$$

Diagonal tensile failure

In Figure 3.8 it can be seen that the confinement of the masonry by the bands and columns create more load paths and therefore increases the shear resistance of the wall. If the confinement consists of more timber elements, the load is distributed more evenly over the wall.

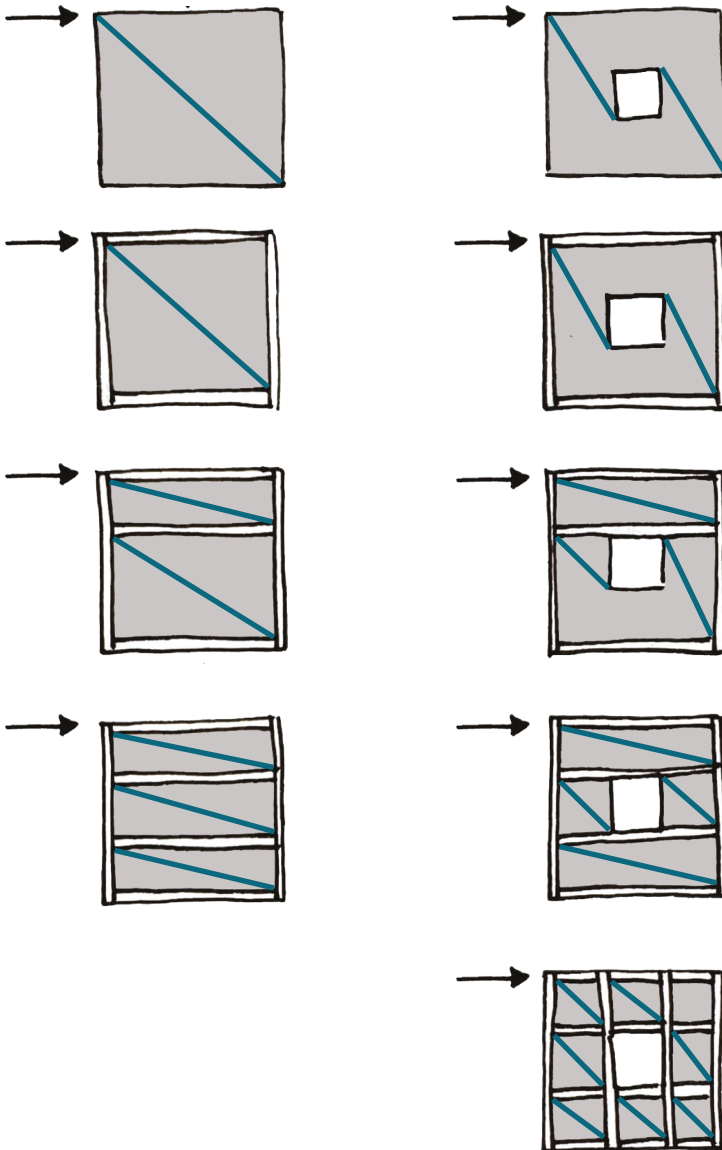


Figure 3.8: Schematic representation of the diagonal compressive struts that are expected to develop in the masonry.

## 3.4 CONCLUSIONS CHAPTER 3

Performing the analytical study has provided an initial estimation of the ultimate resistance and failure mechanisms of this type of Nepali masonry, as well as the contribution of the timber frame confinement to the resistance. Furthermore, insight is obtained in the applicability of the simplified models used for this analytical study.

### 3.4.1 Applicability of strut and tie models

Strut and tie models have been proven to be a reliable simplified method to assess concrete and masonry structures. However, in this particular case this method is not applicable: the lack of superimposed vertical loads prevents from establishing a reliable strut and tie mechanism.

### 3.4.2 Applicability of NPR calculations

For this research, no experimental data could be found for the specific Nepali masonry that is investigated. Whether or not the formulas as recommended by the NPR 9998 (based on Dutch masonry) are valid for Nepali masonry as well, will be assessed using a numerical study in Chapters 5 and 6.

The values obtained for the drift limit of the structure ( $\theta$ ) are expected to be overestimated, since the drift limit for brick masonry with cement mortar is larger than for rubble stone masonry with mud mortar. Since  $P_{add}$  is determined by the dilatancy of the stones and therefore depends on the drift limit, it is uncertain how much force will actually develop in the columns. This will be further investigated in the numerical study.

### 3.4.3 Timber frame

An important observation made during this analytical study, concerns the strength of the timber frame. When calculating the load carrying capacity of the connections, it was found that the dimensions of the bands and columns as stated in the Nepali building codes are not sufficient to fit the fasteners when following the edge distances requirements as recommended by the European standards (EN 1995-1-1, 2004). The cross-sectional dimensions of the bands and columns are therefore increased to 140x140 mm. With these new dimensions, the load carrying capacity of the connections is calculated which determines  $P_{add,max}$ . In all of the confined wall models, this limit of  $P_{add}$  is expected to be reached, based on the estimated displacement of the wall. This means that the strength of the connections of the timber frame could be governing for the collapse mode of the global structure.

### 3.4.4 Estimated ultimate strength

When observing the effect of the confinement by the timber frame on the closed wall, it is estimated that adding only the roof band and the floor band increases the ultimate strength of the wall, whereas adding more bands has no structural benefit: it leads to interrupting the masonry and which actually weakens it. However, when observing the effect of these bands on the wall with opening, it becomes clear why adding these bands could benefit the masonry structure: by confining not only the top and bottom of the wall, but also the top and bottom edges of the opening, the governing piers are compressed such that their estimated resistance quadruples. Figure 3.9 shows bar diagrams of the estimated strength of the walls.

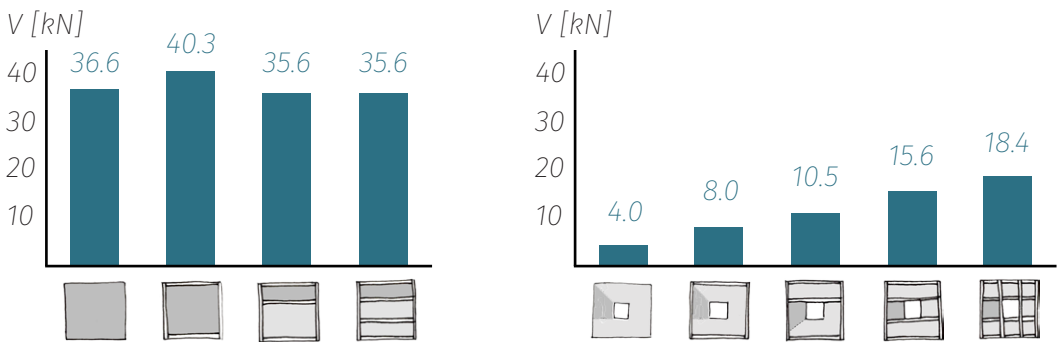


Figure 3.9: Bar diagram of the estimated ultimate resistance of the closed walls (left) and walls with opening (right), when increasing the amount of confinement.

### 3.4.5 Failure modes

The wall configurations without window opening are expected to develop shear mechanisms, either brittle (diagonal tensile failure) or ductile (bed-joint sliding). By increasing the amount of bands, the likeliness of a bed-joint sliding mechanism to develop is expected to increase as well. The development of a ductile mechanism instead of a brittle mechanism is desirable concerning safety. However, the resistance to bed-joint sliding is estimated to be only slightly lower than the resistance to diagonal tensile failure, so the probability of a brittle failure mechanism to develop cannot be excluded.

For the walls with opening the governing mechanism is found in the piers next to the opening. The piers of the first three models are more slender than the fully confined piers of the last two models. Therefore, the flexural mechanism is expected to be governing in the first three models. By confining also the top and bottom edges of the opening, the piers are compressed such that their flexural strength becomes greater than their diagonal tensile strength, so by increasing the amount of timber confinement the failure mode shifts from ductile to brittle which is undesirable.

# CHAPTER 4

---

## Discretisation of the masonry structure

*This chapter explains the theoretical background of performing a finite element analysis (FEA) in the solver software DIANA. In order to perform numerical calculations, the masonry structure needs to be discretised into a numerical model. This chapter discusses the possibilities within applying material models and element models to represent the masonry structure, and the force model that will represent earthquake loads. The chapter starts with background information on a finite element analysis in the first two paragraphs, followed by the realisation of the material models, element models, and force models. The chapter concludes with an overview of the choices that are made to establish the numerical model.*

### 4.1 BASIC ROUTINE FEA

A finite element analysis (FEA) translates mathematical formulations of reality, which has an infinite domain, into a finite amount of elements, and links these elements to each other by means of nodes. This transition from continuous to discrete is called discretisation. A finite element analysis is used when analytical calculations are inadequate or become too complex.

Figure 4.1 represents one iteration of a displacement controlled finite element analysis, consisting of five steps. A prescribed displacement is attached to the nodes, which causes strains and stresses in the element. The strains are calculated in integration points in the element by means of interpolation from the nodes. The stresses follow from the stress-strain relation. By integrating over the element's volume, the internal forces in the nodes and element stiffness is calculated. The last step of the iteration is considering equilibrium in the node from the internal forces of the connected elements and the external forces. If the nodes are in equilibrium the next load increment can be taken, if not, a new nodal displacement is applied and the routine is repeated until step five converges. (Hendriks, 2016b).

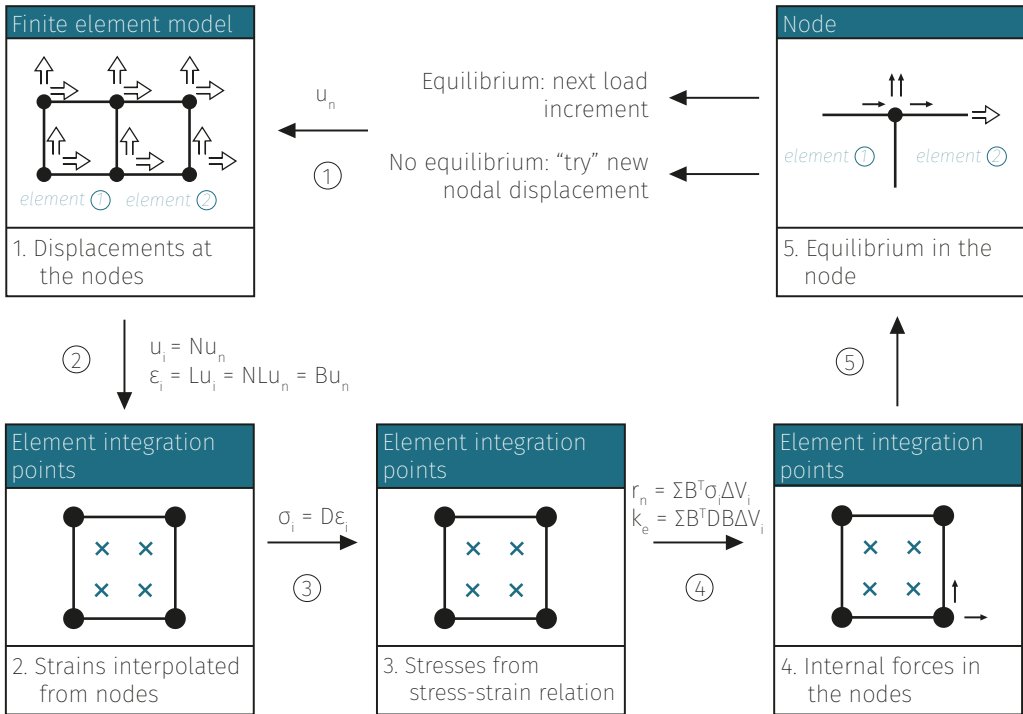


Figure 4.1: Basic routine of one FEA iteration in DIANA (source: adapted from Hendriks, 2016b)

## 4.2 SCALE LEVEL

By translating the real structure into a finite element model, assumptions concerning the elements have to be made. The more detailed the model, the more accurate the results, but the longer the simulation time. A consideration must be made between accuracy and computational burden.

Three approaches to the discretisation of masonry can be identified: micro-scale, meso-scale, and macro-scale (Alshawa, 2017), shown in Figure 4.2. Creating a model on micro-scale level follows the reality of the appearance of the structure closely. Modelling masonry on this scale means that every brick is modelled as a separate plane element, the mortar between them is modelled as line elements, and the interaction between the mortar and the brick units is represented by interface elements. The orthotropic behaviour of masonry is integrated in the geometry of the model since each stone is modelled separately. This modelling strategy is very detailed, and not an appropriate approach for rubble stone masonry, since the configuration of the stones is random.

A slightly less detailed modelling approach is to disregard the interaction between the mortar and the stones, which allows to model the mortar joints with interface elements. Usually, for this meso-scale level, the brick units are modelled as linear

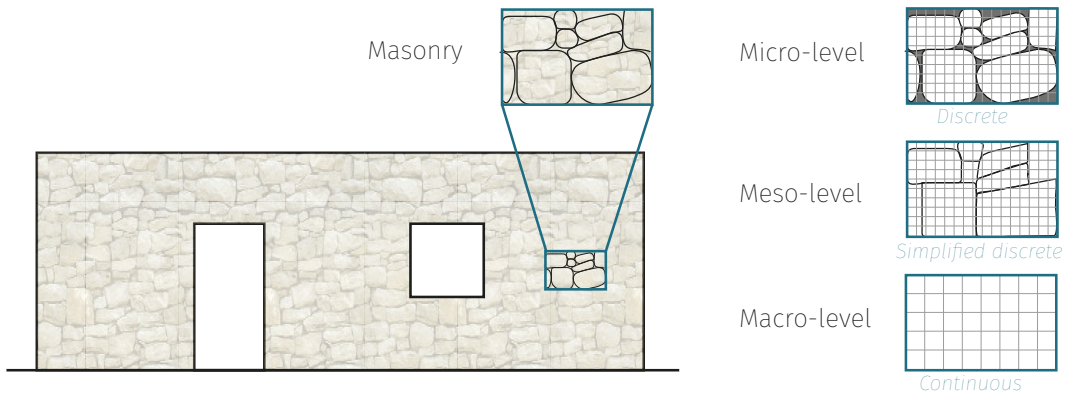


Figure 4.2: *Micro-, macro-, and meso-scale discretisation (source: adapted from Van Wijnbergen, 2016)*

elastic (DIANA-10.1, 2017a). For this approach it holds as well that the random stone configuration does not allow for a model on meso-scale level.

Creating a model on micro-scale or on meso-scale results in a so called discrete model. Alternatively, a model on macro-scale is called a continuum model. The macro level is less detailed, and is used to simulate the global behaviour of the masonry (DIANA-10.1, 2017b). The bricks and joints are modelled together as a single homogeneous material by homogenising the stone and mortar properties over an surface, creating a so called “smeared cracking model”. This modelling approach will be used for this research, since the uncertainty of the stone sizes and their configuration eliminates the possibility to model the structure in great detail. Consequently, a global analysis will be performed on the masonry to investigate the most important mechanisms and structural vulnerabilities, rather than predicting the actual response under seismic loading.

## 4.3 MODELLING OF MASONRY

### 4.3.1 Element model

When discretising a structure to a finite element model, it is important to carefully choose the element types and the material model. The finite element model must represent the reality accurately to obtain reliable results. DIANA offers many different elements with different properties, which in combination with the right material model can represent the actual structure fairly well.

The masonry walls are modelled as sheets, and will be analysed in a two-dimensional flat plane. The loading acts in the plane of the element. Therefore, regular plane stress elements are applied (see Figure 4.3 for the characteristics). A quadratic mesher type is assigned with a linear mesh order, i.e. the plane stress elements have four integration points.

### 4.3.2 Material model

Assigning a material model to a certain element is determining which material properties are assigned to that element. It is important to realise which material properties are important to include in the model for the model to describe the behaviour of the materials properly, and which material properties are not.

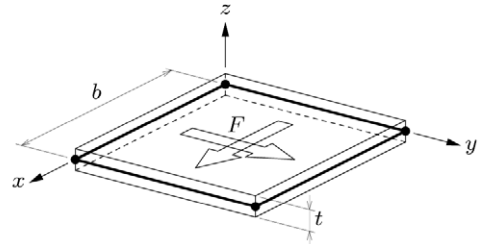


Figure 4.3: Characteristics of plane stress elements (source: DIANA-10.1, 2017c)

Masonry is an orthotropic material, meaning the properties of the material are direction-dependent. It is possible to model this orthotropic behaviour in DIANA by means of the “Engineering Masonry model”. This model allows for the consideration of several failure mechanisms that could model complex cracking behaviour. Consequently, this model needs quite some input parameters that are not precisely known, making the application of this model less reliable. For this study, the behaviour of masonry will be simplified to isotropic behaviour, meaning the different behaviour in different directions is neglected. DIANA offers the “Total strain based crack model” to analyse isotropic materials.

The total strain based crack model describes the stress as a function of the strain. One approach within the total stress-strain relations, is to evaluate the stress-strain relations in the principal directions of the strain vector. This approach is known as the “Rotating crack model”, the crack directions are continuously rotating with the principal directions of the strain vector. This describes the non-linear behaviour of the masonry. The total strain based crack model knows different predefined crushing and softening curves for compression and tension respectively, varying from vastly simplified to close to the behaviour in reality. In this study, the tension softening curve chosen for the model is linear and ultimate strain based. The compression crushing curve is parabolic, shown in Figure 4.4. The ultimate crack strain ( $\epsilon_u$ ) of the material can be calculated from the strength of the material and the fracture energy for a constant crack bandwidth ( $h$ ). The fracture energy divided by the crack bandwidth represents the area under the stress strain curve. The predefined crushing and softening curves describe these relations as follows:

$$\begin{cases} \epsilon_t = \frac{E}{f_t} \\ \epsilon_{t,u} = 2 \frac{G_{f,t}}{f_t h} \\ \epsilon_c = \frac{5}{3} \frac{f_c}{E} \\ \epsilon_{c,u} = \epsilon_c - \frac{2}{3} \frac{G_{f,c}}{f_c h} \end{cases}$$



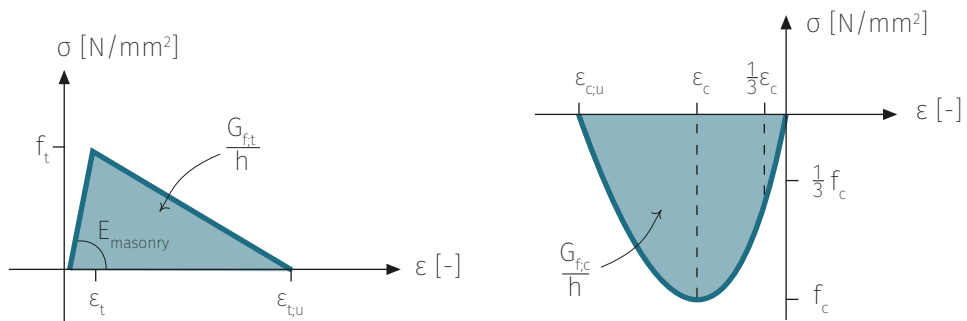


Figure 4.4: Predefined tensile (left) and compressive (right) behaviour of the total strain based crack elements (source: Diana10-1, 2017b).

Schreppers et al. (2017) proposes a relation between the strength of a material and its fracture energy, for tension and compression:

$$\begin{cases} G_{ft} = 0.025(2f_t)^{0.7} \\ G_{fc} = 15 + 0.43f_c - 3.6 \cdot 10^{-3} \cdot f_c^2 \end{cases}$$

The shear behaviour for the total strain based crack model is taken into account by the shear stress-strain relation. The ratio between the shear stress and shear strain depends on the shear stiffness ( $G$ ) which is related to the Young's modulus and Poisson's ratio. Since Poisson's ratio and the Young's modulus are input parameters for the total strain based crack model, the shear parameters need not be defined separately.

### 4.3.3 Material properties

The total strain based crack model depends on several material properties that describe the linear behaviour, the tensile and compression behaviour, and the crack behaviour of the masonry. Some of these material properties correspond to those introduced in Chapter 3. Due to the lack of experimental tests on the masonry, the exact values of the material properties are unknown for this research. Therefore, the material properties are defined within a certain range that is conform values found in literature. By means of a parameter study performed in Chapter 5 of this research, the effect of the uncertainty of the material properties on the behaviour of the structure will be investigated. Subsequently, for the numerical modelling that will follow to answer the research question, each material property will be assigned a set value in Chapter 5.

Table 4.1 gives an overview of the masonry material properties including the range of their value which is based on values found in literature.

**Table 4.1:** Overview material properties masonry

Material property	Range	Source	Unit
Young's modulus	$1800 \leq E \leq 3300$	Sorour et al. (2009)	N/mm <sup>2</sup>
Mass density	$2000 \leq \rho \leq 3000$	Dhital (2015)	kg/m <sup>3</sup>
Poisson's ratio	$0.01 \leq \nu \leq 0.25$	Cavaleri et al. (2013)	-
Tensile strength	$0.01 \leq f_t \leq 0.10$	Milosevic et al. (2013)	N/mm <sup>2</sup>
Fracture energy in tension	$0.0016 \leq G_{ft} \leq 0.010$	Schreppers et al. (2017)	N/mm
Compressive strength	$1.50 \leq f_c \leq 5.00$	Lekshmi (2016); Giaretton et al. (2015)	N/mm <sup>2</sup>
Fracture energy in compression	$1.5f_c \leq G_{fc} \leq 5$	Nakamura & Higai (2001); Pina-Henriques et al. (2005)	N/mm

## 4.4 MODELLING OF BANDS AND COLUMNS

### 4.4.1 Element model

The dimensions of the cross sections of the bands and columns are small in relation to the length. The bands and columns are therefore modelled as beam elements. Beam elements (class-III for non-linear analyses) can undergo axial deformation ( $\Delta L$ ), shear deformation ( $\gamma$ ), curvature ( $\kappa$ ) and torsion. This allows for analysing the axial force, shear force and bending moments in the bands and columns, shown in Figure 4.5.

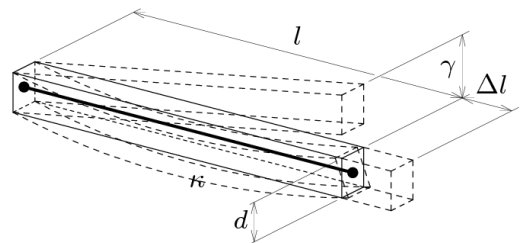


Figure 4.5: Beam elements, characteristics  
(source: Diana-10.1, 2017c)

### 4.4.2 Material model

Timber has a much higher strength and stiffness compared to the rubble stone masonry. Therefore, when the masonry is loaded beyond its capacity, it is assumed that the bands and columns are still in their elastic phase. This assumption allows to model the bands and columns as linear elastic materials. The stress-strain relations of the class-III beam elements are shown in Figure 4.6.

### 4.4.3 Material properties

The input parameters for the linear elastic beam elements consist of the timber Young's modulus, mass density and Poisson's ratio. Like the masonry, the exact values of these material properties are unknown, but unlike the masonry the varieties in the timber material properties do not result in a different global response of the structure, since this is determined by the much weaker masonry. Therefore, no range in the timber material properties are considered. The values assigned are shown in Table 4.2 and are based on the strength classes for softwoods of the NEN-EN 338.

**Table 4.2:** Overview material properties timber

Material property	Value	Unit
Young's modulus	$E_{0,mean} = 11500$	N/mm <sup>2</sup>
Mass density	$\rho_{mean} = 450$	kg/m <sup>3</sup>
Poisson's ratio	$\nu = 0.3$	-

Note. Values obtained from NEN-EN 338

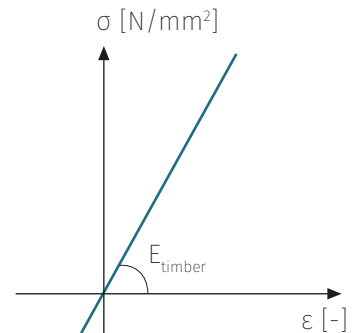


Figure 4.6: Predefined behaviour of the class-III beam elements (source: DIANA10-1, 2017b)

## 4.5 MODELLING OF BAND-TO-MASONRY CONNECTION

### 4.5.1 Element model

Geometrical imperfections of the stones and the timber cause friction between the two materials. This friction will provide resistance from the materials to detach, but there is no strong bond between the materials; in practise mud is used when stacking them upon each other, as opposed to a strong bonding material like cement. Figure 4.7 shows a picture of a lintel beam above a door opening to give an impression of the behaviour between the stones and the timber. In this particular picture, there seems to be little interaction between the stones and the timber, since the lintel beam is fairly straight. However, the seismic bands are on the top-side provided with transverse batten, which cause an interlocking behaviour between band and masonry, shown in Figure 4.8. This behaviour can be described by interface elements.

Interface elements are used to link two different elements in order to exchange information. To connect the plane stress elements of the masonry to the beam elements of the bands, DIANA offers two-dimensional line interface elements: to be placed between truss elements, beam elements or edges of two-dimensional



Figure 4.7: Example of a timber-to-masonry connection in Nepali structure (source: own photograph)

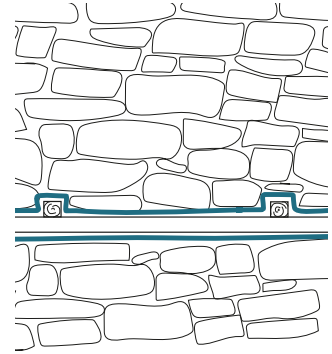


Figure 4.8: Interlock between band and masonry

elements. The surface and the directions of the interface is generated by DIANA automatically from the geometry of the elements.

Interface elements connect the nodes of one element to the nodes of the other, it is therefore important that the two connecting elements have the same amount of nodes. This can be regulated by means of the element size and the way the element is meshed (linearly or quadratically). See Figure 4.9 for the characteristics.

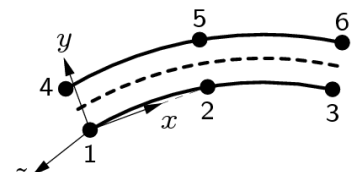


Figure 4.9: Two dimensional line interface element characteristics (DIANA-10.1, 2017c)

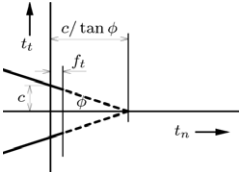
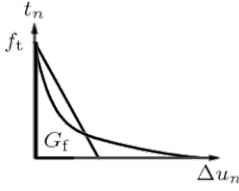
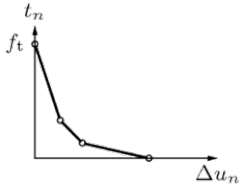
## 4.5.2 Material model

DIANA offers several types of interface elements that can each, to a certain extent, describe the behaviour between the masonry and the bands. When choosing between the different types of interface elements, the following aspects are of importance:

- Detachment of stones and timber should be possible;
- Detachment of the bands and stones initiates at a certain threshold value of the normal stress;
- The stones and timber cannot penetrate each other under compressive stress
- Sliding between bands and stones should be possible;
- Sliding of the bands and stones initiates at a certain threshold value of the shear stress;
- Difference in shear behaviour between top and bottom side of the band.

Three suitable material models for the interface elements are selected based on these prerequisites: Coulomb friction model, discrete cracking model, and non-linear elastic model. Table 4.3 gives an overview of the advantages and disadvantages of each of the models. Coulomb friction interface elements will be applied.

**Table 4.3:** Advantages and disadvantages of the interface material models

Material model	Advantage	Disadvantage
<p><b>Coulomb friction</b></p> 	<p>The Coulomb friction criterion describes a relation between the tensile traction normal and tangent to the interface, depending on the cohesion between the stones and beam, the friction angle and the tensile strength. Since the normal and shear traction are coupled, this material model describes the behaviour according to reality fairly well.</p>	<p>This model requires many input parameters, of which the cohesion, friction angle and the tensile strength are unknown, leading to a larger uncertainty and computational burden.</p>
<p><b>Discrete cracking</b></p> 	<p>A discrete crack arises if the normal traction <math>t_n</math> exceeds <math>f_t</math>. The discrete cracking model couples the normal and shear behaviour by means of a (reduced) shear stiffness which can be derived from the normal and shear traction. Compared to the Coulomb friction model, this model requires less input parameters, restraining the computational burden.</p>	<p>This model allows for different tension softening criteria, but offers only two options to describe the shear behaviour: zero shear traction and zero shear stiffness after cracking; or a constant shear modulus after cracking. A more detailed description of the sliding behaviour is not possible.</p>
<p><b>Nonlinear elastic</b></p> 	<p>This material model actually describes a multi-linear relation between the traction and relative displacement separately for the normal and tangential direction. This material model needs the least input parameters compared to the Coulomb friction and discrete cracking material models.</p>	<p>By decoupling the normal and shear behaviour, the shear behaviour is not a function of the normal behaviour and needs to be setup separately. To describe a dependency of the shear traction on the normal traction is therefore more complex and inadvisable.</p>

Note. Figures obtained from Diana10-1, 2017c

### 4.5.3 Material properties

The Coulomb friction interface elements demand linear and non-linear input parameters. The linear input parameters consist of the initial normal and shear stiffness ( $K_n$  and  $K_s$  respectively). These values must be much greater than the initial stiffness of the surrounding elements, i.e.  $E_{\text{masonry}}$  and  $G_{\text{masonry}}$  (since  $E_{\text{timber}} > E_{\text{masonry}}$  only  $E_{\text{masonry}}$  is considered). The interface elements should not contribute to the displacements of the structure in the linear domain, because the interface elements describe an intangible and can therefore not add deformation to the undamaged structure; they merely describe the opening and sliding behaviour after the elastic stage.

The non-linear parameters of the Coulomb friction line interface elements consist of the cohesion, the friction angle and dilatancy angle. Additionally, a tension strength is applied in order for the interface element to open up, which describes the detachment of the masonry and the timber. The tensile strength of the interface element is equal to the masonry tensile strength, because the bonding material between the stones of the masonry, which is mud, is also applied between the masonry and the timber band. The values for the cohesion, friction angle and dilatancy angle are obtained from literature. Due to the band's geometry, they are different for the interface elements placed on the top side of the beam to those placed on the bottom side.

The friction angle determines when the stones start to slide with respect to the timber band. On the bottom side of the timber band, the materials slide when the angle between the resultant force and normal force acting on them is equal to the internal friction angle ( $\varphi$ ), shown in Figure 4.10. The friction angle is related to the friction coefficient between the masonry and timber:  $\varphi = \tan^{-1}(\mu_f)$ , where the value for  $\mu_f$  is adapted from a study on mortar-to-timber friction in masonry buildings:  $\mu_f = 0.80$  (Almeida et al., 2020). This leads to a friction angle of  $\varphi_{\text{bottom}} = 40^\circ$  of the interface on the bottom side of the band. On the top side, however, a dilatancy of the stones is needed in order for them to displace relative to the timber band, due to the transverse batten that are placed on the band.

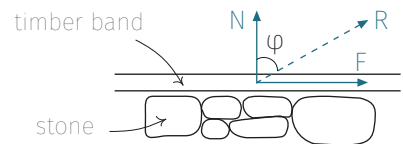


Figure 4.10: Angle of friction between masonry and bottom side timber band

Dilatancy is the change of volume that occurs with shear distortion of a material, characterised by the dilation angle ( $\psi$ ). In common practise, a simplified relation between the angle of friction and the dilation angle is often applied. As a rule-of-thumb, the dilation angle is at least  $20^\circ$  less than the friction angle (Alejano & Alonso, 2006). For this study, a dilation angle of  $\psi = \varphi - 30^\circ$  will be used. This means that the interface elements placed on the bottom side of the band will

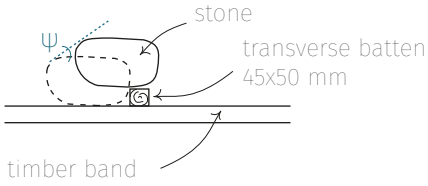


Figure 4.11: Dilatation angle between masonry and top side timber band

be assigned a dilatancy of  $\psi_{\text{bottom}} = 10^\circ$ . The interface elements placed on the top side of the band are assigned a larger dilation angle. A relative displacement in these interface elements takes place when the stones are distorted such that they are able to move over the transverse batten with dimensions 45x50 mm, shown in Figure 4.11. Sliding takes place for a dilatancy angle of  $\psi_{\text{top}} = \tan^{-1}(45/50) = 40^\circ$ .

The cohesion follows from the Mohr-Coulomb model, which gives a relation between the friction angle, tensile cut-off value and the cohesion, shown in Figure 4.12. The cohesion for the interface elements is approximated to be:

$$1.5f_t \cdot \tan(\varphi) \leq c \leq 2f_t \cdot \tan(\varphi), \text{ where } f_t = f_{t,\text{interface}} = f_{t,\text{masonry}}$$

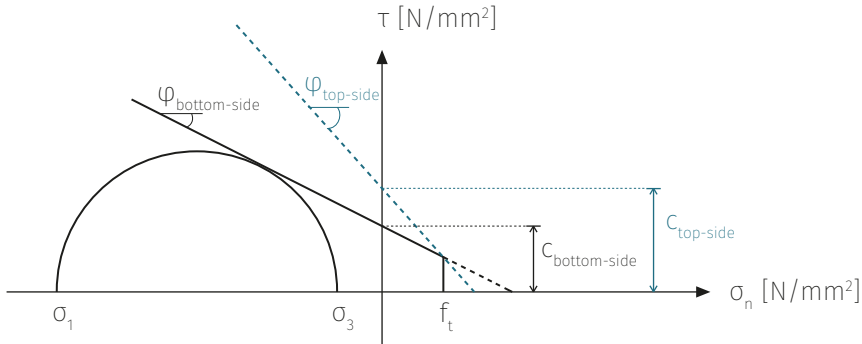


Figure 4.12: Mohr-Coulomb model for material properties of line interface elements

Table 4.4 gives an overview of the material properties of the line interface elements that represent the band-to-masonry connection on the top side and bottom side of the band.

**Table 4.4:** Overview material properties band-to-masonry connection

Material property	Symbol	Value top side	Value bottom side	Unit
Normal stiffness	$K_n$	$1 \cdot 10^5 E_{\text{masonry}}/h$	$1 \cdot 10^5 E_{\text{masonry}}/h$	N/mm <sup>3</sup>
Shear stiffness	$K_s$	$1 \cdot 10^5 G_{\text{masonry}}/h$	$1 \cdot 10^5 G_{\text{masonry}}/h$	N/mm <sup>3</sup>
Cohesion	$c$	$1.5f_t \cdot \tan(\varphi)$	$2f_t \cdot \tan(\varphi)$	N/mm <sup>2</sup>
Fiction angle	$\varphi$	70°	40°	degree
Dilatancy angle	$\psi$	40°	10°	degree

## 4.6 MODELLING OF BAND-TO-COLUMN CONNECTION

As discussed in Chapter 3, the band-to-column connection consists of a timber joint with metal fasteners which has a low rotational stiffness and therefore behaves like a hinge. The joint has a load carrying capacity of 74 kN, and since the bands are connected with a column on each side, the total capacity becomes 14.8 kN. This connection can be realised in DIANA in different ways:

- Apply hinges to the nodes of the two beam elements. This is a linear function and therefore does not allow for assigning an ultimate strength or lateral stiffness to the connection.
- Use node interface elements to connect the nodes of the two beam elements. This is a more complicated solution than applying hinges, which affects the stability of the model, but due to its non-linearity it can describe the failure of the timber joint.

In order to minimise the computational burden, it is chosen to model the band-to-column connection as hinges with an infinite strength and infinite lateral stiffness, which means they will not undergo failure during the analysis. During loading, the stresses at the timber connections will not decrease nor will they redistribute over the timber frame. Therefore, the exact influence of the joint strength and ductility on the timber confinement and, therefore, on the global behaviour of the entire structure will not be shown by the numerical results.

Instead of including the ultimate strength and ductility of the connections to the analysis, their behaviour will be assessed in hindsight by observing the stresses in the timber elements and subsequently determining if the maximum stresses in the connections are reached. This approach is justified by the reasoning that if this method of confining a masonry structure could be successful, the connections of the timber frame may not be governing. If the stresses in the timber frame would exceed the load carrying capacity of the connections, the connections should be redesigned. The disadvantage of this approach is that the timber connections could become over-dimensioned, because their design is based on their ultimate strength and their ductility is not taken into account.

## 4.7 FORCE MODEL

There are four domains in which the force-displacement response of a structure can be analysed: dynamic opposed to static, and linear opposed to non-linear, shown in Figure 4.13. Non-linearity of a structure means its structural properties change during loading, caused for example by the formation of cracks. The masonry that make up the buildings of rural Nepal are of low strength due to the use of mud mortar. Cracks will occur at low ground accelerations, causing the structure to behave non-linear at early stages of loading (Van Wijnbergen, 2016). To obtain



a reliable representation of the resistance of the building to earthquakes, it is therefore preferred to analyse the structure in the non-linear domain.

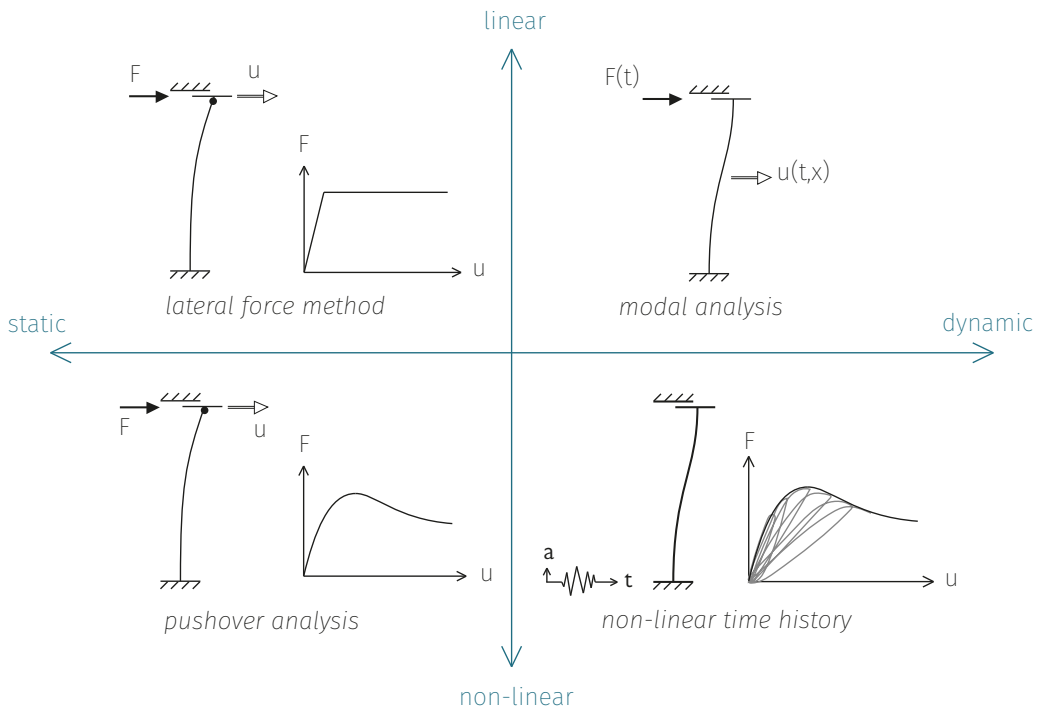


Figure 4.13: Force-displacement analysis domain (source: adapted from Van Wijnbergen, 2016).

In the non-linear domain, DIANA offers a modal pushover force model, which is a static analysis. It does not account for damping, nor for cyclic behaviour. The lateral force is equivalent to the modal distribution and is calculated based on the mode shape. It is also possible to perform a time history analysis in DIANA. This is a transient dynamic analysis for which damping and cyclic behaviour is accounted for. The input for this force model is the acceleration history with time in the three directions. DIANA calculates the external force by solving the equation of motion. Both force models have advantages and disadvantages, they are summarised in Table 4.5 (DIANA-10.1, 2017d).

Considering the relative simple structure, of which the response is dominated by the sway mechanism, it is decided that applying a complex analysis is superfluous. Performing a pushover analysis will be sufficient to answer the research question of this master's thesis, since it calculates the most important mechanisms of the structure. The results give insight in the structural vulnerabilities and identifies the weakest links in the load transfer mechanisms of the structure (NPR 9998, 2017).

**Table 4.5:** Characteristics pushover analysis and time history analysis

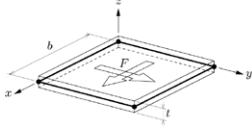
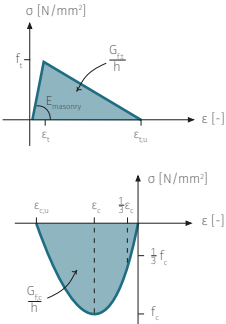
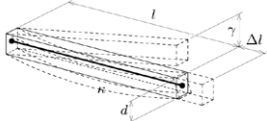
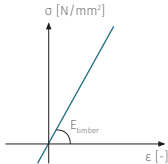
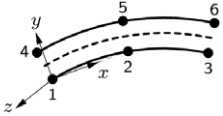
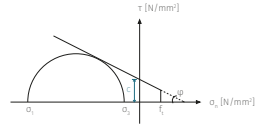
Pushover analysis	Time history analysis
<ul style="list-style-type: none"> <li>+ Simplicity of the analysis, spread use</li> <li>+ Faster, easier to compare</li> <li>+ Well established procedure</li> <li>+ Considered in guidelines and codes (EC8, FEMA, etc.)</li> <li>+ Prediction of the structural capacity under seismic load</li> </ul>	<ul style="list-style-type: none"> <li>+ Accurate structural assessment</li> <li>+ Correlations between modes are accounted for</li> <li>+ “Realistic” prediction of the development of the structural response (damage, displacements, cracks, etc.) in time</li> </ul>
<ul style="list-style-type: none"> <li>- One mode shape is studied at a time</li> <li>- For complex, non-symmetric, or low structures the dominant mode might not be clear. Different mode shapes in different directions need to be studied.</li> <li>- The dominant mode can change due to damage</li> </ul>	<ul style="list-style-type: none"> <li>- Very complex analysis</li> <li>- High computational cost</li> <li>- Limited number of signals can be studied</li> </ul>

Note. Obtained from DIANA (n.d.)

## 4.8 CONCLUSIONS OF CHAPTER 4

This chapter has discussed the possibilities of applying material models and element models to represent the masonry structure, and the force model to represent earthquake loads. The result is a discretisation of the structure in DIANA. The numerical model is created on a macro-scale level, which will simulate the global behaviour of the masonry. Table 4.6 gives an overview of the element models, material models, and material properties that have been assigned to the different elements of the structure. The most important assumptions that have been made for the discretisation of the structure concerns the band-to-column connection, which is modelled as a hinge. The disadvantage of this approach is that the effect of the strength and ductility of the connection is not included in the numerical results. However, the connections of the timber frame may not be governing and should be redesigned if loaded beyond their capacity.

**Table 4.6:** Overview modelling choices

Structural element	Element model	Material model	Material properties
Masonry walls	Plane stress elements 	Total strain based crack model 	$1800 \leq E \leq 3300$ $2000 \leq \rho \leq 3000$ $0.01 \leq \nu \leq 0.25$ $0.01 \leq f_t \leq 0.10$ $0.0016 \leq G_{ft} \leq 0.01$ $1.5 \leq f_c \leq 5$ $1.5 f_c \leq G_{fc} \leq 5$
Timber bands and columns	Class-III beam elements 	Linear elastic isotropic 	$E = 11,500 \text{ N/mm}^2$ $\rho = 450 \text{ kg/m}^3$ $\nu = 0.30$
Band-to-masonry connection	Structural line interface elements 	Coulomb friction 	$K_n = 10^5 \cdot E_{\text{masonry}}/h$ $K_s = 10^5 \cdot G_{\text{masonry}}/h$ $c = 2f_t \cdot \tan(\varphi)$ $40^\circ \leq \varphi \leq 70^\circ$ $10^\circ \leq \psi \leq 40^\circ$
Band-to-column connection	Hinge	-	-



# CHAPTER 5

---

## Parameter study of the numerical model

*Material tests on this type of masonry and its confinement are not performed for this research, therefore the exact values of the material properties are unknown. In Chapter 4, the material properties are defined within a certain range that is conform values found in literature. By means of a parameter study performed in this chapter, the effect of the uncertainty of the material properties on the behaviour of the structure will be investigated. Subsequently, each material property will be assigned a chosen value for the numerical modelling that will follow in Chapter 6 to answer the research question.*

### 5.1 GENERAL

The effect of the material properties on the response of the masonry wall will be investigated by means of performing a pushover analysis in DIANA. The setup of the numerical model is shown in Figure 5.1. The total strain based crack model depends on several material properties that describe the linear and non-linear behaviour of the material. The non-linear behaviour is described by tensile and compression parameters, and the linear behaviour by the Young's modulus, the mass density, and Poisson's ratio. Each of these parameters have an lower and upper bound value as determined by means of a literature study in Chapter 4. The numerical models will be assigned these values after which their response to the pushover load will be observed. Additional to the lower and upper bound values, intermediate values of the parameters will be assigned to the models as well. An overview of the masonry parameters and their varying values is given in Table 5.1.

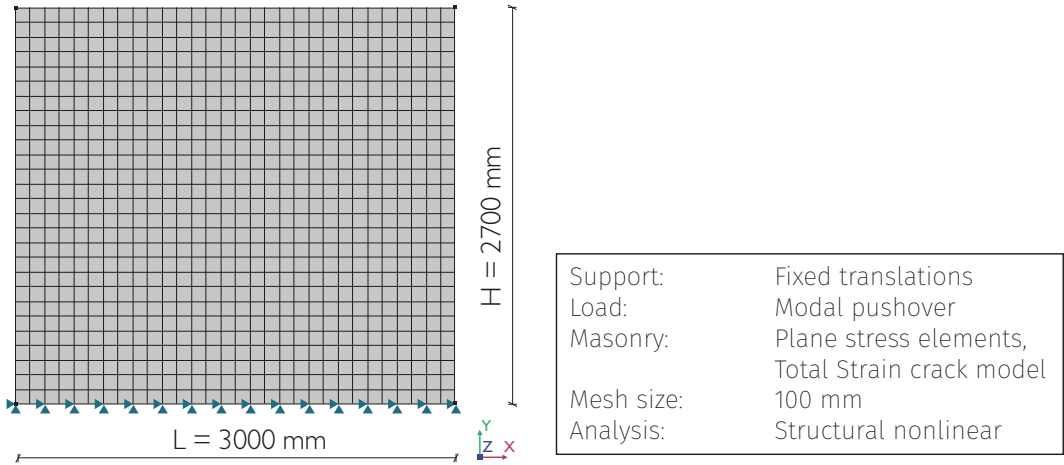


Figure 5.1: Overview of the numerical model of the masonry wall.

**Table 5.1:** Varying values for the masonry material properties

Material property	Lower bound value	Intermediate value	Upper bound value	Unit
Young's modulus ( $E$ )	1800	2000	3300	$N/mm^2$
Mass density ( $\rho$ )	2000	2400	3000	$kg/m^3$
Poisson's ratio ( $\nu$ )	0.10	0.20	0.25	-
Tensile strength ( $f_t$ )	0.01	0.03	0.10	$N/mm^2$
Fracture energy in tension ( $G_{f,t}$ )	0.0016	0.003	0.010	$N/mm$
Compressive strength ( $f_c$ )	1.50	3.00	5.00	$N/mm^2$
Fracture energy in compression ( $G_{f,c}$ )	2.25	4.50	5.00	$N/mm$

## 5.2 TENSILE BEHAVIOUR

The masonry tensile properties belong to the non-linear input parameters of the numerical model, therefore influencing the behaviour of the structure beyond its elastic stage. The non-linear behaviour of a structure includes its ultimate strength, hardening and softening, and crack propagation of the cracks formed in the elastic stage. It is expected that the tensile properties will have an influence on these aspects.

The masonry tensile properties consists of two components: the tensile strength and the fracture energy in tension. The fracture energy is the energy required to open a certain area within the cracking surface, and is related to the tensile strength by the relation proposed by Schreppers et al. (2017):

$$G_{ft} = 0.025(2f_t)^{0.7}$$

The tensile strength of masonry depends on the strength of the stones and on the strength of the mortar. The tensile strength of Nepali masonry is uncertain since the stone type and size is unknown, as well as the thickness of the mud mortar and whether or not it is strengthened by for example lime. From the literature study it follows that the tensile strength of rubble stone masonry has quite a range, varying from 0.01 N/mm<sup>2</sup> to 0.10 N/mm<sup>2</sup> (Milosevic et al., 2013).

### 5.2.1 Numerical results of varying parameters in tension

Figure 5.2 shows the force-displacement diagrams and the crack width contours obtained by the numerical calculations for different values of the tensile strength and related fracture energy. When applying the lower bound value of 0.01 N/mm<sup>2</sup> to the numerical model, the masonry wall shows diagonal tensile failure (shown by the crack width contours in Figure 5.2a). The failure mechanism of the wall experiences a shift from brittle to ductile when the tensile strength of the masonry reaches a value of 0.03 N/mm<sup>2</sup>. This is observed in the force-displacement diagram by the increase of deformation capacity, as well as by the location of the cracks, which are now located at the bottom of the wall. Figures 5.2b and 5.2c show the effect of increasing the tensile strength to the upper bound value of 0.10 N/mm<sup>2</sup>: the cracks only develop along the foundation of the wall, so the wall experiences an uplift while the wall itself stays intact.

The force-displacement diagram shows an ultimate resistance of the lower bound model of 38.9 kN. The ultimate strength of the wall with  $f_t = 0.03$  N/mm<sup>2</sup> is over 70 kN, which is an increase of 180% compared to the lower bound model. Increasing the tensile strength and related fracture energy further, from 0.03 N/mm<sup>2</sup> to the upper bound value of 0.10 N/mm<sup>2</sup>, does not have a noticeable influence on the ultimate strength of the wall nor on the deformation capacity.

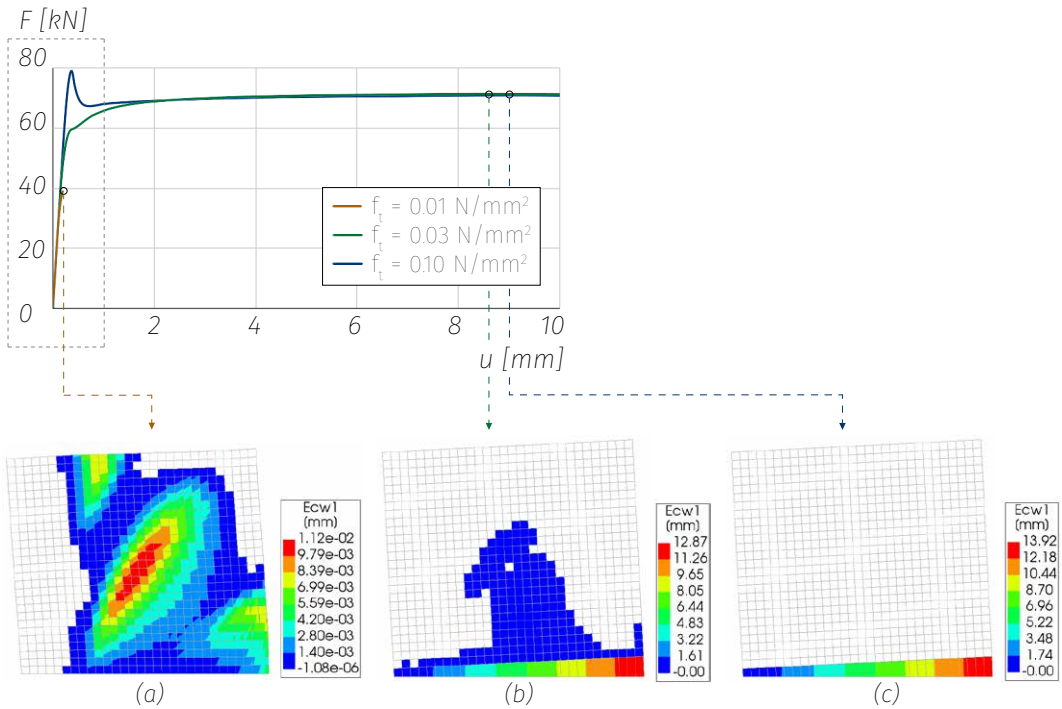


Figure 5.2: Force-displacement diagram for varying values of  $f_t$  with crack width contours at peak load for a) model with  $f_t = 0.01 \text{ N/mm}^2$ ; b) model with  $f_t = 0.03 \text{ N/mm}^2$ ; c) model with  $f_t = 0.10 \text{ N/mm}^2$ ;

Figure 5.3 shows the first part of the force-displacement diagram (indicated in Figure 5.2 by the dashed box) to have a closer look at the elastic stage of the models and their transition to the plastic stage. The crack width contours show the first crack developments of the three models, and at which point during loading they take place. For the model with the highest tensile strength, the first cracks occur at a higher load compared to the lower valued models, so the higher the tensile strength the larger the elastic stage. The first cracks of the lower bound model propagate over the diagonal of the wall, indicating its susceptibility to diagonal tensile failure, whereas the first cracks of the other two models are located only in the corner of the wall.

The force-displacement diagram shows a difference in the transition from the elastic stage to the plastic stage for the two ductile models ( $f_t = 0.03 \text{ N/mm}^2$  and  $f_t = 0.10 \text{ N/mm}^2$ ). This difference is caused by the increase of the fracture energy. The upper bound model can resist higher loads before cracking occurs, and will therefore show elastic behaviour where the other models already show non-linear behaviour. When cracks do occur in the upper bound model, its resistance drops due to the rapid propagation of the cracks that is caused by the high load.



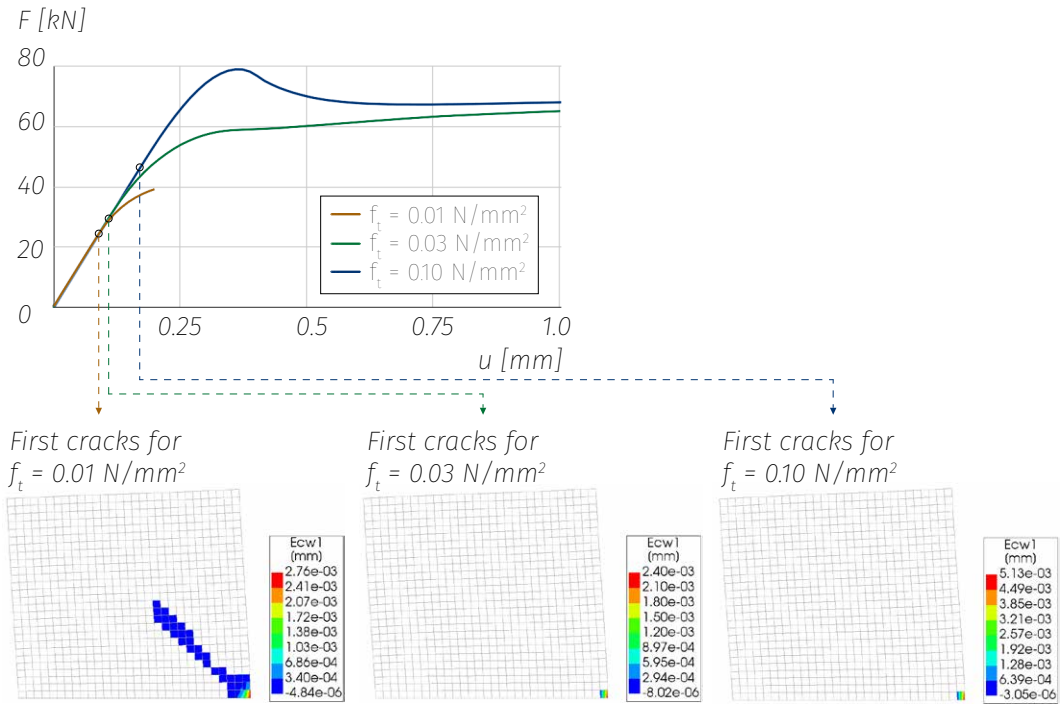


Figure 5.3: Force-displacement diagram for varying values of  $f_t$  with crack width contours of the first cracks at the end of the elastic stage.

## 5.2.2 Comparison with the analytical results

The calculations of Chapter 3 has estimated that the unconfined masonry wall would develop a diagonal tensile failure mechanism, with an ultimate strength of 39 kN. This is conform the numerical calculations for the lower bound value of the tensile strength:  $f_t = 0.01$  N/mm<sup>2</sup>,  $G_{ft} = 0.0016$  N/mm. When increasing the tensile strength of the numerical model, the results diverge from those obtained by the analytical calculations.

Increasing the tensile strength of the numerical model to 0.03 N/mm<sup>2</sup> results in a rocking failure mode with an ultimate strength of over 70 kN, which is, with a difference of 31 kN, almost double the strength of the lower bound model. The analytical calculations of Chapter 3 use different formulas for different failure modes, and the resistance against rocking is based only on the masonry's compressive strength. These calculations have estimated the resistance of the wall to rocking to be indeed higher than the resistance to diagonal tensile failure. However, unlike the numerical results, the difference in ultimate strength between diagonal tensile failure and rocking is only 10 kN.

### 5.2.3 Chosen values tensile behaviour

From this study it followed that the tensile strength of the masonry is of great importance: for the lowest value of  $0.01 \text{ N/mm}^2$ , the structure experiences brittle failure, whereas increasing the tensile strength to the slightly higher value of  $0.03 \text{ N/mm}^2$  (note that this is still considered a low-strength value for masonry according to literature) the structure behaves ductile. Moreover, for a tensile strength of  $0.03 \text{ N/mm}^2$ , the ultimate strength of the wall is almost twice as high compared to a tensile strength of  $0.01 \text{ N/mm}^2$ . Since these values are close to each other and are both realistic values for (Nepali) rubble stone masonry (Milosevic et al., 2013), yet produce very different results, they are both considered in the continuation of this research. The value for the fracture energy in tension is related to the value of the tensile strength as proposed by Schreppers et al. (2017). For the continuation of the parameter study a tensile strength of  $0.03 \text{ N/mm}^2$  will be used, for it provides ductile behaviour which allows for investigating the effect of the other parameters.

## 5.3 COMPRESSIVE BEHAVIOUR

The compressive behaviour of the masonry is described by two parameters: the compressive strength ( $f_c$ ) and the fracture energy in compression ( $G_{fc}$ ). The compressive behaviour is of importance for the resistance of the structure against crushing, which determines the rocking failure mode. The rocking failure mode is considered to be ductile, since it will provide the structure with sufficient deformation capacity before failure: after the structure has reached its peak load, the force in the structure will not immediately drop to zero, but will gradually decrease. This post-peak behaviour can be explained by the fact that the crushed part of the masonry wall allows for redistribution of the stresses and can therefore still resist the compressive force.

Since the compressive behaviour has an influence on the wall's resistance against rocking, the tensile strength needs to be high enough not to result in diagonal tensile failure. Therefore, the influence of the compression parameters is investigated for the numerical model with  $f_t = 0.03 \text{ N/mm}^2$ . An accurate response to the loading will show the gradual decrease of the post-peak force in the force-displacement diagram. The parameters for the compressive behaviour will be adjusted accordingly.

### 5.3.1 Numerical results of varying parameters in compression

The compressive strength of rubble stone masonry is estimated in Chapter 4 to be in between  $1.50$  and  $5.00 \text{ N/mm}^2$  (Lekshmi, 2016; Giaretton et al., 2015). From the study of Pina-Henriques et al. (2005), the fracture energy in compression is estimated to be maximum  $5.00 \text{ N/mm}$ . When applying this value of the fracture

energy to the model, the force-displacement diagram does not show a decrease in force after reaching its peak, shown in Figure 5.4. This behaviour does occur for values of the fracture energy below 0.1 N/mm in combination with lower values of the compressive strength, shown in Figure 5.5. A fracture energy of 0.1 N/mm is much lower than what is suggested by literature to be common for rubble stone masonry.

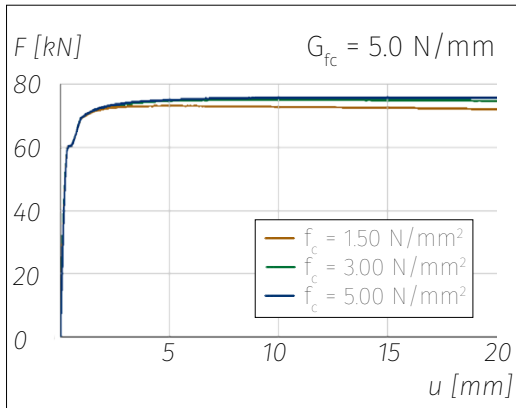


Figure 5.4: Force-displacement diagram for  $G_{fc} = 5.0 \text{ N/mm}$

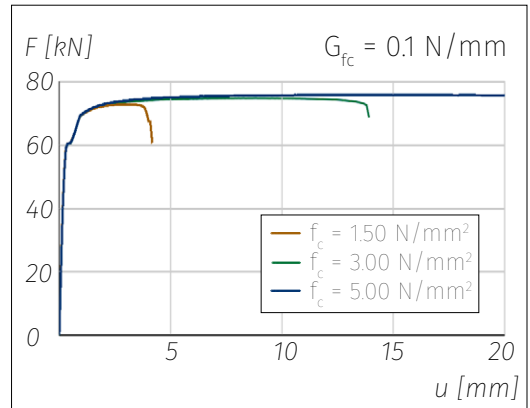


Figure 5.5: Force-displacement diagram for  $G_{fc} = 0.1 \text{ N/mm}$

The magnitude of the compressive strength has some influence on the ultimate strength of the in-plane wall, as can be seen in both Figure 5.4 and Figure 5.5, where the ultimate strength increases by 4% going from the lower bound to the upper bound value of the compressive strength. A greater difference between the upper and lower bound values of the compressive strength concerns the deformation capacity of the wall, as can be seen in Figure 5.5. When the masonry compressive strength doubles from 1.50 to 3.00 N/mm<sup>2</sup>, the ductility of the wall triples.

### 5.3.2 Chosen values compressive behaviour

For further modelling, it is chosen to assign a compressive strength of 3.0 N/mm<sup>2</sup>, and a fracture energy of 0.1 N/mm to the masonry. Judging by the literature study, this value for the fracture energy is very low, but judging by the force-displacement curve this value gives an appropriate post-peak behaviour. When plotting the compressive stress against the strain by means of the predefined parabolic curve as discussed in Chapter 4, it can be seen that this low value for the fracture energy leads

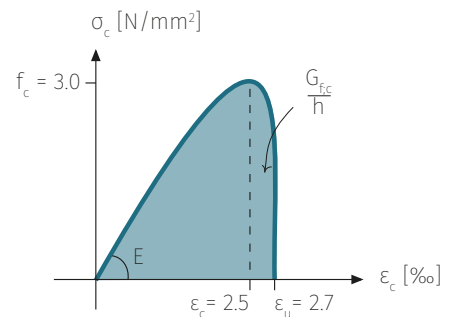


Figure 5.6: Stress-strain curve in compression for  $f_c = 3.0 \text{ N/mm}^2$  and  $G_{fc} = 0.1 \text{ N/mm}$ .

to a steep softening part of the curve (Figure 5.6). This means that the masonry will experience crushing quickly after reaching its compressive strength. This deformed parabolic curve suggests that the compressive strength and fracture energy are indeed not proportionate to each other. For the continuation of this research it is therefore of importance to realise that the deformation capacity of the structure can be underestimated when the governing failure mechanism is determined by crushing.

## 5.4 YOUNG'S MODULUS

The Young's modulus measures the tensile stiffness of the masonry, which is described by Hooke's law in the elastic stage of the stress-strain curve. The larger the Young's modulus, the more stress is needed to reach a certain deformation of the material.

### 5.4.1 Numerical results of varying Young's modulus

From literature the value of the Young's modulus is estimated between 1800 and 3300 N/mm<sup>2</sup>. Additional to these lower and upper bound values, an intermediate value of 2000 N/mm<sup>2</sup> is assigned to the Young's modulus of the numerical model. Figure 5.7 shows the force-displacement curves of the three models as a result of the pushover analysis. The stresses at failure show that all three models experience toe crushing due to the rocking mechanism. The upper bound model, with  $E = 3300$  N/mm<sup>2</sup>, reaches its maximum compressive stresses in the toe at a smaller global displacement compared to the models with a lower modulus of elasticity. When zooming in on the first part of the force-displacement diagram, shown in Figure 5.8, it can be seen that the higher initial stiffness of the wall leads to a higher yield strength, but also higher compressive stresses in the toe of the wall.

From these numerical results a possible conclusion on the effect of the Young's modulus could be that the higher this value, the stiffer the model, the sooner the wall reaches its rocking limit due to toe crushing. Therefore, the value of the Young's modulus has an effect on the deformation capacity of the wall when the governing failure mechanism is determined by crushing.

### 5.4.2 Chosen value Young's modulus

The magnitude of the Young's modulus has an influence on both the linear and non-linear behaviour of the masonry wall, of which the non-linear behaviour is most interesting since the objective of this research concerns failure of the structure. The Young's modulus does not have an effect on the ultimate strength of the wall, but the larger the Young's modulus, the less deformation capacity

the wall has. This holds for both tensile and compressive failure mechanisms, since a higher Young's modulus results in reaching both the tensile strength and compressive strength at smaller displacements of the masonry compared to lower values of the Young's modulus. For the continuation of this research it is chosen to work with an intermediate value for the Young's modulus of 2000 N/mm<sup>2</sup>.

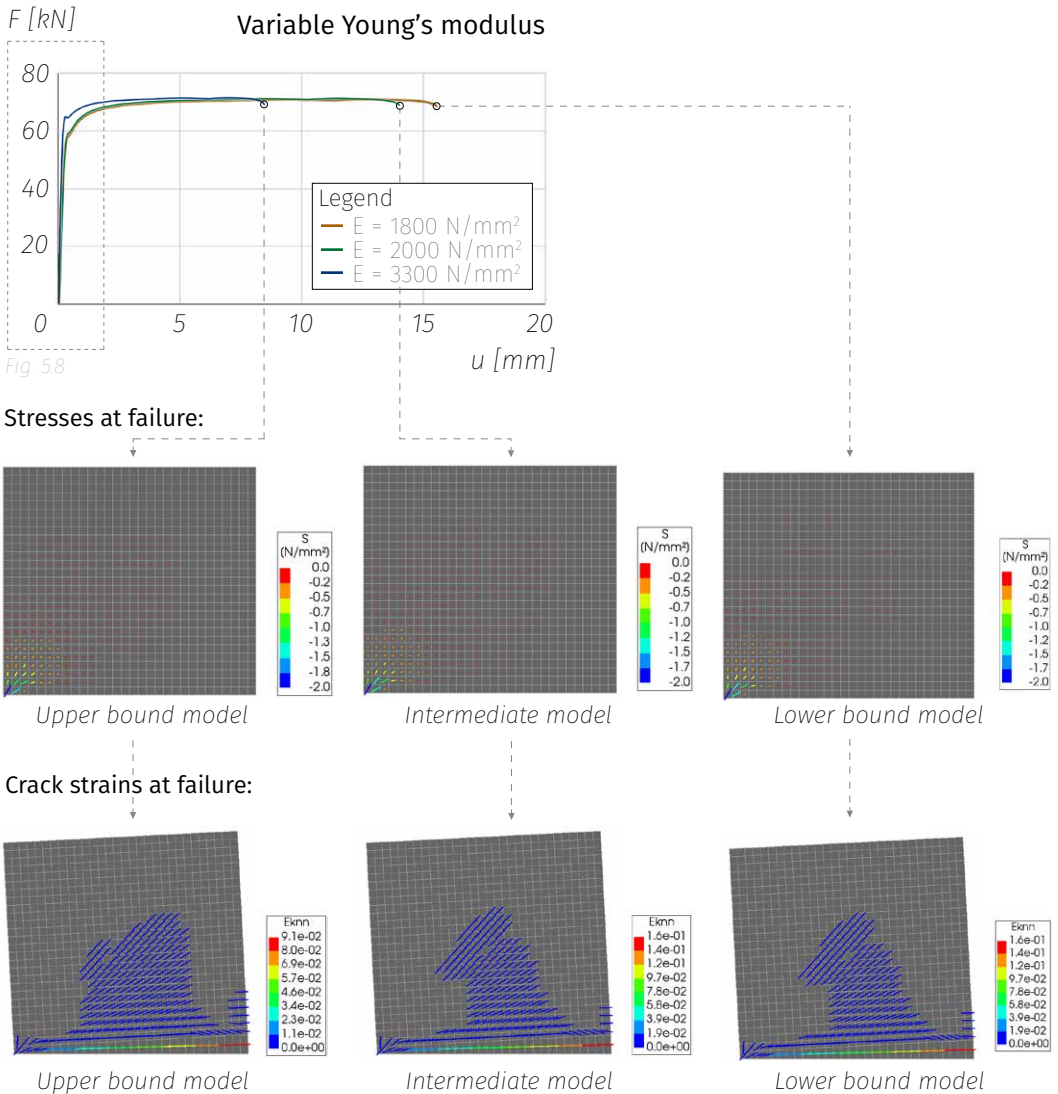


Figure 5.7: Force-displacement diagram for varying values of  $E$ , with stresses and crack strains for the three models at failure.

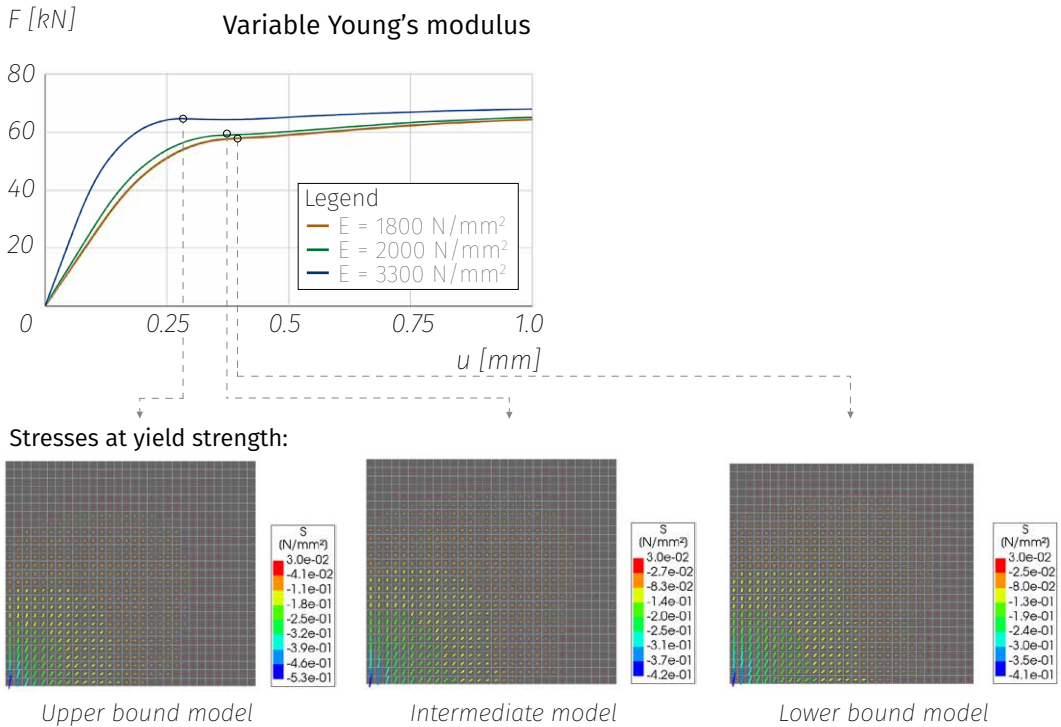


Figure 5.8: First part of the force-displacement diagram for varying values of  $E$ , with stresses for the three models at yield strength.

## 5.5 MASS DENSITY

The mass density of the masonry determines the self weight of the wall. From the analytical study of Chapter 3 it is known that the larger this downward force, the larger the wall's resistance to the pushover load due to force equilibrium.

### 5.5.1 Numerical results of varying the mass density

Figure 5.9 shows the force-displacement curves as a result of the pushover analysis for the three different values for the mass density. As can be seen from the curves, the ultimate resistance of the wall is proportionate to the magnitude of the mass density: if the mass density increases by 20% from  $2000 \text{ kg/m}^3$  to  $2400 \text{ kg/m}^3$ , the ultimate strength increases by 20% as well, going from 60 kN to 71 kN. And again, and increase of 25% from  $2400 \text{ kg/m}^3$  to  $3000 \text{ kg/m}^3$  results in a 25% strength increase, going from 71 kN to 87 kN. This is as expected since the wall develops a rocking mechanism, therefore its strength is determined by horizontal and vertical

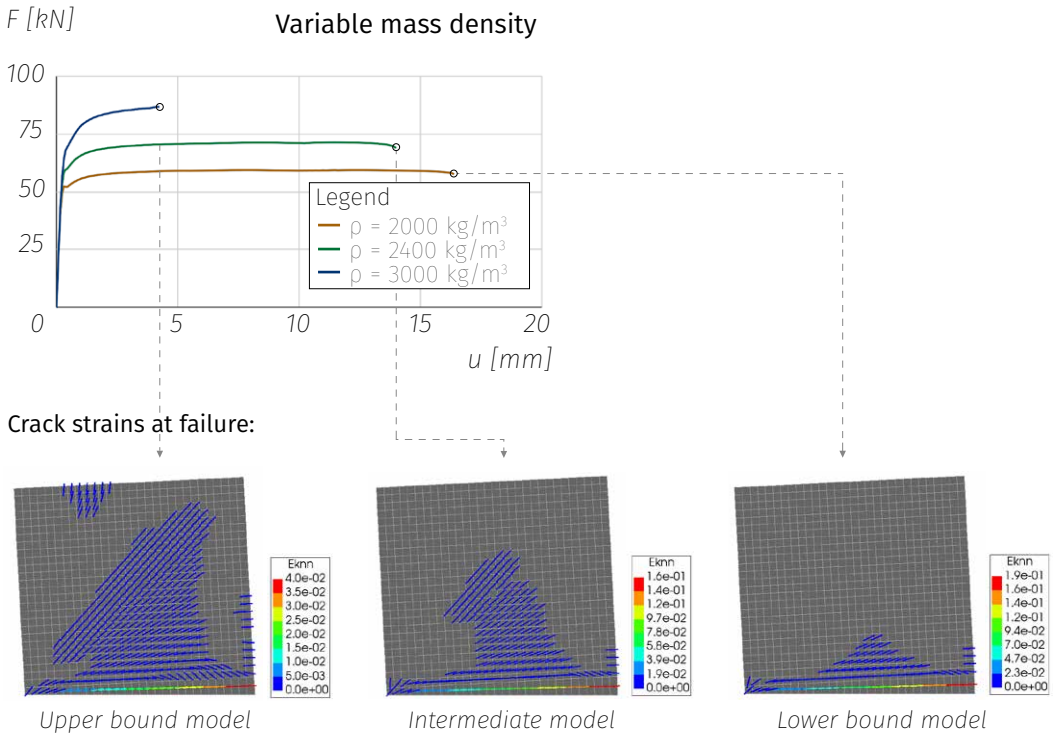


Figure 5.9: Force-displacement diagram for varying values of  $\rho$ , with crack strains for the three models at failure.

force equilibrium around the toe, so a larger vertical force results in a relatively larger horizontal force.

Additionally to the wall's ultimate strength, the mass density has an influence on the wall's displacement capacity: the larger the mass density, the less displacement capacity the wall has. Judging from the crack strains of the three models at failure (Figure 5.9), a possible explanation for this brittle behaviour could be due to the cracks developing over the diagonal of the wall for the heavier models: it seems that the top corner of the wall slides down due to its self weight. Since the cracks at the bottom of the wall due to rocking are much larger it is difficult to see these diagonal cracks, but if when observing the strain contours in only the X-direction it can be concluded that for the upper bound model a combination of toe crushing and diagonal sliding takes place at failure (shown in Figure 5.10).

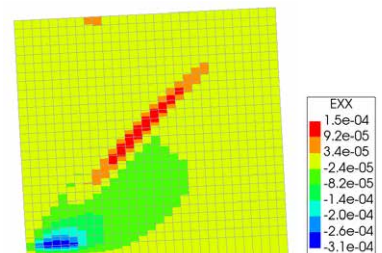


Figure 5.10: Strain contours in X-direction for the upper bound model at failure.



## 5.5.2 Chosen value mass density

The magnitude of the mass density has a significant influence on both the ultimate strength and on the displacement capacity of the wall. Where it would be beneficial for the strength of the wall to have a larger mass density, it takes away from its ductility since the tensile strength of the masonry is not sufficient to avoid sliding of the top part of the wall. The lower values of the mass density seem to be in better proportion to the tensile strength of the masonry. For the continuation of this research it is chosen to work with an intermediate value of  $2400 \text{ kg/m}^3$ , which is considered a plausible value for the mass density.

## 5.6 POISSON'S RATIO

When masonry is compressed in one direction, it will get thicker in the other direction, and vice versa, if it is stretched in one direction it tends to get thinner in the other direction. The ratio between the strain in the direction of the load and the strain perpendicular to the load is called Poisson's ratio. The larger Poisson's ratio, the more the material will deform in the direction perpendicular to the load. Since the Poisson effect describes deformations, it is expected that this parameter mostly influences the crack strains and crack widths.

### 5.6.1 Numerical results of varying Poisson's ratio

The value of Poisson's ratio for masonry is estimated to be in between 0.10 and 0.25. Figure 5.11 shows the force-displacement diagram due to the pushover load for the models with these lower and upper bound values as well as an intermediate value for Poisson's ratio. The curves show a slight difference in displacement capacity for the different models. Additional to the force-displacement curves, Figure 5.10 shows crack width contours for the models at failure. The higher Poisson's ratio, the more concentrated the cracks are developed. This is as expected since the material with a high Poisson's ratio can elastically deform more in the direction perpendicular to the load, whereas the material with a low Poisson's ratio will crack sooner in the direction perpendicular to the load.

### 5.6.2 Chosen value Poisson's ratio

Since Poisson's ratio does not have a severe influence on the behaviour of the structure nor on its failure, it is chosen to proceed the numerical study with the lower bound value of 0.10, to be on the safe side when it comes to overestimating this parameter.



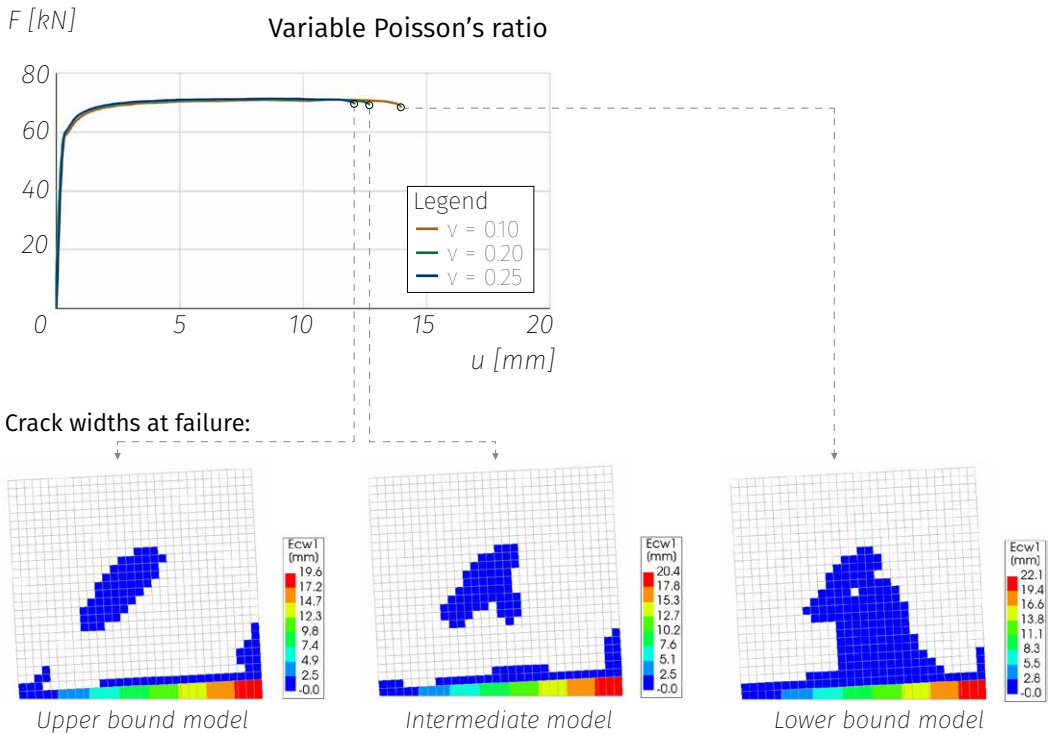


Figure 5.11: Force-displacement diagram for varying values of  $\nu$ , with crack width contours for the three models at failure.

## 5.7 CONCLUSIONS CHAPTER 5

The effect of the material properties on the response of the masonry wall has been investigated by means of performing a number of pushover analyses in DIANA. The material properties that have a significant influence on the behaviour and ultimately failure of the structure are the mass density and the tensile strength and fracture energy. Moreover, the compressive strength and fracture energy have a considerable influence on the deformation capacity of the wall. Table 5.1 shows the chosen values for the material properties, as well as their influence on the global behaviour of the structure. Only for the tensile strength and fracture energy two values have been chosen to proceed with, since these values are close to each other and are both realistic values for Nepali rubble stone masonry, yet produce very different results, they are both considered in this numerical study.

**Table 5.2:** Chosen values for the masonry material properties

Material property	Symbol	Value	Unit	Main influence
Young's modulus	$E$	2000	N/mm <sup>2</sup>	· Yield strength · Displacement capacity
Mass density	$\rho$	2400	kg/m <sup>3</sup>	· Ultimate strength · Displacement capacity
Poisson's ratio	$\nu$	0.10	-	· Crack distribution
Tensile strength	$f_t$	0.01 & 0.03	N/mm <sup>2</sup>	· Ultimate strength · Failure mechanism
Fracture energy in tension	$G_{ft}$	0.0016 & 0.003	N/mm	· Ultimate strength · Failure mechanism
Compressive strength	$f_c$	3.00	N/mm <sup>2</sup>	· Displacement capacity
Fracture energy in compression	$G_{fc}$	0.10	N/mm	· Displacement capacity

# CHAPTER 6

---

## Numerical study on the effect of the confinement

*The set-up of the numerical model of Chapter 4 and the parameter study of Chapter 5 have led to a numerical model that is considered sufficient reliable to estimate the influence of the timber confinement on the masonry structure. As in the analytical study of Chapter 3, a total of nine configurations of the shear wall will be studied, gradually increasing the amount of the timber elements. Their response to the pushover load will be studied, followed by a comparison with the results obtained in Chapter 3. This chapter will close with conclusions.*

### 6.1 GENERAL

The parameter study of Chapter 5 has been performed on the closed wall without confinement, so the structural response of this model has been obtained. From this study it followed that the tensile strength of the masonry is of great importance: for the lowest value of  $0.01 \text{ N/mm}^2$  the structure experiences brittle failure, whereas increasing the tensile strength to the slightly higher value of  $0.03 \text{ N/mm}^2$  (note that this is still considered a low-strength value for masonry as was determined in Chapter 4.3) the structure behaves ductile. Since these values are close to each other and are both realistic values for Nepali rubble stone masonry, yet produce very different results, they are both considered in this numerical study.

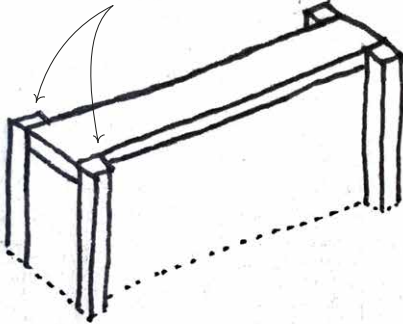
### 6.2 CLOSED WALLS

#### 6.2.1 Numerical model

Timber bands and columns are added to the numerical model that was used for Chapter 5. Since the numerical model is a two-dimensional model, the columns are placed in the same plane as the bands instead of in front and behind the

bands. Therefore, the geometry of the columns in the numerical model is 280x140 mm since one column in the numerical model represents two columns in reality, shown in Figure 6.1.

140x140 mm column on each side of the band



280x140 mm column on the head end of the band

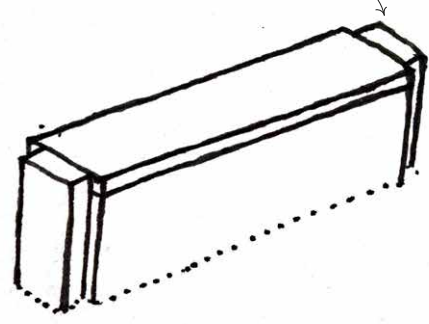


Figure 6.1: Impression of the position of the columns: two columns at each side of the band as is suggested in reality (left), one equivalent column on the head end of the band (right).

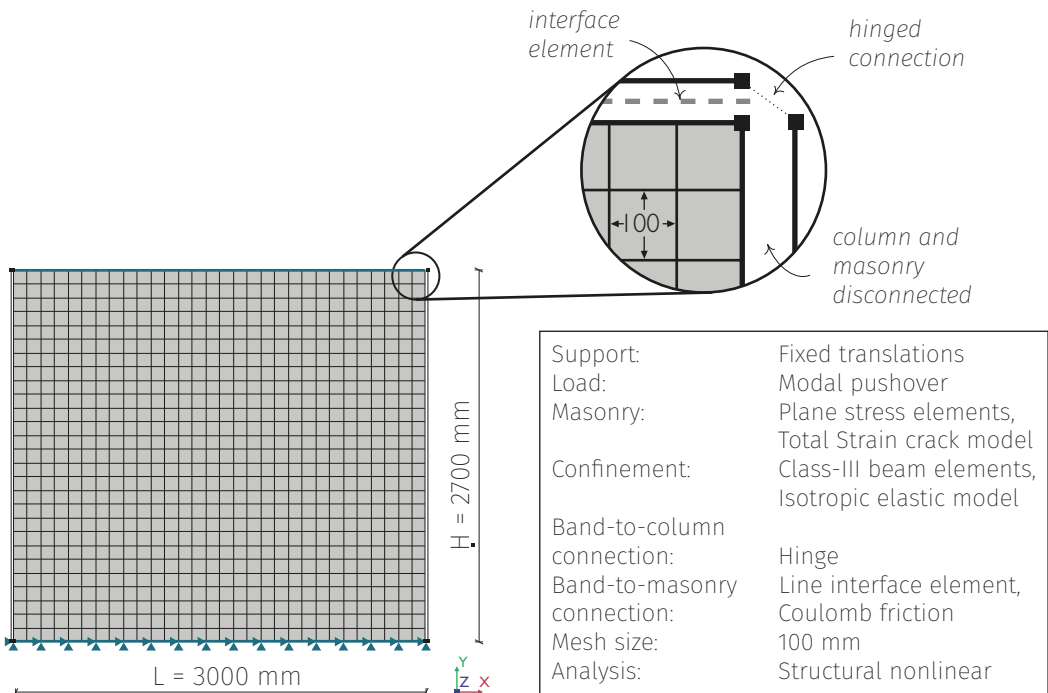


Figure 6.2: Overview of the numerical model of the masonry wall confined by a roof and floor band and two columns.

Figure 6.2 shows the numerical model of the masonry wall confined by columns and a roof and floor band. As explained in Chapter 4, the connection between the masonry and the timber band is described by Coulomb friction line interface elements. Since the geometry of the band is different on the top- and bottom-side, the properties of the interface elements are different as well on the top- and bottom-side. A complete overview of the properties of the numerical model, including the analysis settings, is given in Appendix C.

Figure 6.3 shows the numerical models of the masonry wall confinement by two columns and three bands (left) and four bands (right). The third and fourth bands are placed at the location where the top and bottom of a window opening would be, and are named the lintel band and sill band respectively. The lintel band is connected to the column at 1800 mm height and the sill band at 900 mm height. In order to place a hinged connection in the numerical model, the column needed to be divided into different parts to create nodes at this location. The column parts are connected as if they are not separate parts, by placing tyings at the intermediate nodes.

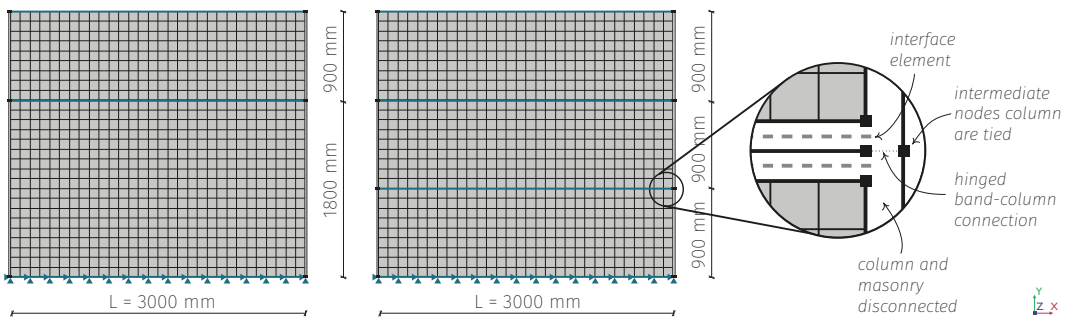


Figure 6.3: Overview of the numerical model of the masonry wall confined by two columns, and a roof, floor and lintel band (left) and a roof, floor, lintel and sill band (right).

The walls are subjected to a modal pushover load and their responses are compared to study the effect of the amount of bands making up the wall's confinement.

### 6.2.2 Results for $f_t = 0.01 \text{ N/mm}^2$

Figure 6.4 shows the force-displacement diagram as a result of the pushover load on the confined walls compared to the unconfined wall, with a masonry tensile strength of  $f_t = 0.01 \text{ N/mm}^2$ . Judging by these curves, incorporating confinement to the wall is beneficial for both the ultimate strength as the ductility of the wall. If the confinement exists of only a roof and floor band, the ultimate strength of the wall increases by 10 kN compared to the unconfined wall. Adding a third band increases the wall's displacement capacity as well as its ultimate strength. Adding a fourth band to the confinement results in an ultimate strength similar to the three-band-

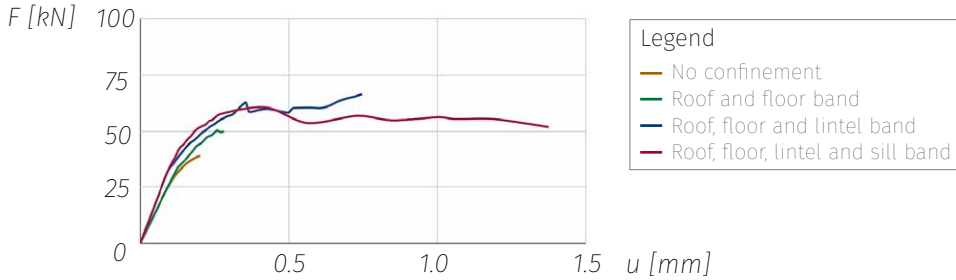


Figure 6.4: Force-displacement diagram as a response to the pushover load on the unconfined wall and confined walls, for  $f_{t,masonry} = 0.01 \text{ N/mm}^2$ .

model, yet the ductility is increased considerably. The force-displacement curve of the three-band-model shows some fluctuations in the hardening phase. At these points, the numerical model did converge, but in this phase the part of the wall above the lintel band started to detach and slide from the bottom part of the wall, which might explain the irregularity of the curve. This detachment is shown in Figure 6.5 by the relative displacements of the line interface elements at the first drop in the curve ( $u = 0.36 \text{ mm}$ ) and at failure ( $u = 0.75 \text{ mm}$ ), in the left and right figure respectively.

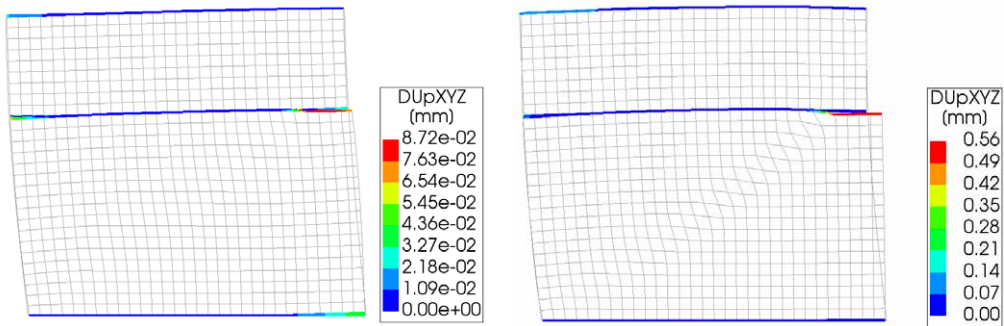


Figure 6.5: Relative displacement of the interface elements of the three band model, during the hardening phase at  $u = 0.36 \text{ mm}$  (left) and  $u = 0.75 \text{ mm}$  (right).

Figure 6.6 shows the crack strains of the models at failure. Due to the pushover load, all models develop cracks of the diagonal of the wall. Note that the crack strains over the diagonal of the two-band-confined wall are of similar size of the unconfined wall, yet the colour scales are different because the confined model develops severe strains at the top of the wall at the location where the roof band detaches from the masonry. The crack strains of the three-band-model and four-band-model are even greater since the confinement leads to an increased ultimate strength and increased global displacement of the wall at failure, and therefore larger stresses and strains locally. Due to sliding of the top part of the three-band-

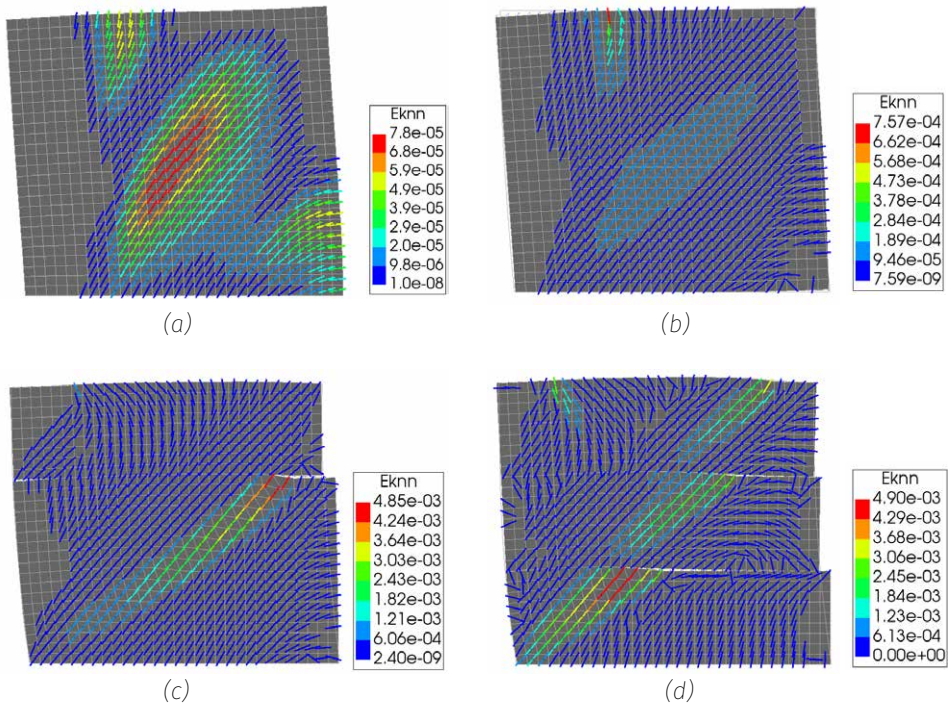


Figure 6.6: Crack strains at failure of (a) unconfined wall; (b) wall confined by roof and floor band; (c) wall confined by roof, floor and lintel band; (d) wall confined by roof, floor, lintel and sill band.

model, diagonal cracks in the masonry mostly develop in the bottom part of the wall. For the four-band-model, however, diagonal tensile crack patterns develop over all three parts of the wall, even though these wall parts undergo sliding as well. It seems that placement of the bands over even distances of the wall, as is the case for the four-band-model, results in a better interaction between the wall parts, which could explain a better spread crack pattern compared to the three-band-model.

Apart from the strength, ductility and crack development of the masonry, it is important to check the response of the timber frame. As was determined in Chapter 3, the timber connection is able to carry a force of 7.2 kN in the columns and of 8.4 kN in the bands, which corresponds to a tensile stress limit of 0.37 N/mm<sup>2</sup> and 0.43 N/mm<sup>2</sup> respectively. If larger loads arise in the band-to-column connection, the connection would fail due to a combination of reaching the timber embedded strength and plasticity of the fastener. For the connections at the top of the frame, connecting the columns to the roof band, these stress limits apply to both the column and the band. For the other connections, the column is a continuous element which transfers the normal stresses directly to the foundation, shown in Figure 6.7, so for these connections the stress limit applies to the band only.



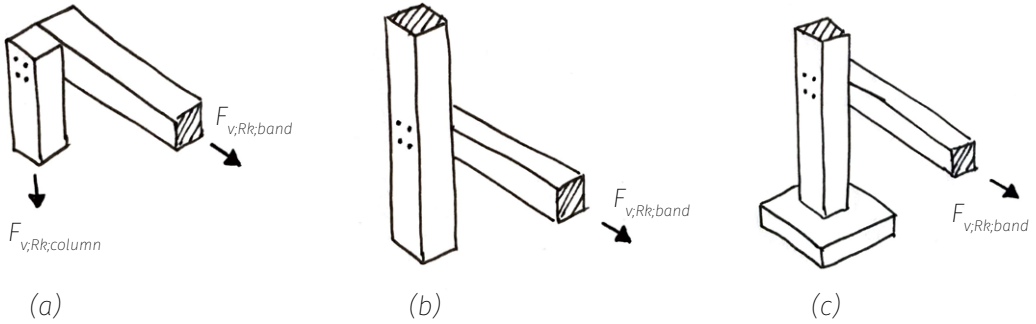


Figure 6.7: Load transfer of the joints in the timber frame, with (a) column-to-roof band connection; (b) column-to-lintel band connection; (c) column-to-floor band connection.

Figure 6.8 shows the stresses in the timber elements at failure for the models confined by two, three and four bands. In the model confined by two bands (roof and floor band) the stresses in the timber elements do not exceed the transfer limit. This holds as well for the model confined by three bands, however the stresses in the roof band are close to reaching their limit of  $0.43 \text{ N/mm}^2$ . In the model confined by four bands, the top right joint which connects the column to the roof band has exceeded its transfer capacity. At the point of global failure of the structure the stresses in the column and band at the joint are  $1.46 \text{ N/mm}^2$ . For this joint, the stress limit in the column was reached at  $u = 0.74 \text{ mm}$ , and the stress limit in the band was reached at  $u = 1.19 \text{ mm}$ . This means that if the design of the timber joint is not addressed, it will be governing for the global failure of the structure: the timber confinement is expected to fail and the ultimate strength and ductility as presented by the force-displacement curves will not be reached. During the continuation of this numerical study, it will be observed that the stress limit in the timber elements is reached in other models as well, so later on in this chapter it will be explained how the timber joints should be designed in order for them withstand the pushover loads.

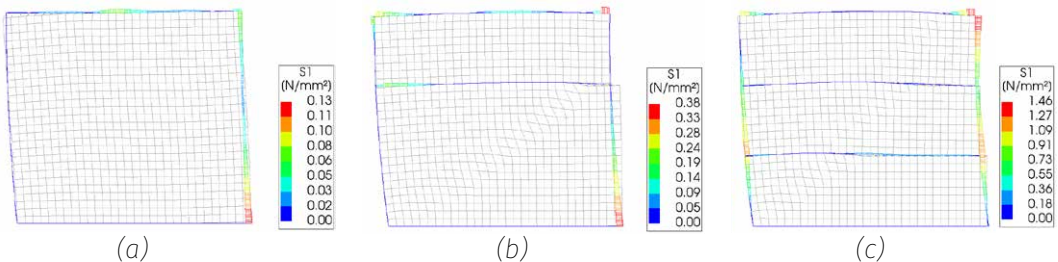


Figure 6.8: Principal stresses in the timber elements at global failure of the structure with  $f_{t,masonry} = 0.01 \text{ N/mm}^2$ , for the models confined by (a) roof and floor band; (b) roof, floor and lintel band; (c) roof, floor, lintel and sill band.



### 6.2.3 Results for $f_t = 0.03 \text{ N/mm}^2$

Figure 6.9 shows the force-displacement diagram as a result of the pushover load on the confined walls compared to the unconfined wall, with a masonry tensile strength of  $f_t = 0.03 \text{ N/mm}^2$ . Figure 6.10 shows the first part of the force-displacement diagram to study the response of the confined models more closely, indicated by the dashed box in Figure 6.9. For this higher value of tensile strength, the unconfined model behaves ductile due to the development of a rocking mechanism. Contrary to the unconfined wall, the models with confinement have little deformation capacity and experiences brittle failure shortly after the elastic capacity of the wall is reached, causing non-convergence of the model.

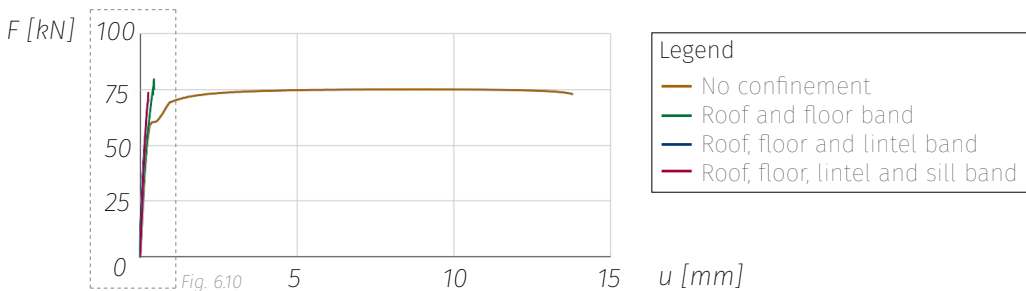


Figure 6.9: Force-displacement diagram as a response to the pushover load on the unconfined wall and confined walls, for  $f_{t,masonry} = 0.03 \text{ N/mm}^2$ .

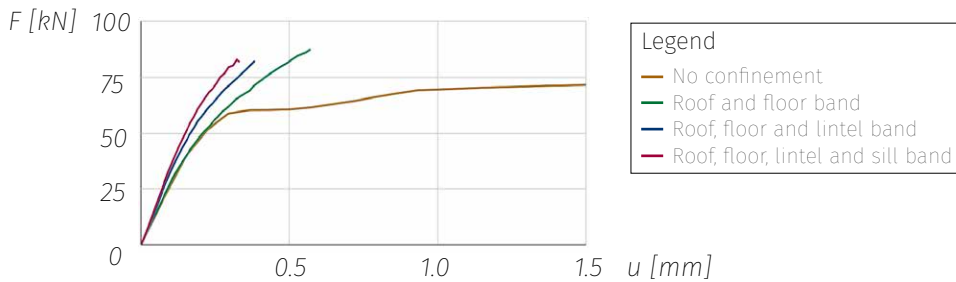


Figure 6.10: First part of the force-displacement diagram as a response to the pushover load on the unconfined wall and confined walls, for  $f_{t,masonry} = 0.03 \text{ N/mm}^2$ .

Due to the confinement, the rocking mechanism cannot fully develop. This might be counter-intuitive, because it might be expected that the confinement would lead to a higher ductility. P.B. Lourenço observes a similar phenomenon in one of his studies (Lourenço, 1996), and provides an explanation. The softening regime of the unconfined wall is governed by failure of the compressed toe of the wall. The confinement leads to an increased strength of the shear wall. This higher failure load causes higher stresses at the support of the wall, which make it more difficult for the stresses at the compressed toe to redistribute upon crushing.

Figure 6.11 shows the vertical stresses over the length of the wall at the support for the unconfined model compared to the two-band-confined model. This shows the discontinuous stress distribution of the confined model, which confirms that rocking cannot fully develop for this wall.

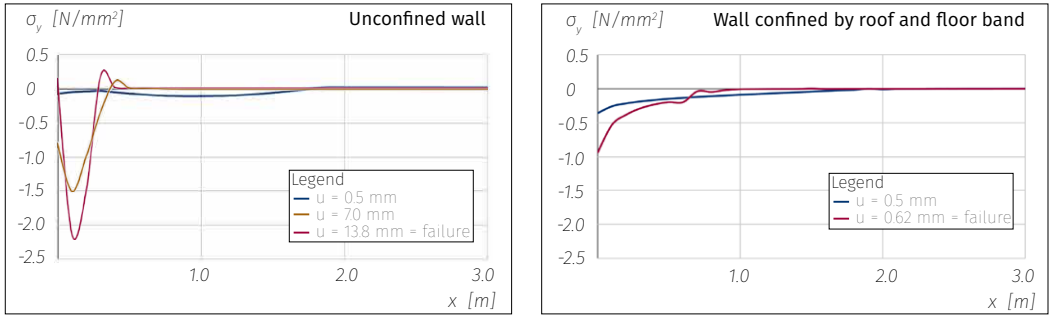


Figure 6.11: Vertical stresses over the length of the wall at the support, for different values of the horizontal displacement of the wall, with stress diagram of the unconfined wall (left) and of the wall confined by two bands (right).

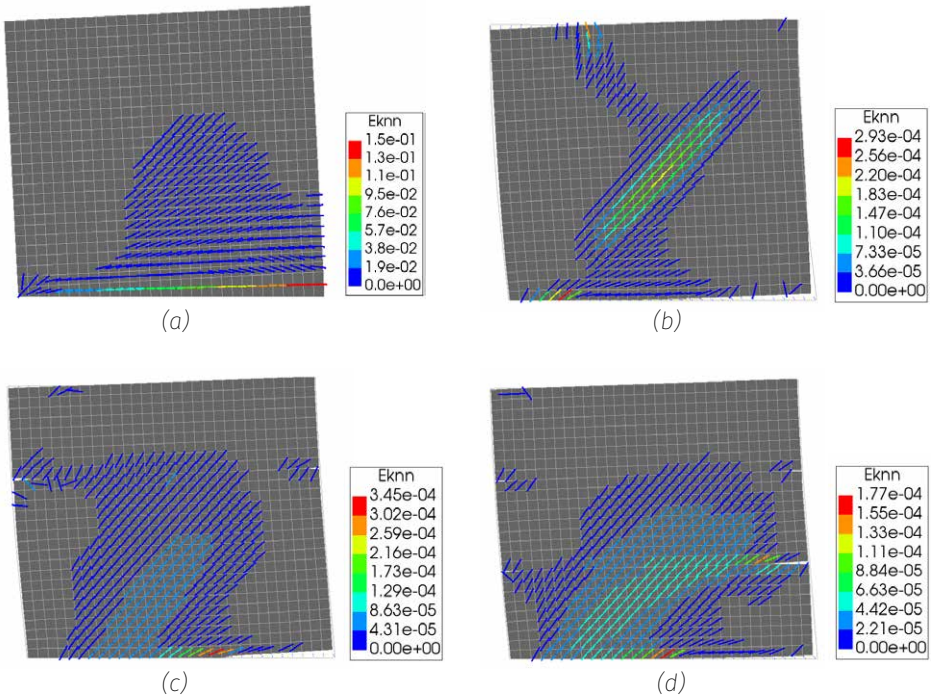


Figure 6.12: Crack strains at failure for  $f_{t, \text{masonry}} = 0.03 \text{ N/mm}^2$ , of (a) unconfined wall; (b) wall confined by roof and floor band; (c) wall confined by roof, floor and lintel band; (d) wall confined by roof, floor, lintel and sill band.

Figure 6.12 shows the crack strain contour plots of the four models at failure. The cracks of the confined models have developed over the diagonal of the wall indicating diagonal tensile failure, which corresponds to the brittle behaviour that is observed in the force-displacement diagram. Each of the confined models show a similar response to the pushover load concerning their ultimate strength and displacement capacity. However, the global stiffness of the wall increases when the amount of bands increases. A possible explanation of this increased global stiffness could be that by adding more bands, the height over which the diagonal cracks develop decreases, so failure occurs in a less slender wall. For the models with the lower tensile strength, this difference in global stiffness was less noticeable, because the cracks developed over the diagonal of each wall part, whereas for the higher tensile strength models the crack propagation stops at the bands.

Figure 6.13 shows the principal stresses in the timber elements for the models confined by the bands and columns. Contrary to the models with a lower masonry tensile strength, the internal forces and stresses remain in the lower part of the wall. Therefore, the largest stresses occur in the column loaded in tension at the location of the support. Since the behaviour and the capacity of the supports is not included in this study, it is concluded that the timber frame of all three the confined models can resist the pushover load.

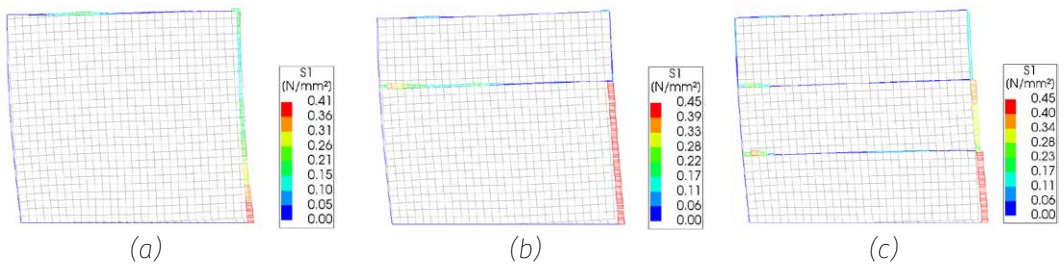


Figure 6.13: Principal stresses in the timber elements at global failure of the structure with  $f_{t, \text{masonry}} = 0.03 \text{ N/mm}^2$ , for the models confined by (a) roof and floor band; (b) roof, floor and lintel band; (c) roof, floor, lintel and sill band.

## 6.3 WALLS WITH WINDOW OPENING

### 6.3.1 Numerical model

Figure 6.14 shows a picture of a typical Nepali window: a timber frame with shutters. The frame is extended into the masonry to interlock the window, since no adhesives are used to keep the window in place. Figure 6.15 shows the numerical model of the unconfined wall with window opening. The window opening is placed in the middle of the wall. The window frame is represented by the numerical model by

means of beam elements. Due to the low tensile strength of the masonry it is necessary to place these beam elements to avoid the collapse of the wall part above the opening. The frictional interaction between the horizontal beams of the window frame and the masonry is described by Coulomb friction interface elements, with the same properties as the interface elements on the bottom side of the seismic bands. The vertical beams of the window frame are physically disconnected from the masonry because the friction between these elements is negligible.

Like the wall without window opening, this wall will be confined by columns at each side of the wall, and four seismic bands. Additionally to these bands and columns, two extra columns will eventually be added to the confinement at both sides of the window opening. Figure 6.16 shows the models that make up the numerical study on the confined wall with window opening.



Figure 6.14: Typical Nepali window: timber frame connected to the masonry by interlock (source: own photo).

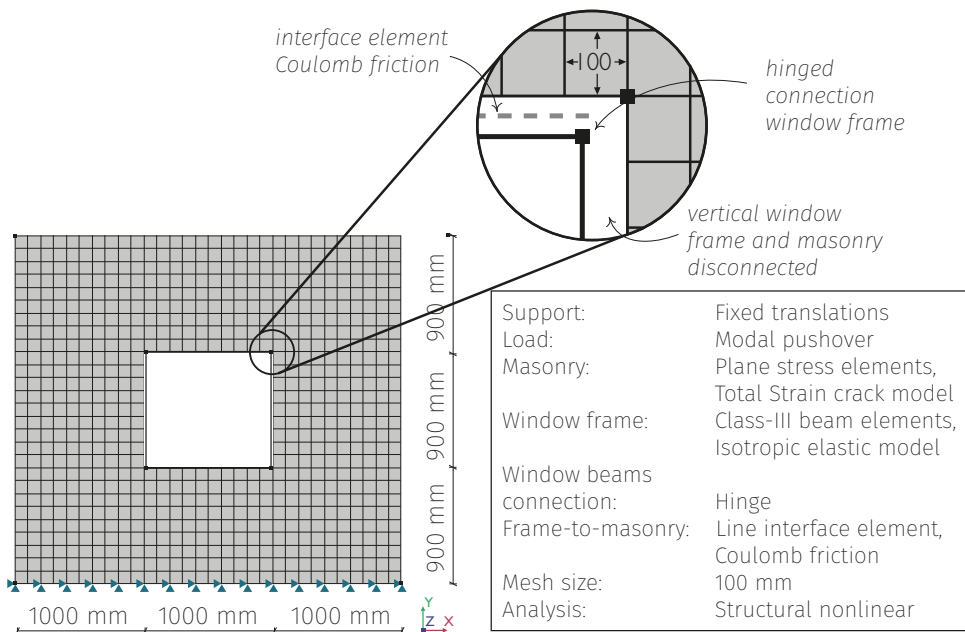


Figure 6.15: Overview of the numerical model of the unconfined masonry wall with window opening.

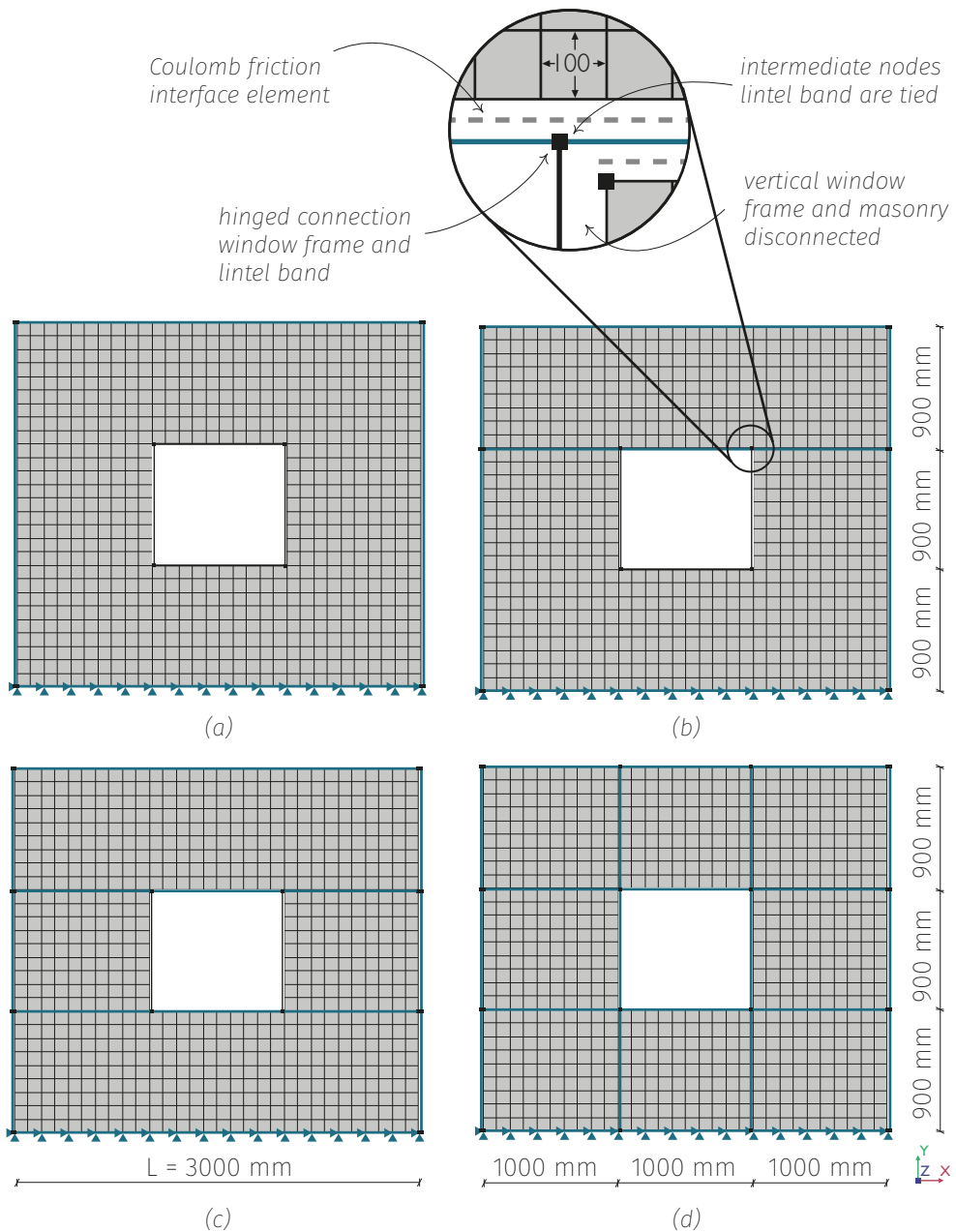


Figure 6.16: Overview of the numerical models of the masonry walls with window opening, confined by (a) two columns and roof and floor band; (b) two columns and roof, floor and lintel band; (c) two columns and roof, floor, lintel and sill band; (d) four columns and roof, floor, lintel and sill band.

### 6.3.2 Results for $f_t = 0.01 \text{ N/mm}^2$

Figure 6.17 shows the force-displacement diagram as a response to the modal pushover load for the models with a masonry tensile strength of  $f_t = 0.01 \text{ N/mm}^2$ , and the crack strains obtained by the numerical model at failure. From the force-displacement curves it is observed that the confinement has an effect on both the ultimate strength and the ductility of the wall, both positively and negatively.

The unconfined wall shows ductile behaviour, and judging by the crack strain contours, this ductility comes from the rocking mechanism that has developed in the pier on the right side of the window. When confining the wall by a roof and floor band, and two columns on each side of the wall, the response remains similar to the unconfined wall: the wall fails due to rocking of the right side pier. However, compared to the unconfined model the crack strains are smaller and the ultimate strength of the wall is larger.

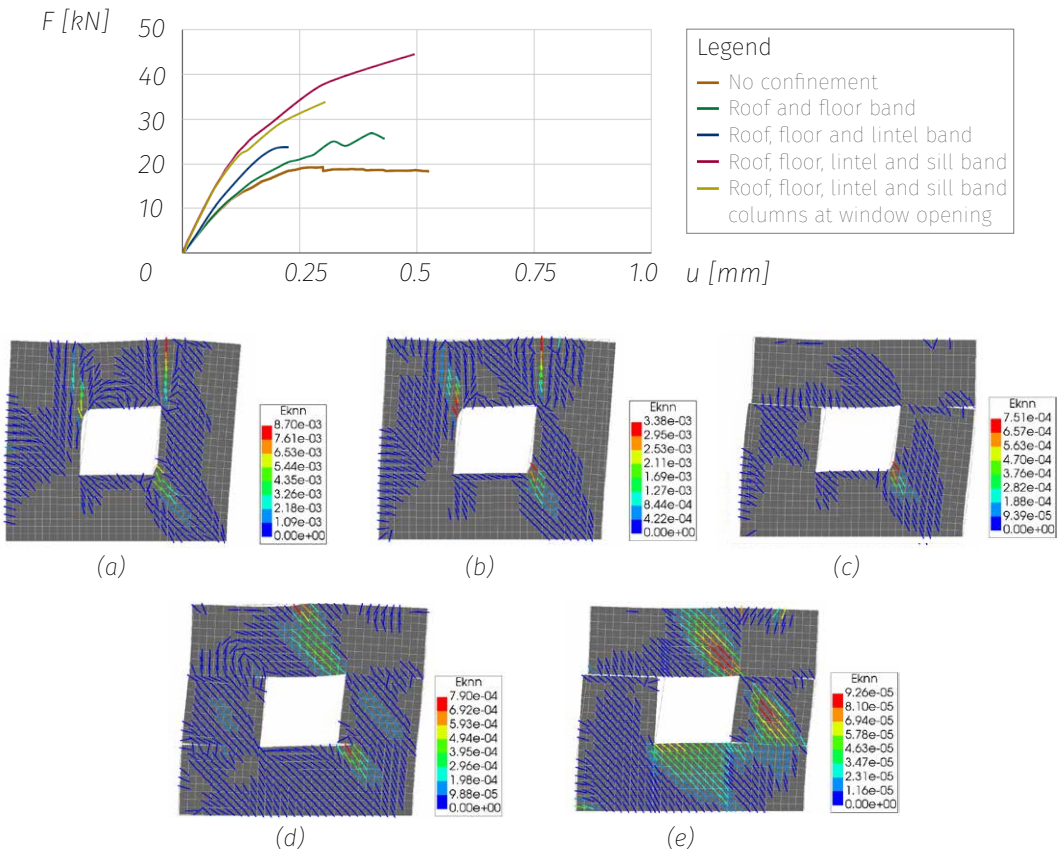


Figure 6.17: Force-displacement diagram of the walls with window opening, with crack strain contour plots at failure for (a) unconfined wall; (b) two-band-confined wall; (c) three-band-confined wall; (d) four-band-confined wall; (e) four-band-confined wall with two extra columns.



Adding also a lintel band to the model seems to have a negative effect on both the ultimate strength and displacement capacity of the wall, compared to the two-band-model. Judging by the contour plot, it seems that the lintel band causes sliding of the top part of the wall. This doesn't seem to be the case when adding the fourth band. With the addition of the sill band at the bottom of the window opening, the piers next to the window opening can develop a rocking mechanism, which can be observed by their detachment from the sill band. The horizontal displacement of the top part of the wall can now be followed by the piers, so their relative displacements are much smaller compared to the three-band-model. The model confined by four bands has approximately the same displacement capacity as the unconfined wall, but its ultimate strength is more than twice as large. Eventually, the model confined by four bands fails due to diagonal tensile failure of the top part of the wall, judging by the crack strain contours.

Adding two extra columns to the four-band-model increases the confinement effect, causing a similar effect that has been observed in Paragraph 6.2.3: the confinement prevents the full development of the rocking mechanism of the pier, and causes sudden failure due to crack development over its diagonal. With the restrained displacement of the piers, the top part of the wall is sliding relative to the piers, as was observed in the three-band-model. The crack strains in the model confined by four bands and four columns, are much smaller than have been observed in the previous models. However, for this shear wall, adding more confinement is not beneficial for the ductility, and due to sudden failure it is not beneficial for the ultimate strength either.

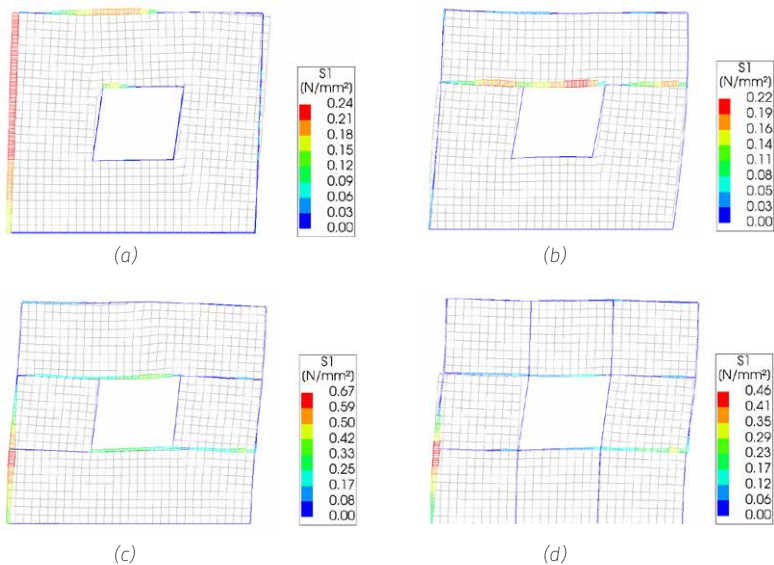


Figure 6.18: Principal stresses in the timber elements at the point of failure of the structure with  $f_{t,masonry} = 0.01 \text{ N/mm}^2$ , for the walls confined by (a) roof and floor band; (b) roof, floor and lintel band; (c) roof, floor, lintel and sill band; (d) roof, floor, lintel and sill band and four columns.

Confining the shear wall by four seismic bands increases its ultimate strength, however, it is important to check the response of the timber frame. Figure 6.18 shows the principal stresses in the timber elements for the confined models at the point of failure of the structure. For none of the models the stress limit in the timber elements at their connections is reached.

### 6.3.3 Results for $f_t = 0.03 \text{ N/mm}^2$

Figure 6.19 shows the force-displacement diagram as a response to the modal pushover load for the models with a masonry tensile strength of  $f_t = 0.03 \text{ N/mm}^2$ . Based on the force-displacement curves, the confinement seems to have a similar effect on these walls compared to those with a lower tensile strength, although the higher tensile strength allows for further loading and a larger displacement capacity of the walls, with the exception of the four-band-model with two columns, which is almost the same for both the values of the tensile strength.

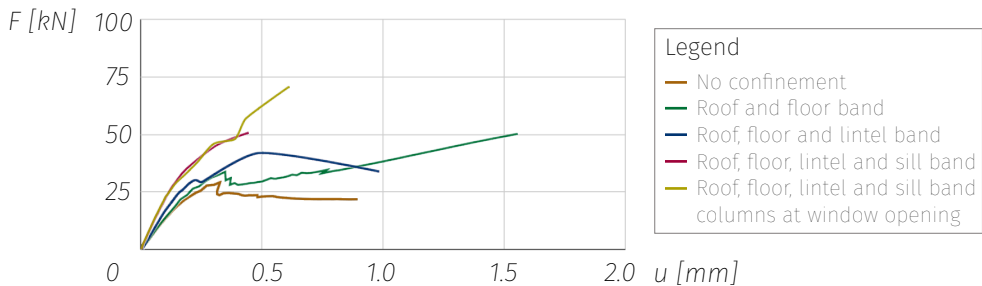


Figure 6.19: Force-displacement diagram of the unconfined and confined walls with window opening as response to the pushover load, for  $f_{t,masonry} = 0.03 \text{ N/mm}^2$ .

Figure 6.20 shows the crack strain contours of the five models at failure. The failure mechanisms are as well very similar to the models with  $f_t = 0.01 \text{ N/mm}^2$ . The unconfined wall and wall with roof and floor band confinement develop a rocking mechanism in the pier on the right side of the window, thus explaining their ductility. The three-band-model and both four-band-models experience a combination of sliding and rocking. Sliding takes place at the lintel band where the top of the wall slides off of both piers. The pier on the right hand side of the window opening experiences rocking in all models. However, judging by the crack strain contours, it seems that these piers in both the models with four bands also develops cracks over its diagonal. So the failure mode of these models could be exceedance of diagonal tensile capacity, which would explain that these models have less deformation capacity compared to the models with less confinement, observed by the force-displacement curves.



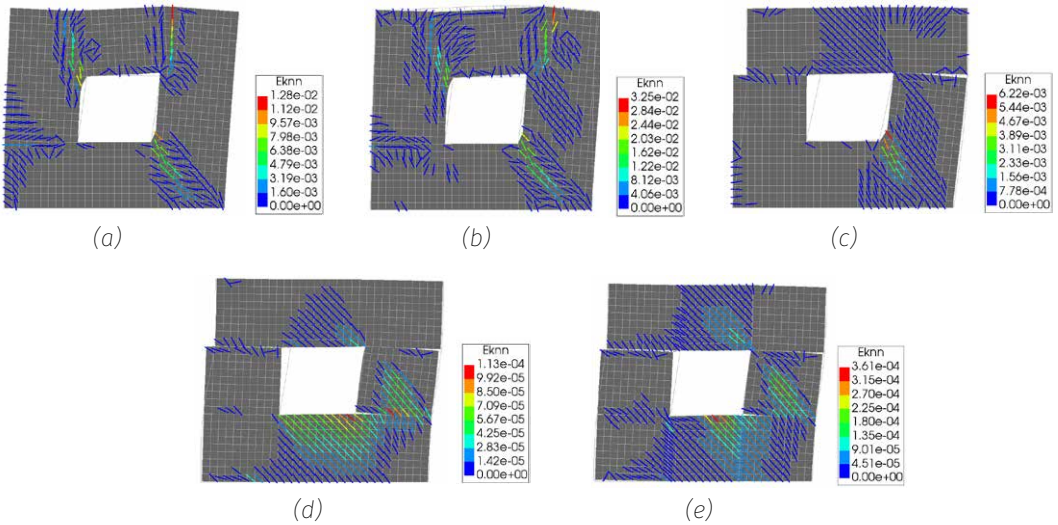


Figure 6.20: Crack strain contour plots for walls with  $f_t = 0.03 \text{ N.mm}^2$  at failure, for (a) unconfined wall; (b) two-band-confined wall; (c) three-band-confined wall; (d) four-band-confined wall; (e) four-band-confined wall with two extra columns.

For the model with four bands and two columns, this decrease in ductility compared to the less confined models, is not compensated by an increase in the ultimate strength: the ultimate strength of this model is equal to the ultimate strength of the model confined by only a roof and floor band.

For the model with four bands and four columns, one could argue that the increase in ultimate strength outweighs the decrease in ductility, since the ultimate strength is almost three times higher compared to the unconfined wall, and 40% higher than the model confined by a roof and floor band. Generally, ductility of a structure is considered an important property when judging its response to loads, since a higher ductility corresponds to a higher safety due to the possibility of a person to flea before collapse. Whether or not this increase in ultimate strength outweighs the decrease in ductility depends on the magnitude of the earthquake loads: if these loads remain below the ultimate strength of the confined structure, the lack of ductility would not create an unsafe situation since the structure would not collapse. However, if the earthquake loads exceed the ultimate strength of the structure, regardless of the amount of confinement applied, the ductility of the structure would be of great importance concerning the safety. The peak horizontal ground acceleration measured of the Gorkha Nepal earthquake of 2015 is  $2.5 \text{ m/s}^2$  (Takai et al., 2016). By using Newton's second law this acceleration corresponds to a horizontal force of 22 kN on a wall with this mass. So the increase of the ultimate strength due to the confinement possibly outweighs the decrease in ductility. However, further research is needed to confirm or reject this hypothesis, where out-of-plane behaviour of the structure is taken into account.

Contrary to the models with the lower masonry tensile strength, the stress limit in the timber elements are exceeded at the point of failure of the structure. Figure 6.21 shows these stresses. It can be seen that for both the models with the four-band-confinement (Figures 6.21c and 6.21d), just at the point of global failure, the stresses in the joint that connects the column on the right side of the wall with the sill band, are around 0.40 N/mm<sup>2</sup>. To be sure that the structure fails on the masonry and not on the timber frame, these connections should be made stronger. This holds as well for the wall confined by three band (Figure 6.21b), where at the point of global failure, the stresses at the roof band connection have just exceeded their limit. However, the model confined by only the roof and floor band shows much higher stresses at the roof band connection, and judging by the force-displacement curves it might be likely that the masonry structure will be confined by only these two bands. If this would be the case, it is of utmost importance to reinforce these timber joints, otherwise the timber frame will be governing for the global failure of the structure and the ultimate strength and ductility as presented by the force-displacement curve will not be reached. Instead, the joint of the two-band-confinement will fail at  $u = 0.56$  mm, which is at a third of the wall's potential displacement if the joint would be strong enough.

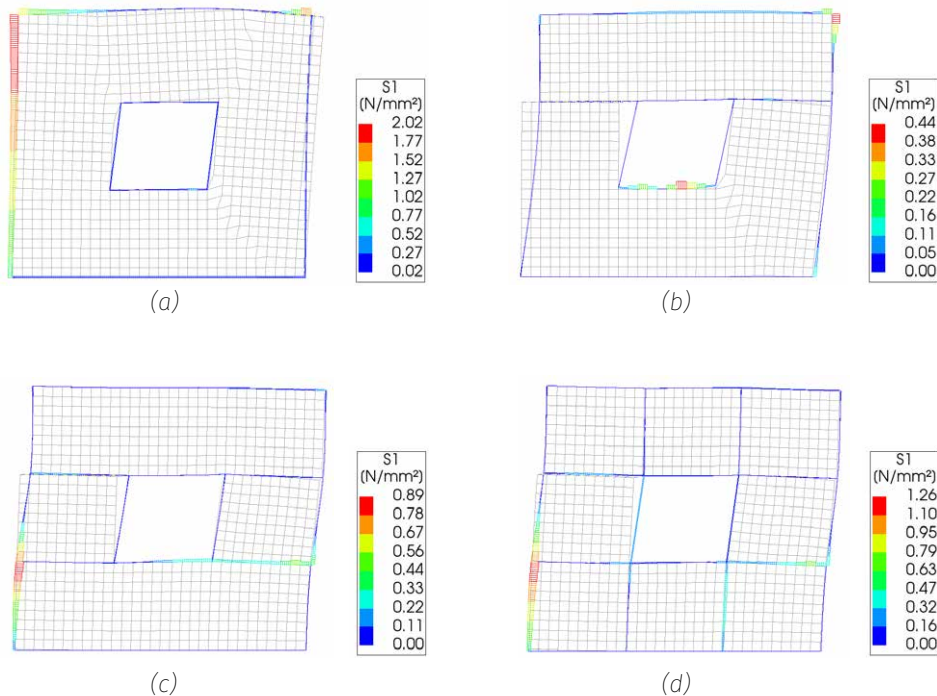
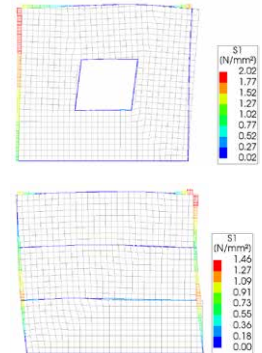


Figure 6.21: Principal stresses in the timber elements at the point of failure of the structure with  $f_{t,masonry} = 0.03$  N/mm<sup>2</sup>, for the walls confined by (a) roof and floor band; (b) roof, floor and lintel band; (c) roof, floor, lintel and sill band; (d) roof, floor, lintel and sill band and four columns.

## 6.4 REDESIGN BAND-TO-COLUMN CONNECTION

The timber joints in the numerical model consist of hinges that behave linearly; their failure is not included in the model. However, it has been observed that during loading of the different shear wall configurations, in reality the joints would fail due to the stresses that arise in the columns and bands. For the redesign of the timber joint two cases are considered:

- Case 1: The masonry structure will be confined by two bands only (floor and roof band). In this case the stresses in the timber elements can become  $\sigma_{\max} = 2.02 \text{ N/mm}^2$  (in the model with window opening and  $f_{t,\text{masonry}}^{\max} = 0.03 \text{ N/mm}^2$ ).
- Case 2: The masonry structure will be confined by all four bands. In this case the stresses in the timber elements can become  $\sigma_{\max} = 1.46 \text{ N/mm}^2$  (in the model without opening and  $f_{t,\text{masonry}}^{\max} = 0.01 \text{ N/mm}^2$ ).



These two cases are considered because they are both adequate confinement solutions to increase the resistance of the masonry structure. Appendix D provides the calculations used to determine the load-carrying capacity and splitting capacity of the two new designs for the timber joint. This paragraph provides a summary of the two design cases.

### 6.4.1 Case 1: Timber confinement consists of two bands

The greatest stress that has developed in the frame is  $\sigma_{\max} = 2.02 \text{ N/mm}^2$ , and has developed in the roof band-to-column connection, in the model with window opening confined by two bands and  $f_{t,\text{masonry}}^{\max} = 0.03 \text{ N/mm}^2$ . This corresponds with a carrying capacity of the connection of 39.6 kN. Therefore, the resistance of the connection must be greater than:

$$F_{v,\text{ef},\text{Rd}} \geq F_{v,\text{Ed}} = 39.6 \text{ kN}$$

First, the splitting capacity of the joint must be checked. The current dimensions of the timber elements do not provide sufficient resistance to splitting of the timber. In order for the frame to resist these loads, the dimensions of the bands must become 200x200 mm, and the dimensions of the columns must become 175x200 mm. Due to the larger dimensions of the timber elements, a larger nail size

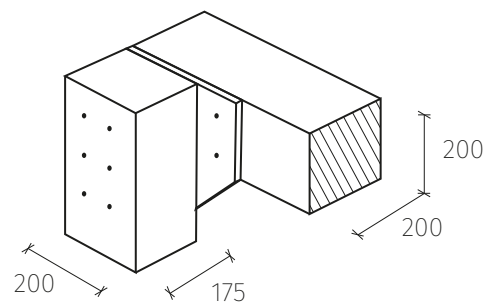


Figure 6.22: Redesign timber joint for Case 1.

of 260x76 mm will be used. The connection will be strengthened by a thin steel plate, shown in Figure 6.22. Adding the steel plate allows for increasing the amount of fasteners without compromising the edge distances. The connection is now a steel-to-timber connection with a combination of single and double shear. The design load carrying capacity of the connection becomes:

$$F_{v,ef;Rd} = \frac{k_{mod}}{Y_M} \cdot F_{v,ef;Rk} = \frac{0.90}{1.3} \cdot 61.4 = 42.5 \text{ kN}$$

### 6.4.2 Case 2: Timber confinement consists of four bands

The greatest stress that has developed in the frame is  $\sigma_{max} = 1.46 \text{ N/mm}^2$ , and has developed in the roof band-to-column connection, in the model without opening confined by four bands and  $f_{t,masonry} = 0.01 \text{ N/mm}^2$ . This corresponds with a carrying capacity of the connection of 28.6 kN. Therefore, the resistance of the connection must be greater than:

$$F_{v,ef;Rd} \geq F_{v;Ed} = 28.6 \text{ kN}$$

First, the splitting capacity of the connection must be checked. The current dimensions of the timber elements do not provide sufficient resistance to splitting of the timber. In order for the frame to resist these loads, the dimensions of the bands and columns must become 150x150 mm. These dimensions are not much larger than the 140x140 mm used up until now, so the same nail size of 180x6 mm can be used.

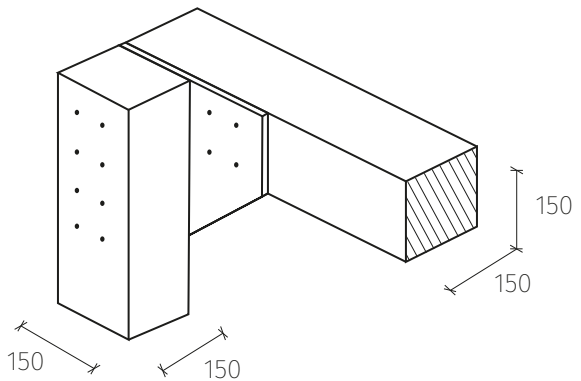


Figure 6.23: Redesign timber joint for Case 2.

The connection will be strengthened by a thin steel plate, shown in Figure 6.23. Adding the steel plate allows for increasing the amount of fasteners without compromising the edge distances. The connection is now a steel-to-timber connection with a combination of single and double shear. The design load carrying capacity of the connection becomes:

$$F_{v,ef;Rd} = \frac{k_{mod}}{Y_M} \cdot F_{v,ef;Rk} = \frac{0.90}{1.3} \cdot 46.3 = 32.1 \text{ kN}$$

## 6.5 VALIDATION NUMERICAL MODELS

By comparing the results that are obtained by the numerical model to the results obtained by the analytical calculations of Chapter 3, a rough validation of the models can be made. The calculations used in the analytical study are not specifically designed for rubble stone masonry but for brick masonry, so their results are to be regarded as estimations of the response of the structure, and can therefore not provide a well-founded validation of the numerical model. In common practise, experimental tests are performed to validate numerical models, however, this is outside the scope of this research.

### 6.5.1 Unconfined closed wall

To investigate the effect of the confinement method by means of the numerical study, two different values for the masonry tensile strength have been considered ( $f_t = 0.01 \text{ N/mm}^2$  and  $f_t = 0.03 \text{ N/mm}^2$ ). This decision has been made since a slightly different tensile strength resulted in a different failure mechanism and ultimate strength of the wall. The analytical study follows a different approach: each failure mechanism is described by a separate formula, each with different parameters. For these calculations, initially only one set of values for the material properties has been applied. The tensile strength of the masonry is represented by the diagonal tensile strength, which only occurs in the formula for the diagonal tensile capacity. If this value is increased from  $0.02 \text{ N/mm}^2$  (which is the value used for the calculations in Chapter 3) to  $0.03 \text{ N/mm}^2$ , the estimated resistance to diagonal tensile failure becomes larger than the resistance against rocking.

Table 6.1 shows the resistance and failure mechanism estimated by the analytical and numerical calculations for the unconfined wall without window opening, for different values for the masonry tensile strength.

**Table 6.1:** Estimated resistance and failure mechanism found by the analytical and numerical studies, for different values for the masonry tensile strength.

	Analytical study		Numerical study	
	$f_{dt} = 0.02$ N/mm <sup>2</sup>	$f_{dt} = 0.03$ N/mm <sup>2</sup>	$f_t = 0.01$ N/mm <sup>2</sup>	$f_t = 0.03$ N/mm <sup>2</sup>
Ultimate strength	$V_{dt} = 37 \text{ kN}$	$V_{rt} = 47 \text{ kN}$	$V = 39 \text{ kN}$	$V = 75 \text{ kN}$
Failure mechanism	Diagonal tensile failure	Rocking	Diagonal tensile failure	Rocking

For both the analytical approach as for the numerical approach it is found that the masonry tensile strength has a great influence on the failure mechanism of the wall: a slightly higher value results in a rocking mechanism instead of diagonal tensile failure. However, the ultimate strength found by the numerical model for the rocking mechanism is much higher than is found by the analytical calculations. This can be explained by the differences in the applied force: the analytical calculations assume the pushover load to be applied at the top of the wall for the rocking mechanism, whereas the model pushover load in DIANA applies the load at the mean displacement of the wall, which is at approximately two-thirds of the height, shown in Figure 6.24.

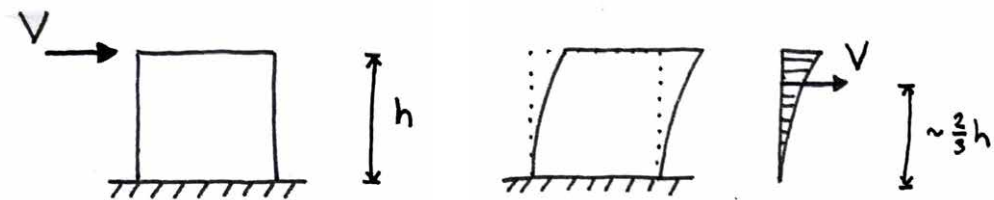


Figure 6.24: Applied load according to NPR calculations (left) and as applied by the model pushover load in DIANA (right).

If the ultimate strength obtained by the numerical model is scaled by two-thirds, it should be similar to the resistance against rocking obtained by the analytical model:

$$V_{\text{rocking,numerical,scaled}} = 75 \cdot \frac{2}{3} = 50 \text{ kN} \approx V_{\text{rocking,analytical}} = 47 \text{ kN}$$

### 6.5.2 Confined closed wall configurations

Figure 6.25 gives an overview of the ultimate strength and failure mechanisms of the closed shear wall configurations, obtained from the analytical and numerical studies. Several observations can be made:

- The numerical models estimate the ultimate resistance of the confined walls to be much higher than estimated by the analytical models.
- The numerical results show a considerable increase in the ultimate strength of the walls with a higher masonry tensile strength. For the analytical results this difference is smaller and only observed when diagonal tensile failure is governing, since the diagonal tensile strength has no influence on the other failure mechanisms.
- Confining the wall by more than two bands results in a decrease of the ultimate strength for the analytical models and for the higher strength numerical models, since the extra bands results in sliding of the wall parts.

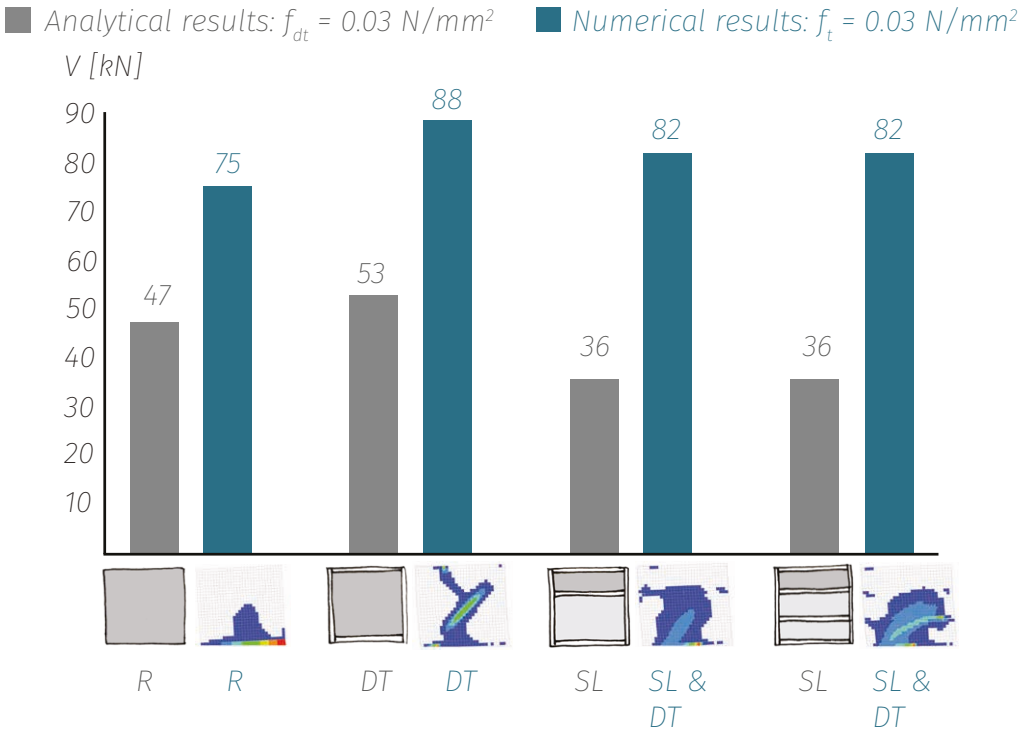
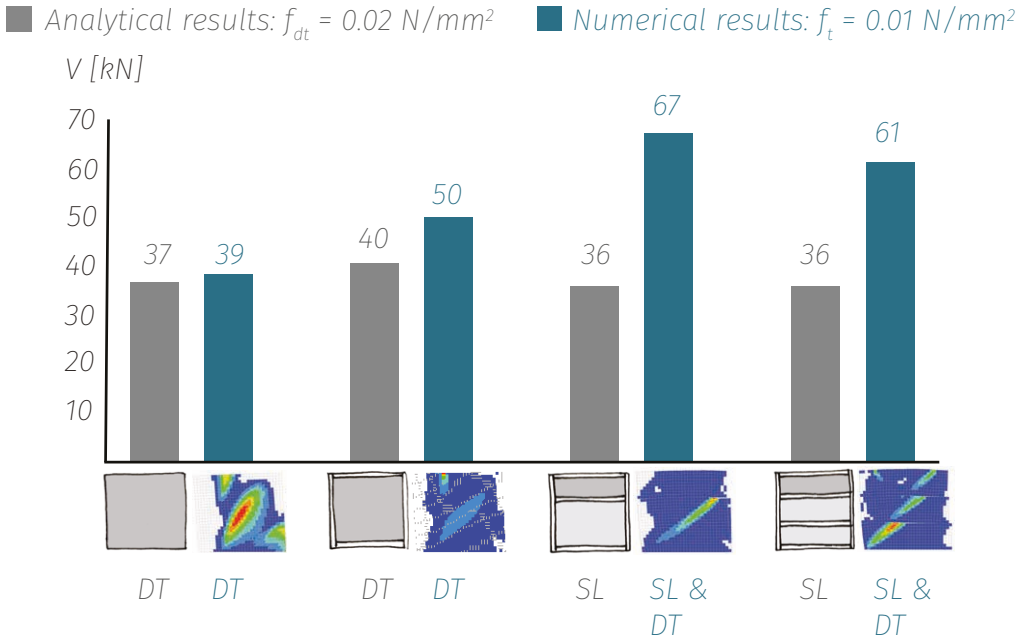


Figure 6.25: Ultimate strength and failure mechanisms of the closed shear wall configurations, obtained from the analytical and numerical studies, for the lower (top) and higher (bottom) values of the masonry tensile strength.

Considering these observations, both studies predict comparable failure mechanisms, but the ultimate strength is considerably different. It is to be expected that the analytical results are conservative compared to the numerical results, however, this does not explain the significant differences that are observed in the ultimate strength. The following aspects contribute to the strength differences as well:

- The location of the applied force, as explained in Paragraph 6.5.1.
- The analytical calculations are applied on the part of the wall that is expected to be governing for global failure. For the walls with more than two bands, it was expected that the top part of the wall would be governing for failure since this part has the lowest normal stresses in the masonry (whereas the other wall parts have higher normal stresses due to the self weight of the wall part(s) above it). Figure 6.25 shows the parts of the walls that are considered in the analytical calculations, together with the failure observed by the numerical analyses. It can be seen that according to the numerical results, failure does not occur in the top part of the wall, as was assumed in the analytical study. Therefore, in the analytical calculations a higher normal stress could have been applied, which would have led to a higher ultimate strength.
- The analytical approach applies a limit to the contribution of the timber frame to the resistance, which is determined by the load carrying capacity of the band-to-column connections. The numerical approach does not apply this limit and is therefore overestimating the resistance of one of the confined shear wall configurations, namely the four-band-model with  $f_t = 0.01 \text{ N/mm}^2$ . Additionally, the cut-off approach applied for the analytical calculations is conservative, since it does not allow for the development of larger stresses at any location of the column, whereas the stress distributions of the timber frame obtained by the numerical calculations show that the stresses in the columns are not constant and can be larger in between the connections with the bands.

### 6.5.3 Walls with window opening

Figure 6.25 gives an overview of the ultimate strength and failure mechanisms of the unconfined and confined walls with window opening, obtained from the analytical and numerical studies. Several observations can be made:

- The numerical models estimate the ultimate resistance of the walls to be much higher than estimated by the analytical models.
- The failure mechanisms estimated by the numerical models match the failure mechanisms estimated by the analytical models.
- For both the analytical models and the numerical models an increase in the ultimate strength is observed when increasing the amount of confinement, with the exception of the last numerical model with  $f_t = 0.01 \text{ N/mm}^2$ .
- A higher masonry tensile strength results in a higher ultimate strength for all



numerical models, but for the analytical models this only has an effect on the ultimate strength if diagonal tensile failure is governing.

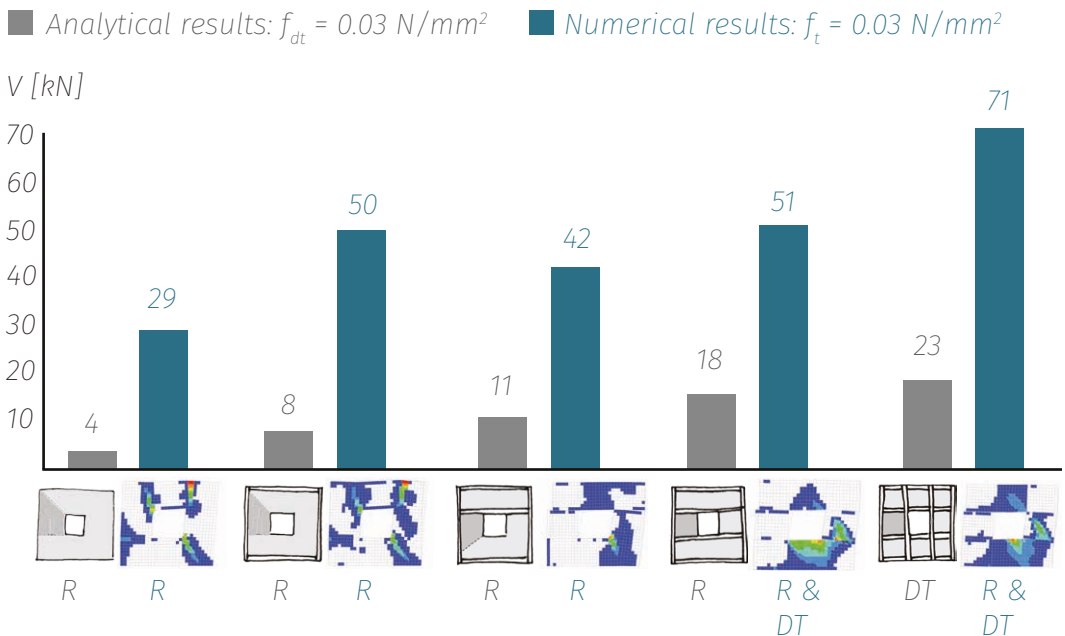
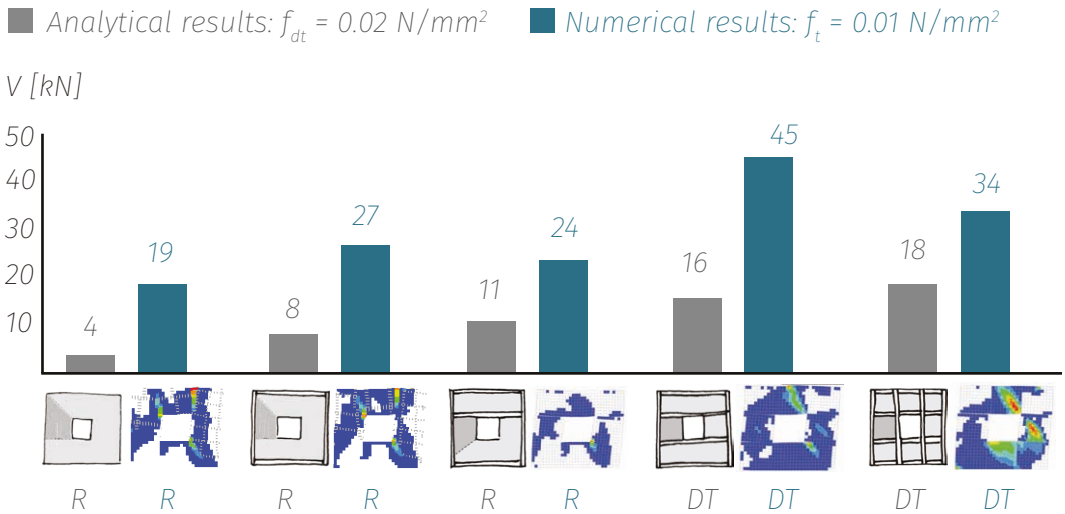


Figure 6.26: Ultimate strength and failure mechanisms of the shear wall configurations with window opening, obtained from the analytical and numerical studies, for the lower (top) and higher (bottom) values of the masonry tensile strength.

Considering these observations, it is likely that the failure mechanisms are correctly estimated by the numerical analysis. Moreover, the positive effect that the confinement has on the ultimate strength is observed in both studies. The absolute value of the ultimate strength, however, is considerably different. Part of this difference could be explained by the conservative nature of the analytical calculations, however, this does not cover the entire gap in between the results. The following aspects contribute to the strength differences as well:

- The location of the applied pushover load, as explained in Paragraph 6.5.1.
- The wall part assumed to be governing in the analytical calculations: for the unconfined wall and the wall confined by two bands, the rocking pier is assumed smaller for the analytical calculations compared to the numerical results. Therefore, in the analytical calculations a higher normal stress could have been applied, which would have led to a higher ultimate strength of these two wall configurations.
- The numerical approach does not apply a limit to the stresses that develop in the columns, and is therefore overestimating the resistance of one of the confined shear wall configurations, namely the two-band-model with  $f_t = 0.03 \text{ N/mm}^2$ .
- The cut-off value for the loads in the columns that is applied in the analytical calculations leads to a conservative contribution of the confinement to the ultimate resistance, since it does not allow for larger stresses in the columns at any location, whereas these stresses are only limited at the connections with the bands.

## 6.6 CONCLUSIONS CHAPTER 6

### 6.6.1 Validation of the numerical model

The results of the numerical analyses have been compared to the results of the analytical study. Similarities have been found in the estimated failure mechanisms of the models, therefore it is likely that the failure mechanisms are correctly estimated by the numerical analysis. Differences have been found in the ultimate strength of the analytical and numerical models. Even though the difference in strength can partly be explained, it does not validate which of them are closest to the reality. However, since the analytical calculations are developed by the NPR for unconfined masonry, it is expected, based on the comparison to the numerical results, that these formulas are not applicable to confined masonry. In order to provide a well-founded validation of the numerical model, experimental tests need to be performed.

### 6.6.2 The effect of the confinement on masonry with $f_t = 0.01 \text{ N/mm}^2$

Force-displacement diagrams have been obtained from the numerical analyses, which are shown again in Figure 6.27 for comparison. For the closed wall, the force-displacement curves show that the confinement has a positive effect on both the ultimate strength and the ductility of the wall. This positive effect is greatest for the four-band-confinement. For the wall with window opening, the force-displacement curves show that the masonry wall with this very low tensile strength has little deformation capacity, regardless of the amount of confinement. So for the wall with window opening it is beneficial to add the timber confinement, since it will increase the ultimate strength of the wall.

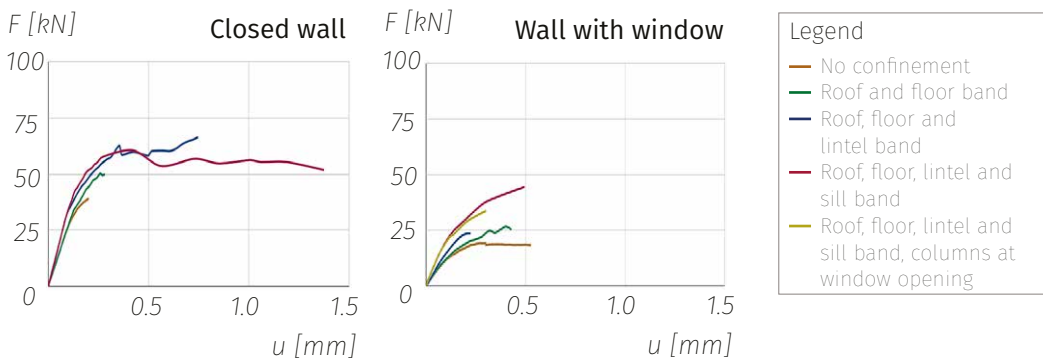



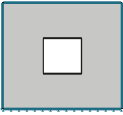
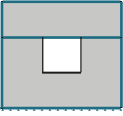

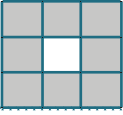


Figure 6.27: Force-displacement curves of the unconfined and confined walls with  $f_{t,masonry} = 0.01 \text{ N/mm}^2$ , of the closed walls (left) and of the walls with window opening (right).

Table 6.2 gives an overview of the benefit of confinement in percentage with respect to the unconfined wall. Based on these numbers it seems most beneficial to confine the masonry structure with four bands. For this low value of the masonry tensile strength it is advisable not to add the extra columns next to the window opening to the confinement, since this has a negative effect on the ductility of the wall.

If the masonry were to be confined by this timber frame consisting of four bands, the design of the timber joints needs to be addressed, since the connection of the roof band with the column would experience higher stresses than can currently be carried by the connection. Moreover, the size of the timber members needs to be increased to 150x150 mm to avoid splitting when loaded perpendicular to the fibre.

**Table 6.2:** The benefit of confinement for a masonry tensile strength of 0.01 N/mm<sup>2</sup>

Wall type	Confinement	Strength benefit	Ductility benefit
Closed wall		+ 28%	+ 41%
		+ 72%	+ 229%
		+ 56%	+ 595%
Wall with window opening		+ 39%	- 19%
		+ 22%	- 58%
		+ 131%	- 6%
		+ 76%	- 43%

Note. Benefit in percentage with respect to the unconfined wall.

### 6.6.3 The effect of the confinement on masonry with $f_t = 0.03 \text{ N/mm}^2$

Figure 6.28 shows the force-displacement diagrams of the unconfined and confined walls, with and without window opening. Table 6.3 gives an overview of the benefit of confinement in percentage with respect to the unconfined wall.

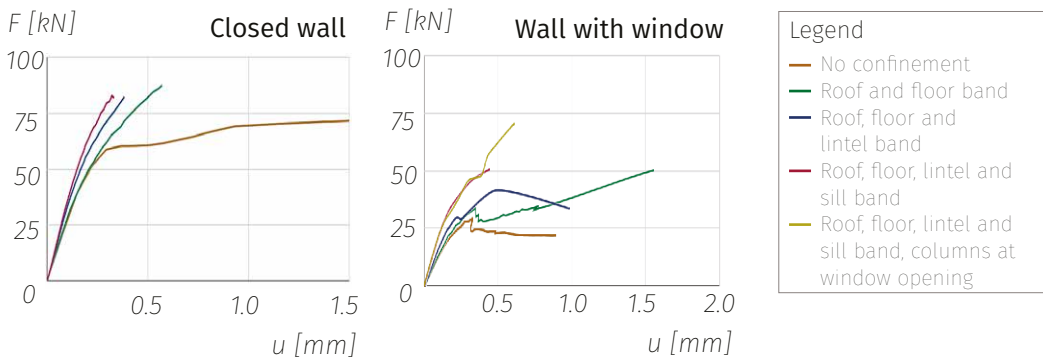


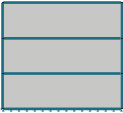
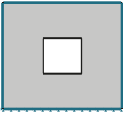
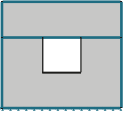

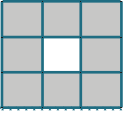


Figure 6.28: Force-displacement curves of the unconfined and confined walls with  $f_{t,masonry} = 0.03 \text{ N/mm}^2$ , of the closed walls (left) and of the walls with window opening (right).

From the force-displacement diagram can be observed that the ultimate strength of the closed walls is approximately the same, regardless of the amount of confinement. The unconfined wall shows a rocking behaviour, allowing for a global displacement of 14 mm before failure. Confining the wall limits the rocking motion and the masonry's diagonal tensile capacity becomes governing, resulting in brittle failure. This leads to the conclusion that confining the closed wall is not beneficial, since the ultimate strength of the wall is not increased considerably compared to the unconfined wall, yet its ductility is lost. However, confining the wall with window opening by these bands and columns, has a positive effect on the ultimate strength, and does not have a negative effect on the ductility of the wall since the ductility for all these analyses is limited.

Based on the force-displacement curves of both the closed wall and wall with opening, it seems best to confine the masonry by a floor and roof band only, since this increases both the ultimate strength and ductility of the wall with opening. However, this results in high stresses at the timber connections, and the columns and bands must increase in size to 200x200 mm. Therefore, it is advised to confine the masonry wall with a timber frame consisting of four bands, and columns at wall corners and window openings, since this increases the ultimate strength of the wall with opening significantly.

**Table 6.3:** The benefit of confinement for a masonry tensile strength of 0.03 N/mm<sup>2</sup>

Wall type	Confinement	Strength benefit	Ductility benefit
Closed wall		+ 17%	- 96%
		+ 10%	- 97%
		+ 9%	- 98%
Wall with window opening		+ 129%	+ 74%
		+ 89%	+ 10%
		+ 132%	- 49%
		+ 224%	- 29%

Note. Benefit in percentage with respect to the unconfined wall.

# CHAPTER 7

---

## Conclusions

*As a response to the Gorkha earthquake in 2015, and to advance to safe reconstruction, the government of Nepal has published a new building code, as well as a catalogue with designs for houses using approved building methods. This master's thesis research has investigated the response of one of these designs to determine if it indeed increases the resistance of the masonry to earthquake loads. In this chapter, the findings of this research will be summarised and the research question will be answered.*

### 7.1 ANSWER TO THE RESEARCH QUESTION

An analytical and numerical pushover analysis on a shear wall have been performed to answer the following research question: Does the confinement of timber bands and columns increase the resistance of rubble stone masonry shear walls against earthquake loads?

Confining the rubble stone masonry shear wall by the timber frame confinement increases the ultimate strength of the wall. However, the dimensions of the timber frame need to be increased in order for the connections to resist the loads.

To elaborate on this answer, two factors are of importance concerning the resistance of a shear wall against earthquake loads: the ultimate strength of the wall, and its displacement capacity. The displacement capacity is of importance since this determines the amount of time to flee the building when it is facing collapse. On the other hand, if the ultimate strength of the building is sufficient, it might not collapse under the earthquake loads at all.

These two considerations are of importance for answering the research question, since it is found that the confinement has a positive effect on the ultimate strength of the wall, but on the other hand can have a negative effect on the displacement

capacity. Whether or not it is wise to confine the masonry by this frame of timber bands and columns, ultimately depends on how strong the masonry actually is. The strength of the masonry is here described, for convenience, by its tensile strength, which is selected as the most relevant parameter.

In practise it is not feasible to determine the tensile strength of the masonry before constructing the building, especially not in rural Nepal, where civilians build their own houses without any schooling in construction work. Based on the findings of this research, the masonry should be confined by a timber frame consisting of four timber bands, and columns at each wall junction. Figure 7.1 shows the design of the confinement method as recommended by the Nepali building codes and the design as recommended by this research. This creates a more brittle structure compared to an unconfined wall, but it will increase its ultimate strength. The loss of ductility is not a problem as long as the increase of ultimate strength is sufficient to allow the structure to resist the earthquake loads. This, however, should be assessed for each individual building, depending also on the location and the expected ground motion.

## 7.2 PARAMETER STUDY

The effect of the confinement is tested by the numerical analysis on masonry with two different tensile strengths:  $f_t = 0.01 \text{ N/mm}^2$  and  $f_t = 0.03 \text{ N/mm}^2$ . Both of these tensile strengths are considered low in comparison to the strength of brick masonry for example. By the parameter study it was found that this slight difference in tensile strength, results in a different failure mechanism of the structure, and therefore result in a vastly different displacement capacity.

Other material properties of the masonry that have a significant influence on the behaviour and ultimately failure of the shear wall are:

- The mass density, which has a considerable influence on both the ultimate strength and on the deformation capacity of the wall.
- The compressive strength and fracture energy, which have a considerable influence on the deformation capacity of the wall.

## 7.3 VALIDATION OF THE NUMERICAL RESULTS

The results of the numerical analyses have been compared to the results of the analytical study. Similarities have been found in the estimated failure mechanisms of the models, therefore it is confirmed that the failure mechanisms are correctly estimated by the numerical analysis. Due to large differences in the estimated ultimate strength, these results could not be validated. Even though the difference in strength can partly be explained, experimental tests need to be performed in



Recommended design by Nepali building codes

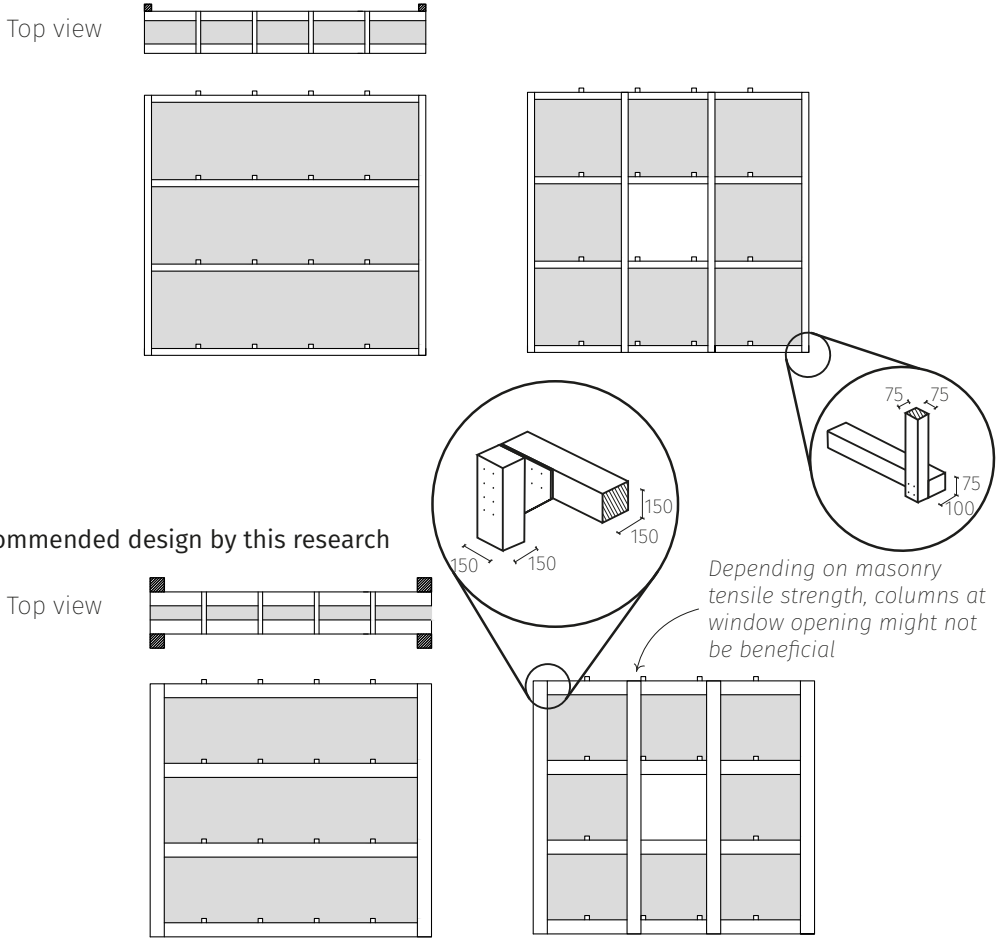


Figure 71: Design of the confinement method as recommended by the Nepali building code (top) and by this research (bottom).

order to provide a well-founded validation of the numerical model. Moreover, since the analytical calculations are developed by the NPR for unconfined masonry, it is expected, based on the comparison to the numerical results, that these formulas are not applicable to confined masonry.

## 7.4 DESIGN OF THE TIMBER FRAME

The design of timber connections as recommended by the Nepali building codes is in this study determined not to provide sufficient strength to the frame, and

must be altered in order to actually have this positive effect on the structure's resistance. The following aspects have to be taken into account:

- Place columns on both sides of the band instead of only on the inner side to avoid torsional loads on the bands due to eccentricity.
- In order for the nails to safely transfer the loads from the bands to the columns with respect to edge distances and splitting capacity, the shear plane of the joint needs to be larger: the cross-sectional dimensions of the timber members need to be at least 150x150 mm, as opposed to the 70x70 mm suggested by the Nepali building codes.
- The load transfer capacity of the timber joint could be governing for the resistance of the global structure. It is advised to eliminate this risk by strengthening the joint by means of steel plates, which allows for applying more fasteners.

# CHAPTER 8

---

## Discussion of the limitations of the study

*Throughout this master's thesis research, several assumptions and simplifications have been made that have an influence on the results and, therefore, limits the conclusions. The conclusions of Chapter 7 will be discussed, which includes the argumentation behind these assumptions and their influence on the results of this research.*

### 8.1 ANSWER TO THE RESEARCH QUESTION

The research question is answered by means of an in-plane analysis on the confined and unconfined masonry wall. Since the earthquake loads are resisted by the shear stiffness of the walls of the building, an in-plane analysis determines the ultimate strength and displacement capacity of the masonry. Additionally to the ultimate strength and displacement capacity, it is important to investigate collapse of the walls, which is governed by the out-of-plane resistance: to avoid collapse, the connections of the out-of-plane walls to the in-plane walls must be sufficient to resist the earthquake loads. An out-of-plane study is outside the scope of this research, therefore, the effect of the confinement on the resistance of the masonry covers only the ultimate strength of the masonry wall and does not cover collapse.

The effect of the confinement is tested by the numerical analysis on masonry with two different tensile strengths. The extremely low tensile strength of  $0.01 \text{ N/mm}^2$  corresponds roughly to the assumption that the stones are loose, which is likely to occur when the mortar is degraded and its bond is very limited. If the building is constructed with this value for the masonry tensile strength, then the timber frame confinement will benefit the resistance of the building against earthquakes, and it is recommended to include this confinement to the structure. The confinement then must consist of four bands, placed at the top and bottom of the wall, and at the top and bottom of window openings.

However, if the building is constructed with masonry having a tensile strength of  $0.03 \text{ N/mm}^2$  or higher, the confinement has such a negative influence on the ductility that it could be best not to confine the masonry at all. This effect is most observed in the closed wall configurations. For the shear wall with window opening, although decreasing its ductility, the confinement triples its ultimate strength. Therefore, in the case of a higher masonry tensile strength, an analysis on a three-dimensional structure is needed to fully answer the research question. In a three-dimensional study, the closed walls and walls with opening give a combined response to the load and therefore the advantages and disadvantages of the confinement are combined as well. Additionally, this research does not study the out-of-plane behaviour of the walls, which represent in most cases the highest vulnerability to earthquake loads due to sudden collapse.

## 8.2 PARAMETER STUDY

Apart from the tensile strength, the numerical study on the effect of the confinement is performed with only one set of material properties, which values were chosen by means of force-displacement curves obtained by the parameter study. For most masonry material properties, no significant difference was observed in the response between the lower and upper bound value, and an intermediate value was assigned to the properties. As was concluded in Chapter 7, two properties (apart from the tensile strength) had a significant influence on the response, yet one value was assigned to them:

- A larger mass density resulted in a larger ultimate strength and a smaller displacement capacity. To investigate the effect of the confinement method, it is not of importance to know the absolute value of the resistance of the masonry structure is; the relative value of the resistance between the unconfined and confined structures is of importance. Therefore, the results of this research are not influenced by assuming this one value for the mass density.
- This might not be the case for the fracture energy in compression. Based on the force-displacement curves of the parameter study, it was decided to continue the numerical study with a low value for the compressive fracture energy relative to the compressive strength, since this value resulted in softening behaviour. Consequently, the masonry undergoes crushing rapidly after reaching its compressive strength. For the shear wall configurations for which diagonal tensile failure is governing, this consequence is not of importance, since the displacements of the structure remain small. However, for the wall configurations that develop a rocking mechanism, the relatively low fracture energy could lead to an underestimation of the ductility of the wall.

The parameter study has been performed on the material properties of the masonry only, and not on the frictional behaviour between the bands and the masonry. This behaviour is described in the numerical model by means of Coulomb friction

interface elements, of which the properties were found in literature as well. For this research, the values for the line interface elements were chosen such that it would result in a stable numerical model. Consequently, the bond between the masonry and the timber could be overestimated, which would influence both the results of the ultimate strength and the results of the ductility.

### **8.3 VALIDATION OF THE NUMERICAL RESULTS**

By comparing the numerical to the analytical results, it is concluded that the absolute value of the ductility and the ultimate strength of the shear wall configurations cannot be validated. The numerical analyses were stopped when non-convergence occurred in several steps in a row, leading to unreliable results. Further validation of the numerical models is of importance to determine whether the currently obtained ductility of the models is accurate, or if improvements of the numerical model would lead to a more stable model, and therefore a higher ductility and ultimate resistance of the structure.

### **8.4 DESIGN OF THE TIMBER FRAME**

The connections of the timber frame are redesigned based on the stresses that will develop in the connections and the requirement that the capacity of the connections needs to be sufficient to carry these stresses. The redesign of the connections could therefore be conservative, since the ductility of the connections is not taken into account. Concerning the edge distances and the splitting capacity of the connections, it is unquestionable that the dimensions of the timber frame need to be increased. However, taking account the ductility of the connections, a lower load carrying capacity could be sufficient for the connections not to fail after reaching this capacity.



# CHAPTER 9

---

## Recommendations for further research

*By performing numerical analyses on shear walls with and without the timber confinement, an indication is obtained of the effect of the confinement on the response of the masonry. However, further research is needed to judge the effect of the confinement with more certainty. This chapter summarises aspects that are outside the scope of this research but are important to investigate.*

- Perform experimental tests on the materials to determine their actual properties. Chapter 5 of this research has concluded that some of the material properties have a significant influence on the behaviour and ultimately failure of the structure, namely the tensile strength and fracture energy, the mass density, and the compressive strength and fracture energy. To simulate the actual response of the structure in a numerical analysis, it is important to determine the actual values of these material properties. Moreover, experimental tests need to be performed on the frictional behaviour between the masonry and the timber bands, also taking into account a possible interlocking effect, due to the geometry of the bands, which is of importance for validating the numerical model. Additionally, further research on the interacting between the masonry and the bands would lead to the possibility of investigating the effect of other band materials as well, since a different band material in the numerical model would be expressed in different values for the line interface properties.
- Validate the numerical in-plane models with experimental tests. For this research an analytical study has validated the estimated failure mechanisms of the shear walls, as well as the positive effect that the confinement has on the ultimate strength. However, the actual ultimate strength and ductility of the confined shear walls could not be validated by the analytical study. At this point it is uncertain whether the numerical analyses showed non-convergence

because of failure of the structure, or because the numerical model requires improvements.

- Include the non-linear behaviour of timber connections to the numerical models. The connections of the timber frame elements are modelled as hinges that behave linearly; their failure is not included. However, it has been observed that during loading of the different shear walls, the connections could fail due to the stresses that arise in the columns and bands. It would be interesting to investigate what effect failure of the connections would have on the global response of the structure: will failure of the frame's connections remove the entire effect of the confinement and result in immediate global failure of the structure? Or will the structure find a new load path and preserve some of its strength and ductility?
- Perform an out-of-plane analysis to study the effect of the confinement method on out-of-plane failure. In the introduction of this research it is stated that out-of-plane failure is a common governing failure mode for rubble stone masonry. The timber frame, consisting of several bands, divides the masonry walls into different parts with a decreased height. This decreased height could have a positive effect on the out-of-plane failure of the walls. This is a potential important benefit of the confinement method that is not investigated in this study.
- Perform a three-dimensional analysis to study the behaviour of the structure when closed walls and walls with openings are combined. Their interaction, combining out-of-plane and in-plane behaviour, is expected to result in a different global ductility and ultimate strength of the structure.
- For this study it is assumed that the wall and the timber frame are both connected to the foundation such that their translations are fixed. In reality, the supports of the wall and timber frame are more complex and will be able to move both horizontally as well as vertically with respect to the foundation. This simplification might have caused an overestimation in the stresses in the timber elements, and might have caused an underestimation in the ductility of the structure. It is therefore recommended to include the non-linear behaviour of the foundation to the numerical model, instead of the simplified fixed translational supports applied in this study.



# REFERENCES

---

Alejano, L.R., & Alonso, E. (2006). Considerations of the dilatancy angle in rocks and rock masses. *International Journal of Rock Mechanics and Mining Sciences*, Volume 43, Issue 5, July 2006, Pages 836. Retrieved from <https://doi.org/10.1016/j.ijrmms.2005.01.003>

Ali, Q., Badrashi, Y.I., Ahmad, N., Alam, B., Rehman, S., & Banori, F.A.S. (n.d.). Experimental Investigation on The Characterization of Solid Clay Brick Masonry for Lateral Shear Strength Evaluation.

Almeida, J.P., Beyer, K., Brunner, R., & Wenk, T. (2020). Characterization of mortar-timber and timber-timber cyclic friction in timber floor connections of masonry buildings. *Materials and Structures*, 53:51. Retrieved from <https://doi.org/10.1617/s11527-020-01483-y>

AlShawa, O., Sorrentino, L., & Liberatore, D. (2017). Simulation of shake table tests on out-of-plane masonry buildings. Part (II): Combined Finite-Discrete Elements. *International Journal of Architectural Heritage*, 11:1, 79-93. DOI: 10.1080/15583058.2016.1237588

Carabbio, R., Pieraccini, L., Silvestri, S. & Schildkamp, M. (2018). How Can Vernacular Construction Techniques Sustain Earthquakes: The Case of the Bhatar Buildings. Retrieved from <https://doi.org/10.3389/fbuil.2018.00018>

Central Bureau of Statistics (2012). *National population and housing census 2011* (National report). Kathmandu, Nepal: Government of Nepal.

Cominelli, S., Giuriani, E., Marini, A. (2016). Mechanisms governing the compressive strength of unconfined and confined rubble stone masonry. *Materials and Structures* (2017) 50:10. DOI 10.1617/s11527-016-0905-6

Department of Urban Development and Building Construction (2015a). *NBC 204: Guidelines for earthquake resistant building construction: Earthen building* (Nepal National Building Code). Kathmandu, Nepal: Government of Nepal.

Department of Urban Development and Building Construction (2015b). *Design catalogue for reconstruction of earthquake resistant houses - Volume I*. Kathmandu, Nepal: Government of Nepal.

Dhital, M.R. (2015). *Geology of the Nepal Himalaya: Regional perspective of the classic collided orogen*. DOI: 10.1007/978-3-319-02496-7

DIANA - Finite Element Analysis (2017a). *User's Manual release 10.1 - Theory*. Retrieved from <https://dianafea.com/manuals/d101/Theory/Theory.html>

DIANA - Finite Element Analysis (2017b). *User's Manual release 10.1 - Material Library*. Retrieved from <https://dianafea.com/manuals/d101/MatLib/MatLib.html>

DIANA - Finite Element Analysis (2017c). *User's Manual release 10.1 - Element Library*. Retrieved from <https://dianafea.com/manuals/d101/ElmLib/ElmLib.html>

DIANA - Finite Element Analysis (2017d). *User's Manual release 10.1 - Analysis procedures*. Retrieved from <https://dianafea.com/manuals/d101/Analys/Analys.html>

DIANA - Finite Element Analysis (n.d.). *Pushover analysis of a masonry house*. Retrieved from <https://dianafea.com/2017-Tutorial-Pushover-Masonry-House-10.2>

EN 1995-1-1 :2004+A1:2008. Eurocode 5: Design of timber structures - Part 1-1: General - Common rules and rules for buildings, pp.36-52. ICS: 91.010.30; 91.080.20

Giaireton, M., Dizhur, D., da Porto, F., & Ingham, J. M. (2015). Constituent material properties of New Zealand unreinforced stone masonry buildings. *Journal of Building Engineering*, 4, pp.75-85. DOI: 10.1016/j.jobe.2015.08.005

Giaireton, M., Dizhur, D., da Porto, F., & Ingham, J.M. (2016). Seismic assessment and improvement of unreinforced stone masonry buildings: Literature review and application to New Zealand. *Bulletin of the New Zealand Society for Earthquake Engineering*, Vol. 49, No. 2, June 2016.

Hendriks, M.A.N. (2016). *Computational modelling of structures - Lesson: An overview of structural finite element types* [PowerPoint slides]. Retrieved from: [https://blackboard.tudelft.nl/bbcswebdav/pid-2876810-dt-content-rid-9605394\\_2/courses/39621-161701/CIE5148-03%20v01%20Elements.pdf](https://blackboard.tudelft.nl/bbcswebdav/pid-2876810-dt-content-rid-9605394_2/courses/39621-161701/CIE5148-03%20v01%20Elements.pdf)

Lekshmi, M.S., Vishnudas, S., Nair, D.G. (2016). Experimental study on the physical properties of mud mortar in comparison with the conventional mortars. *Civil Engineering and Urban Planning: An International Journal (CIVEJ) Vol.3, No.2, June 2016*. DOI:10.5121/civej.2016.3211

Lourenço, P.B. (1996). *Computational strategies for masonry structures* (Doctoral dissertation). ISBN 90-407-1221-2

Maps of World (2015). *District wise Earthquake severity Map of Nepal*. Retrieved from: <http://www.mapsofworld.com/thematic-maps/earthquake/earthquake-in-nepal.html>

Marino, M., Neri, F., De Maria, A., Borri, A. (2014). Experimental data of friction coefficient for some types of masonry and its correlation with an index of quality masonry (IQM). *Second European conference on earthquake engineering and seismology, Istanbul Aug. 25-29, 2014*.

Milosevic, J., Lopes, M., Bento, R., Sousa Gago, A. (2013). Testing and modeling the diagonal tension strength of rubble stone masonry panels. *Engineering Structures* 52 (2013) 581–591. <http://dx.doi.org/10.1016/j.engstruct.2013.03.019>

Minke, G. (2001). *Construction manual for earthquake-resistant houses built of earth*. Eschborn, Germany: GATE - BASIN

National Reconstruction Authority (2016). *Periodic Progress Report-1*. Retrieved from: [http://hrrpnepal.org/media/56499/160410\\_nra-periodic-progress-report.pdf](http://hrrpnepal.org/media/56499/160410_nra-periodic-progress-report.pdf)

NPR 9998 (2017). *Assessment of structural safety of buildings in case of erection, reconstruction and disapproval - Basic rules for seismic actions: induced earthquakes, pp.196-176*. ICS: 91.080.01; 93.020

NPR 9998+C1 (2020). *Assessment of structural safety of buildings in case of erection, reconstruction and disapproval - Basic rules for seismic actions: induced earthquakes, pp.198-203*. ICS: 91.080.01; 93.020

Roca, P. (2017). Simplified methods for assessment of masonry shear-walls. *SÍSMICA 2004 - 6º Congresso Nacional de Sismologia e Engenharia Sísmica (2004)* 101-118.

Schildkamp, M. & Araki, Y. (2019). School Buildings in Rubble Stone Masonry With Cement Mortar in Seismic Areas: Literature Review of Seismic Codes, Technical Norms and Practical Manuals. Retrieved from <https://doi.org/10.3389/fbuil.2019.00013>

Shock Safe Nepal Team 3 (2016). *Low-budget Earthquake Resistant Housing Design in Rural Nepal* (Master's project, Delft University of Technology).

Sorour, M. M., Parsekian, G. A., Duchesne, D., Paquette, J., Mufti, A., Jaeger, L., Shrive, N. G. (2009). Evaluation of Young's modulus for stone masonry walls under compression. *11th Canadian Masonry Symposium, Toronto, Ontario, May 31- June 3, 2009*

Takai, N., Shigefuji, M., Bijukchhen, S., Ichiyanagi, M., & Sasatani, T. (2016). Features of ground accelerations in the Kathmandu Valley during the 2015 Gorkha Nepal earthquake. *5th IASPEI / IAEE International Symposium: Effects of Surface Geology on Seismic Motion, August 15-17, 2016*.

USGS (2015). Magnitude 7.8 Earthquake in Nepal & Aftershocks. Retrieved from: [http://www.usgs.gov/blogs/features/usgs\\_top\\_story/magnitude-7-8-earthquake-in-nepal/](http://www.usgs.gov/blogs/features/usgs_top_story/magnitude-7-8-earthquake-in-nepal/)

Worldatlas (2016). *Major Tectonic Plates Of Earth*. Retrieved from: <http://www.worldatlas.com/articles/major-tectonic-plates-on-earth.html>

van Wijnbergen, E.C.M. (2015). *Exploration and analysis of low-cost seismic retrofit measures to improve box-action for traditional brick masonry houses in Nepal* (Master's thesis, Delft University of Technology, The Netherlands).

# APPENDIX

---

- A. Parameters used for the calculations as recommended in NEN NPR9998. . . . . II
- B. Load carrying capacity timber connection. . . . .IV
- C. DIANA report closed shear wall. . . . . VIII
  - C.1 Project details. . . . . VIII
  - C.2 Model characteristics. . . . .IX
  - C.3 Materials. . . . . X
  - C.4 Geometries. . . . . XIII
  - C.5 Supports and loads. . . . . XIV
  - C.6 Analysis settings. . . . . XIV
- D. Redesign timber joint. . . . . XXIV
  - D.1 Case 1: Timber confinement consists of two bands. . . . . XXIV
  - D.2 Case 2: Timber confinement consists of four bands. . . . . XXVI

## APPENDIX A: PARAMETERS USED FOR THE CALCULATIONS AS RECOMMENDED IN NEN NPR9998:2020

The parameters used for the calculations of the analytical study are defined in Tables A1 and A2. Some of these parameters depend on the dimensions of the wall or pier that form the governing mechanism of the structure. These are shown in Table A2 and their values are denoted as “Variable”. The fixed parameters are shown in Table A1, their values are obtained from literature.

**Table A1:** Fixed parameters

Parameter	Description	Value	Unit
$t$	The thickness of the wall or pier	450	[mm]
$\rho$	The masonry mass density	2400	[kg/m <sup>3</sup> ]
$f_{c,m}$	The masonry compressive strength	3.00 (Cominelli et al., 2016)	[N/mm <sup>2</sup> ]
$f_{c,mtr}$	The mortar compressive strength	1.80 (Lekshmi, 2016)	[N/mm <sup>2</sup> ]
$f_{dt}$	The masonry diagonal tensile strength	0.02 (Ali et al., n.d.)	[N/mm <sup>2</sup> ]
$f_t$	The masonry tensile strength	0.01 (Milosevic et al., 2013)	[N/mm <sup>2</sup> ]
$c$	The masonry bed-joint cohesion	0.01 (Ali et al., n.d.)	[N/mm <sup>2</sup> ]
$\mu_{f,m}$	The masonry coefficient of friction	0.70 (Marino et al., 2014)	[-]
$\mu_{f,t}$	The mortar-timber coefficient of friction	0.80 (Almeida et al., 2020)	[-]

**Table A2:** Variable parameters

Parameter	Description	Value	Unit
$P_{\text{tot}}$	The total axial action $P_{\text{tot}} = P_w + P + P_{\text{add}}$	<i>Variable</i>	[N]
$P_w$	The self-weight of the wall or pier above the cross section being considered. <ul style="list-style-type: none"> <li>· For bed-joint sliding and rocking: <math>P_w = \rho \cdot g \cdot h \cdot t \cdot L</math></li> <li>· For diagonal tensile failure: <math>P_w = \rho \cdot g \cdot 0.5h \cdot t \cdot L</math></li> </ul>	<i>Variable</i>	[N]
$P$	The superimposed load at the top of the wall or pier, consisting of the self-weight of the roof structure and the self-weight of wall parts on top of the wall or pier.	<i>Variable</i> $P_{\text{roof}} = 1000$	[N]
$P_{\text{add}}$	Additional superimposed load from the column internal normal force, limited by the load transfer capacity of the timber joint. $P_{\text{add}} \leq 2 \cdot F_{v,Rk;\text{column}} = 14.8 \text{ kN}$	<i>Variable</i>	[N]
$h$	The wall or pier height	<i>Variable</i>	[mm]
$L$	The wall or pier length	<i>Variable</i>	[mm]
$\sigma_n$	The mean compressive stress over the full cross section of the wall or pier $\sigma_n = P_{\text{tot}} / (L \cdot t)$	<i>Variable</i>	[N/mm <sup>2</sup> ]
$\beta$	A factor to correct nonlinear stress distribution which depends on the dimensions of the wall or pier: $\beta = 1.0$ for $0 \leq h/L < 0.5$ $\beta = 0.84$ for $h/L = 1.0$ $\beta = 0.67$ for $h/L \geq 1.5$	<i>Variable</i>	[-]

## APPENDIX B: LOAD CARRYING CAPACITY TIMBER CONNECTION

The load transfer capacity of the joints of the timber frame is determined by means of the calculations as recommended in the Eurocode 5 (EN 1995-1-1, 2004).

Figure B.1 shows the band-to-column connection as stated in the Nepali building codes (DUDBC, 2015a), which states that the dimensions of the column should be 75x75 mm, the bands should consist of 100x75 mm beams, and the fasteners should be four nails of minimal 4 mm. After checking these dimensions with the minimal edge distances according to the Eurocode 5 (see Appendix C for the calculation of the joint stiffness), it turns out that the dimensions of the columns and beams should be almost twice the size recommended by the DUDBC.

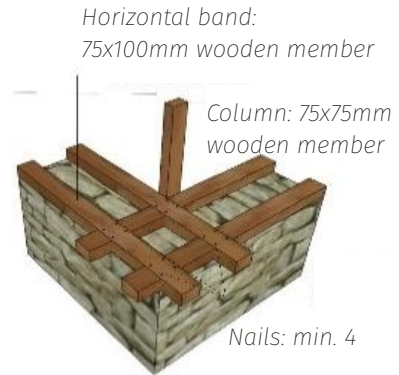


Figure B.1: Joint for wood connection, obtained from DUDBC (2015), p. 141

Throughout this research column and beam sizes of 140x140 mm will be used. Considering these dimensions of the timber members, a nail size of 180x6.0 mm is chosen. Figure B.2 shows the dimensions of the joint. The density of the timber is assumed to be similar to that of softwood with strength class C27:  $\rho_k=370 \text{ kg/m}^3$

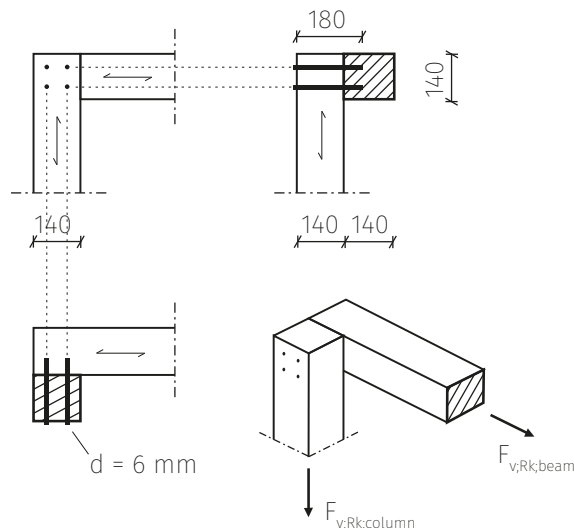


Figure B.2: Dimensions timber joint as used for this research



The total characteristic load carrying capacity of the timber joint consists of the sum of the load carrying capacity according to the Johansen yield theory and the contribution of the rope effect, which is limited to the Johansen part, per shear plane per fastener:

$$F_{v,Rk;tot} = n \left( F_{v,Rk} + \frac{F_{ax,Rk}}{4} \right)$$

with:  $\frac{F_{ax,Rk}}{4} \leq 0.15 \cdot F_{v,Rk}$  for round nails

The Johansen yield theory distinguishes six failure modes for the connection per fastener per shear plane:

$$a) F_{v,Rk} = f_{h,1;k} t_1 d$$

$$b) F_{v,Rk} = f_{h,2;k} t_2 d$$

$$c) F_{v,Rk} = \frac{f_{h,1;k} t_1 d}{1 + \beta} \left[ \sqrt{\beta + 2\beta^2 \left[ 1 + \frac{t_2}{t_1} + \left( \frac{t_2}{t_1} \right)^2 \right] + \beta^3 \left( \frac{t_2}{t_1} \right)^2} - \beta \left( 1 + \frac{t_2}{t_1} \right) \right] + \frac{F_{ax,Rk}}{4}$$

$$d) F_{v,Rk} = 1.05 \left( \frac{f_{h,1;k} t_1 d}{2 + \beta} \right) \left[ \sqrt{2\beta(1 + \beta) + \left( \frac{4\beta(2 + \beta)M_{y,Rk}}{f_{h,1;k} d t_1^2} \right)} - \beta \right] + \frac{F_{ax,Rk}}{4}$$

$$e) F_{v,Rk} = 1.05 \left( \frac{f_{h,1;k} t_2 d}{1 + 2\beta} \right) \left[ \sqrt{2\beta^2(1 + \beta) + \left( \frac{4\beta(1 + 2\beta)M_{y,Rk}}{f_{h,1;k} d t_2^2} \right)} - \beta \right] + \frac{F_{ax,Rk}}{4}$$

$$f) F_{v,Rk} = 1.15 \sqrt{\frac{2\beta}{1 + \beta}} \sqrt{2M_{y,Rk} f_{h,1;k} d} + \frac{F_{ax,Rk}}{4}$$

The ratio between the embedment strengths of the members is denoted by  $\beta$ . For smooth round nails, with a minimum tensile strength ( $f_u$ ) of 600 N/mm<sup>2</sup>, the following characteristic values for yield moment ( $M_{y,Rk}$ ) and embedment strength ( $f_{h,k}$ ) are used:

$$\beta = \frac{f_{h,2;k}}{f_{h,1;k}}$$

$$M_{y,Rk} = 0.3f_u \cdot d^{2.6}$$

$$f_{h,0;k} = 0.082\rho_k \cdot d^{-0.3}, \quad \text{without predrilled holes}$$

$$f_{h,90;k} = \frac{f_{h,0;k}}{k_{90}}$$

$$k_{90} = 1.35 + 0.015d, \quad \text{for softwoods}$$

Appendix B: Load carrying capacity timber connection

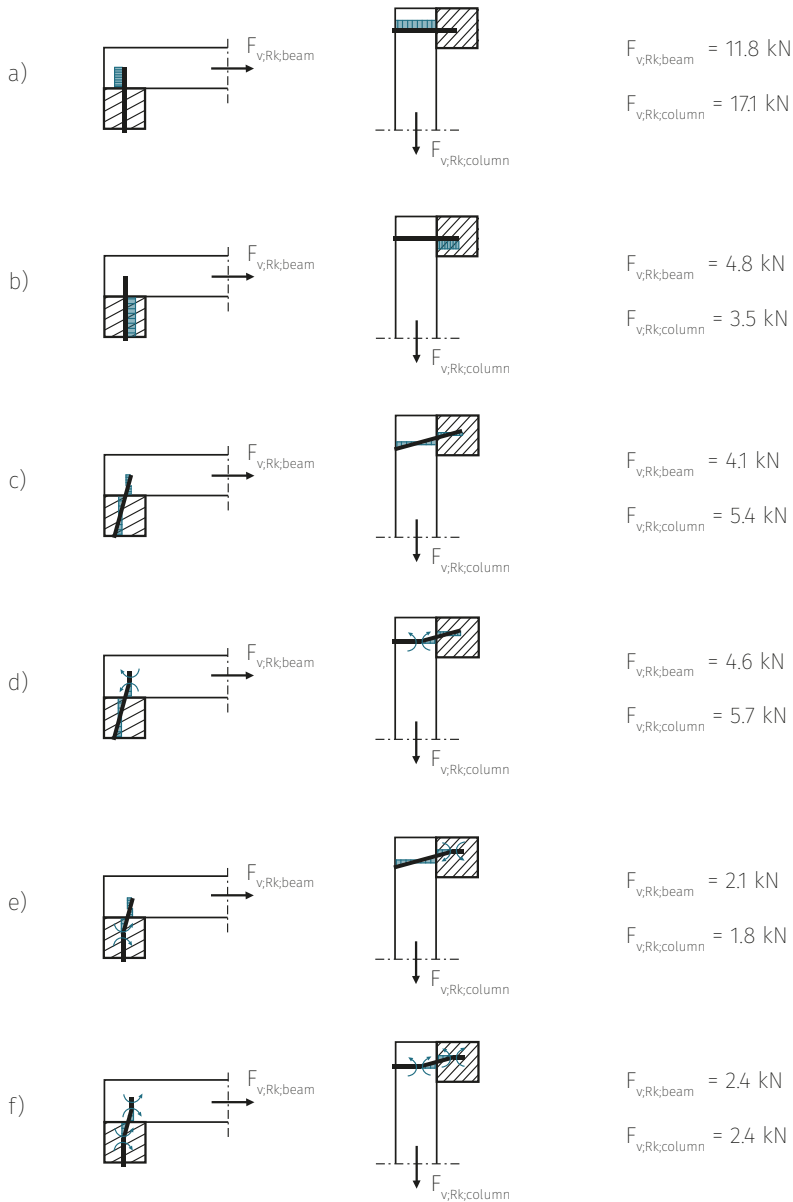


Figure B.3: Failure modes of the joint for the tensile force applied in the beam (left) and in the column (right), with their corresponding capacity per fastener

Since  $t_1 > t_2$ , and the directions of the fibres of the beam is perpendicular to the direction of the fibres of the column so  $f_{h,1;k} \neq f_{h,2;k}$ , the maximum force that can develop in the beam is not equal to that in the column. Figure B.3 shows the different failure modes for the joint when the tensile force is applied in the beam and when applied in the column, and their corresponding capacities.

The governing failure mode is failure mode “e”, which is a combination of yielding of the fastener and reaching the embedded strength of the timber. The total characteristic load carrying capacity of the timber joint with four nails becomes:

$$F_{v,ef;Rk;column} = 4 \cdot F_{v;Rk;column;e} = 7.2 \text{ kN}$$

$$F_{v,ef;Rk;band} = 4 \cdot F_{v;Rk;band;e} = 8.4 \text{ kN}$$

When dividing over the cross-sectional area of the timber elements, this load carrying capacity corresponds to a tensile stress limit of:

$$\begin{aligned} \sigma_{\max;column} &= 0.37 \text{ N/mm}^2 \\ \sigma_{\max;band} &= 0.43 \text{ N/mm}^2 \end{aligned}$$

## APPENDIX C: DIANA REPORT CLOSED SHEAR WALL

### C.1: PROJECT DETAILS

#### C.1.1: Project information

Diana project name	./IP-unconfined/IP-unconfined.dpf
Analysis aspects	['Structural']
Model dimension	['Two dimensional']
Default mesher type	HEXQUAD
Default mesher order	LINEAR
Diana version	Diana 10.4, Latest update: 2020-10-02 21:36:39
System	Windows NT 6.2 Build 9200
Model sizebox	10.0

#### C.1.2: Dimensions

<b>Axes</b>	<b>Minimum coordinate [mm]</b>	<b>Maximum coordinate [mm]</b>
X	-10	3e+03
Y	0	2.7e+03
Z	0	0

#### C.1.3: Units

<b>Quantity</b>	<b>Unit</b>	<b>Symbol</b>
Length	millimeter	mm
Mass	ton	T
Force	newton	N
Time	second	s
Temperature	kelvin	K
Angle	radian	rad

### C.1.4: Directions

Name	X	Y	Z
X	1	0	0
Y	0	1	0
Z	0	0	1

### C.1.5: Definitions

Name	Value
Acceleration of gravity	-9810 mm/s <sup>2</sup>
Fluid density	1e-09 T/mm <sup>3</sup>
Reference point for total head	0 0 0
Rayleigh damping coefficients	a: 0 b: 0
Design safety factor concrete compressive strength	1
Design safety factor concrete uniax. tensile strength	1
Design safety factor concrete stiffness	1
Design safety factor steel yield stress	1
Design safety factor steel stiffness	1
Direction of gravity	Y

## C.2: MODEL CHARACTERISTICS

The model consists of the following shapes, reinforcements, piles and interfaces:

### C.2.1: Shapes

Name	Set	Element Class	Material	Geometry	Seeding method	Element size [mm]	Division
Wall	Shapes	MEMBRA	Masonry	wall	ElementSize	1e+02	0
band_floor	Shapes	CLS3B2	Timber	band	ElementSize	1e+02	0
band_roof	Shapes	CLS3B2	Timber	band	ElementSize	1e+02	0
column_left	Shapes	CLS3B2	Timber	column	ElementSize	1e+02	0
column_right	Shapes	CLS3B2	Timber	column	ElementSize	1e+02	0

### C.2.2: Interfaces

Name	Interface Type	Element Class	Material
Wall			
Wall	Interface	STLIIF	Interface_band_bottom-side
band_floor	Interface	STLIIF	Interface_band_top-side
band_roof			
band_roof	Hinge		
band_roof	Hinge		
column_left			
column_right			

### C.2.3: Mesh sets

Name	# Elements	Material	geometry	Data
Wall	810	Masonry	wall	Wall
band_floor	30	Timber	band	band
band_roof	30	Timber	band	band
column_left	27	Timber	column	column
column_right	27	Timber	column	column
roof-band	30	Interface_band_bottom-side	interface_band	interface
floor-band	30	Interface_band_top-side	interface_band	interface

## C.3: MATERIALS

### C.3.1: Material: Masonry

Name	Value
Material class	Concrete and masonry
Material model	Total strain based crack model

<b>Name</b>	<b>Value</b>
Color	grey
Young's modulus	2000 N/mm <sup>2</sup>
Poisson's ratio	0.1
Mass density	2.4e-09 T/mm <sup>3</sup>
Crack orientation	Rotating
Tensile curve	Linear-crack energy
Tensile strength	0.01 N/mm <sup>2</sup>
Mode-I tensile fracture energy	0.0016 N/mm
Crack bandwidth specification	Rots
Residual tensile strength	0 N/mm <sup>2</sup>
Reduction model	No reduction
Compression curve	Parabolic
Compressive strength	3 N/mm <sup>2</sup>
Compressive fracture energy	0.1 N/mm
Residual compressive strength	0 N/mm <sup>2</sup>
Reduction model	No reduction
Confinement model	No increase

### C.3.2: Material: Timber

<b>Name</b>	<b>Value</b>
Material class	Steel
Material model	Linear elastic isotropic
Color	steelblue
Young's modulus	9000 N/mm <sup>2</sup>

<b>Name</b>	<b>Value</b>
Poisson's ratio	0.3
Mass density	4.5e-10 T/mm <sup>3</sup>

### C.3.3: Material: Interface\_band\_bottom-side

<b>Name</b>	<b>Value</b>
Material class	Interface elements
Material model	Coulomb friction
Color	silver
Type	2D line interface
Normal stiffness modulus-y	20000 N/mm <sup>3</sup>
Shear stiffness modulus-x	10000 N/mm <sup>3</sup>
Fricti	T
Cohesion	0.02 N/mm <sup>2</sup>
Friction angle	0.7 rad
Dilatancy angle	0.17 rad
Interface opening model	Gapping model
Gap criterion	T
Tensile strength	0.01 N/mm <sup>2</sup>
Model for gap appearance	Brittle

### C.3.4: Material: Interface\_band\_top-side

<b>Name</b>	<b>Value</b>
Material class	Interface elements
Material model	Coulomb friction
Color	silver



<b>Name</b>	<b>Value</b>
Type	2D line interface
Normal stiffness modulus-y	20000 N/mm <sup>3</sup>
Shear stiffness modulus-x	10000 N/mm <sup>3</sup>
Fricti	T
Cohesion	0.05 N/mm <sup>2</sup>
Friction angle	1.22 rad
Dilatancy angle	0.7 rad
Interface opening model	Gapping model
Gap criterion	T
Tensile strength	0.01 N/mm <sup>2</sup>
Model for gap appearance	Brittle

## C.4: GEOMETRIES

### C.4.1: Geometry: Wall

<b>Name</b>	<b>Value</b>
Geometry class	Sheets
Geometry model	Regular membrane stress elements
Thickness	450 mm

### C.4.2: Geometry: Band

<b>Name</b>	<b>Value</b>
Geometry class	Lines
Geometry model	2D Class-III beam elements
Shape	Rectangle
Dimensions of a filled rectangle	140 450 mm

### C.4.3: Geometry: Column

Name	Value
Geometry class	Lines
Geometry model	2D Class-II beam elements
Shape	Rectangle
Dimensions of a filled rectangle	280 140 mm

## C.5: SUPPORTS AND LOADS

### C.5.1: Geometry support sets: Foundation

Name	Target	Translation	Rotation
Foundation_band	POINT	X,Y	

### C.5.2: Geometry load cases

Name	Target	Type	Direction	DOF	Value	Unit
Pushover	BODY	PUSHOV	X		9.8e+03	mm/s <sup>2</sup>
Self-weight	model	WEIGHT				
superimposed	LINE	FORCE	Y		-0.33	N/mm

## C.6: ANALYSIS SETTINGS - PUSHOVER ANALYSIS

### C.6.1: Definition

```

Structural eigenvalue
Structural eigenvalue
Evaluate model
Evaluate elements
Average nodal normals
Tolerance angle = 0.349066
Evaluate composed elements
Assemble elements
    
```

```
Tolerance = 1e-06
Define eigenvalue type
Eigenvalue type = Free vibration
Free vibration
Stiffn
  Stiffness matrix = Linear elastic
  Linear
Mass matrix
  Mass matrix type = Consistent
  Include rotational terms = T
Execute eigenvalue analysis
Solver method = Implicitly restarted Arnoldi method
Solver type = Parallel direct
Number of eigenfrequencies = 1
Maximum number of iterations = 30
Convergence criterion tolerance = 1e-06
Output eigenvalue analysis
Output eigenvalue analysis
Device = DIANA native
Option = Binary
Select
  Blknam = OUTPUT
  Modes
    User selection = ALL
  Casety = MODES
  Modsel = COMPLE
  Seltyp = PRIMAR
  Primar
Analys = LINEAR
Pushover
Structural nonlinear
Evaluate model
Evaluate elements
Average nodal normals
Tolerance angle = 0.349066
```

Evaluate composed elements  
Assemble Elements  
Tolerance =  $1e-06$   
Setup matrices  
Setup load vectors  
Nonlinear effects  
Physical nonlinear  
Plasticity  
Tangent stiffness = First order  
Maximum number of iterations = 25  
Sub-stepping in internal iteration = 0.01  
Yield function tolerance = 0.0001  
Creep  
Creep approximation = Zero order  
Maximum number of iterations = 1  
Stress accuracy tolerance = 0.0001  
Corrosion influence  
Temperature influence  
Concentration influence  
Cracking  
Crack normal stiffness = Secant  
Threshold angle between cracks = 60  
Tension cut-off tolerance = 0.001  
Total strain based cracking  
Crack normal stiffness = Secant  
Nonlinear elastic material  
Viscoelastic material  
Viscoplastic material  
Maturity dependent material  
Degree of reaction dependent material  
Pressure influence  
Hyperelastic material  
Interface nonlinearity  
Tangent stiffness = Consistent  
Maximum number of iterations = 25

Yield function tolerance = 0.0001  
Contact  
Material shrinkage  
Material swelling  
Simple soil material  
Tangen = Linear  
Simple stress dependent material  
Engineering masonry material  
Perfectly matched layer material  
Kotsovos concrete material  
Geometrical nonlinear  
Formulation = Total Lagrange  
Execute steps  
Execute steps  
Step type = Load steps  
Load steps  
Load set = 1  
Steps  
Step size = Explicit  
Explicit  
Equilibrium iteration  
Maximum number of iterations = 50  
Iteration method settings  
Iteration method = Newton-Raphson  
Newton-Raphson  
Convergence criteria  
Force norm  
Displacement norm  
Logging information  
Logging report  
Verbosity = Brief  
Logging sequence = Step  
Plasticity information  
Crack information  
Reaction forces information

Execute steps

Step type = Load steps

Load steps

Load set = 3

Steps

Step size = Explicit

Explicit

Equilibrium iteration

Maximum number of iterations = 20

Iteration method settings

Iteration method = Newton-Raphson

Newton-Raphson

Convergence criteria

Force norm

Displacement norm

Logging information

Logging report

Verbosity = Brief

Logging sequence = Step

Plasticity information

Crack information

Reaction forces information

Execute steps

Step type = Load steps

Load steps

Load set = 2

Steps

Step size = Explicit

Explicit

Equilibrium iteration

Maximum number of iterations = 50

Iteration method settings

Iteration method = Newton-Raphson

Newton-Raphson

Line Search

Maximum scale factor = 1  
Minimum scale factor = 0.1  
Energy stop criterion = 0.8  
Regula-Falsi stop criterion = 0.1  
Maximum number of searches = 5  
Convergence criteria  
Force norm  
Displacement norm  
Logging information  
Logging report  
Verbosity = Brief  
Logging sequence = Step  
Plasticity information  
Crack information  
Reaction forces information  
Solution method  
Method = Parallel Direct Sparse  
Convergence tolerance = 1e-08  
Parallel Direct Sparse  
Factorization  
Output  
Output  
Device = DIANA native  
Option = Binary  
Seltyp = USER  
Select  
Blknam = OUTPUT  
Modsel = Complete  
Casety = STEPS  
Steps  
User selection = ALL  
User  
Displacements  
Displacements  
Form = TRANSL

Oper = GLOBAL  
Type = TOTAL  
Total  
Strains  
Strains  
Form = GREEN  
Oper = PRINCI  
Type = CRKWDT  
Crack width  
Strains  
Form = GREEN  
Type = CRACK  
Crack  
Strains  
Form = GREEN  
Oper = GLOBAL  
Type = TOTAL  
Total  
Strains  
Form = TRACTI  
Oper = GLOBAL  
Type = PLASTI  
Plastic  
Stresses  
Stresses  
Form = TRACTI  
Oper = GLOBAL  
Type = EFFECT  
Effective  
Stresses  
Form = CAUCHY  
Oper = GLOBAL  
Type = TOTAL  
Total  
Stresses



```
Form = CAUCHY
Oper = PRINCI
Type = TOTAL
Total
Forces
Forces
Form = TRANSL
Oper = GLOBAL
Type = REACTI
Reaction
Element forces
```

## C.6.2: DCF commands

```
*EIGEN LABEL="Structural eigenvalue"
TYPE FREEVI STIFFN LINEAR
BEGIN EXECUT
  PARDIS
  MAXITE 30
END EXECUT
BEGIN OUTPUT
  TEXT "Output eigenvalue analysis"
  BINARY
  SELECT MODES ALL /
END OUTPUT
*NONLIN LABEL="Pushover"
TYPE GEOMET
BEGIN EXECUT
  TEXT "Self-weight"
  BEGIN LOAD
    LOADNR 1
    STEPS EXPLIC SIZES 0.5(2)
  END LOAD
  BEGIN ITERAT
```

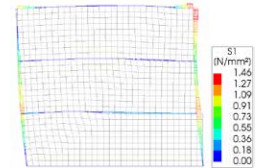
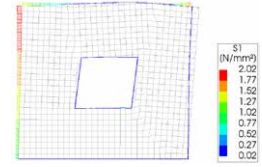
```
MAXITE 50
METHOD NEWTON
END ITERAT
END EXECUT
BEGIN EXECUT
  TEXT "superimposed"
  BEGIN LOAD
    LOADNR 3
    STEPS EXPLIC SIZES 0.5(2)
  END LOAD
  BEGIN ITERAT
    MAXITE 20
    METHOD NEWTON
  END ITERAT
END EXECUT
BEGIN EXECUT
  TEXT "Pushover"
  BEGIN LOAD
    LOADNR 2
    BEGIN STEPS
      BEGIN EXPLIC
        SIZES 0.1(30)
        ARCLEN REGULA SET NODES ALL /
      END EXPLIC
    END STEPS
  END LOAD
  BEGIN ITERAT
    MAXITE 50
    METHOD NEWTON
    LINESE
    BEGIN CONVER
      FORCE CONTIN
      DISPLA CONTIN
    END CONVER
```

```
END ITERAT
END EXECUT
SOLVE PARDIS
BEGIN OUTPUT
  TEXT "Output"
  BINARY
  SELECT STEPS ALL /
  DISPLA TOTAL TRANSL GLOBAL
  STRAIN CRKWDT GREEN PRINCI
  STRAIN CRACK GREEN
  STRAIN TOTAL GREEN GLOBAL
  STRAIN PLASTI TRACTI GLOBAL
  STRESS EFFECT TRACTI GLOBAL
  STRESS TOTAL CAUCHY GLOBAL
  STRESS TOTAL CAUCHY PRINCI
  FORCE REACTI TRANSL GLOBAL
END OUTPUT
*END
```

## APPENDIX D: REDESIGN TIMBER JOINT

For the redesign of the timber joint two cases are considered:

- Case 1: The masonry structure will be confined by two bands only (floor and roof band). In this case the stresses in the timber elements can become  $\sigma_{\max} = 2.02 \text{ N/mm}^2$  (in the model with window opening and  $f_{t,\text{masonry}}^{\max} = 0.03 \text{ N/mm}^2$ ).
- Case 2: The masonry structure will be confined by all four bands. In this case the stresses in the timber elements can become  $\sigma_{\max} = 1.46 \text{ N/mm}^2$  (in the model without opening and  $f_{t,\text{masonry}}^{\max} = 0.01 \text{ N/mm}^2$ ).



These two cases are considered because they are both adequate confinement solutions to increase the resistance of the masonry structure.

### D.1 Case 1: Timber confinement consists of two bands

The resistance of the joint must be greater than:

$$F_{v,\text{ef},\text{Rd}} \geq F_{v,\text{Ed}} = 39.6 \text{ kN}$$

Since the force in the connection acts at an angle to the grain for either the columns or the band, the splitting capacity of the joint must be checked:

$$F_{90,\text{Rk}} = 14b \sqrt{\frac{h_e}{1 - \frac{h_e}{h}}}$$

where:  $b$  is the member thickness;

$h$  is the member height;

$h_e$  is the loaded edge distance to the centre of the most distant fastener or to the edge of the punched metal plate fastener, in mm.

The splitting capacity satisfies the resistance requirement for:

$$b = 175 \text{ mm}$$

$$h = 200 \text{ mm}$$

$$h_e = h - 7d = 151 \text{ mm}$$

The joint will be strengthened by a thin steel plate which allows for using more fasteners, shown in Figure D1. Due to the larger member sizes, a larger nail size will be used. The new resistance of the joint now consists of a combination of a steel-to-timber single and double shear connection, shown in Figure D2.

In order to further increase the load-carrying capacity of the joint, the holes for the nails must be predrilled and the nails must be grooved. With these dimensions and requirements of the members, the parameters for the load-carrying calculations become the following:

$$\begin{aligned}
 d &= 7.6 \text{ mm} \\
 \rho_k &= 370 \text{ kg/m}^3 \\
 f_{h,0;k} &= 0.082(1 - 0.01d)\rho_k \\
 &= 28.0 \text{ N/mm}^2 \\
 f_{h,90;k} &= \frac{f_{h,0;k}}{k_{90} + 1} \\
 &= 11.4 \text{ N/mm}^2 \\
 k_{90} &= 1.35 + 0.015d = 1.46 \\
 M_{y,Rk} &= 0.45f_u d^{2.6} \\
 &= 52660 \text{ Nmm} \\
 f_u &= 600 \text{ N/mm}^2 \\
 \frac{F_{ax,Rk}}{4} &= 25\%
 \end{aligned}$$

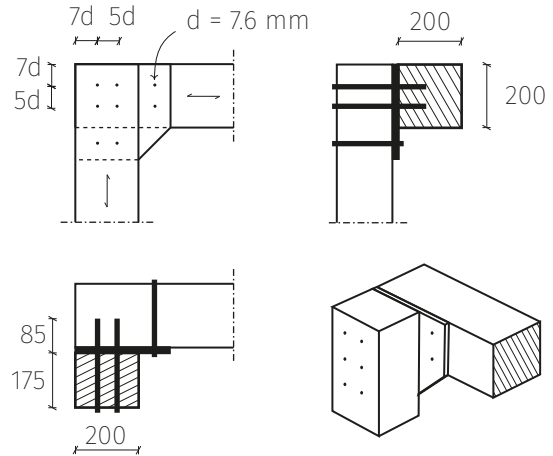


Figure D1: Dimensions of the redesigned timber joint suited for Case 1.

①

$$F_{v,Rk1} = \min \left\{ \begin{aligned} &f_{h,k} t d \\ &f_{h,k} t d \left[ \sqrt{2 + \frac{4M_{y,Rk}}{f_{h,k} d t^2}} - 1 \right] + \frac{F_{ax,Rk}}{4} \\ &2.3 \sqrt{M_{y,Rk} f_{h,k} d} + \frac{F_{ax,Rk}}{4} \end{aligned} \right.$$

$F_{v,Rk1} = 4.9 \text{ kN}$

②

$$F_{v,Rk2} = \min \left\{ \begin{aligned} &0.4f_{h,k} t d \\ &1.15 \sqrt{2M_{y,Rk} f_{h,k} d} + \frac{F_{ax,Rk}}{4} \end{aligned} \right.$$

$F_{v,Rk2} = 6.8 \text{ kN}$

③

$$F_{v,Rk3} = \min \left\{ \begin{aligned} &0.4f_{h,k} t d \\ &1.15 \sqrt{2M_{y,Rk} f_{h,k} d} + \frac{F_{ax,Rk}}{4} \end{aligned} \right.$$

$F_{v,Rk3} = 4.3 \text{ kN}$

Figure D2: Failure modes for steel-to-timber connections

The total characteristic load-carrying capacity of the timber joint is:

$$F_{v,ef;Rk} = 4 \cdot 2 \cdot F_{v,Rk;1} + 2 \cdot F_{v,Rk;2} + 2 \cdot F_{v,Rk;3} = 61.4 \text{ kN} > F_{v,Ed}$$

## D.2 Case 2: Timber confinement consists of four bands

The resistance of the joint must be greater than:

$$F_{v,ef;Rd} \geq F_{v,Ed} = 39.6 \text{ kN}$$

The splitting capacity satisfies the resistance requirement for:

$$\begin{aligned} b &= 150 \text{ mm} \\ h &= 150 \text{ mm} \\ h_e &= h - 7d = 108 \text{ mm} \end{aligned}$$

Like the first case, the joint will be strengthened by a thin steel plate which allows for using more fasteners, shown in Figure D3. Even though the timber members are slightly larger due to the splitting requirement, the nail size of 180x6 mm can still be used. The new resistance of the joint now consists of a combination of a steel-to-timber single and double shear connection, shown in Figure D4.

In order to further increase the load-carrying capacity of the joint, the holes for the nails must be predrilled and the nails must be grooved. With these dimensions and requirements of the members, the parameters for the load-carrying calculations become the following:

$$\begin{aligned} d &= 6 \text{ mm} \\ \rho_k &= 370 \text{ kg/m}^3 \\ f_{h;0;k} &= 0.082(1 - 0.01d)\rho_k \\ &= 28.5 \text{ N/mm}^2 \\ f_{h;90;k} &= \frac{f_{h;0;k}}{k_{90} + 1} \\ &= 11.7 \text{ N/mm}^2 \\ k_{90} &= 1.35 + 0.015d = 1.44 \\ M_{y;Rk} &= 0.45f_u d^{2.6} \\ &= 28481 \text{ Nmm} \\ f_u &= 600 \text{ N/mm}^2 \\ \frac{F_{ax;Rk}}{4} &= 25\% \end{aligned}$$

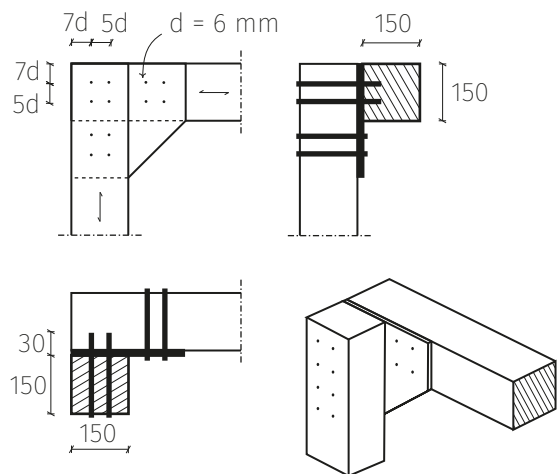
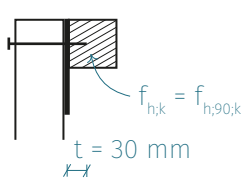


Figure D.3: Dimensions of the redesigned timber joint suited for Case 2.

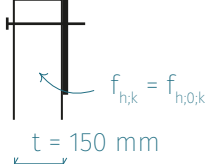
①



$$F_{v,Rk1} = \min \left\{ \begin{array}{l} f_{h,k} t d \\ f_{h,k} t d \left[ \sqrt{2 + \frac{4M_{y,Rk}}{f_{h,k} t d^2}} - 1 \right] + \frac{F_{ax,Rk}}{4} \\ 2.3 \sqrt{M_{y,Rk} f_{h,k} d} + \frac{F_{ax,Rk}}{4} \end{array} \right.$$

$$F_{v,Rk1} = 2.1 \text{ kN}$$

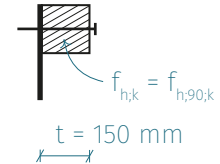
②



$$F_{v,Rk2} = \min \left\{ \begin{array}{l} 0.4 f_{h,k} t d \\ 1.15 \sqrt{2 M_{y,Rk} f_{h,k} d} + \frac{F_{ax,Rk}}{4} \end{array} \right.$$

$$F_{v,Rk2} = 4.5 \text{ kN}$$

③



$$F_{v,Rk3} = \min \left\{ \begin{array}{l} 0.4 f_{h,k} t d \\ 1.15 \sqrt{2 M_{y,Rk} f_{h,k} d} + \frac{F_{ax,Rk}}{4} \end{array} \right.$$

$$F_{v,Rk3} = 2.9 \text{ kN}$$

The total characteristic load-carrying capacity of the timber joint is:

$$F_{v,ef,Rk} = 4 \cdot 2 \cdot F_{v,Rk1} + 2 \cdot F_{v,Rk2} + 2 \cdot F_{v,Rk3} = 46.3 \text{ kN} > F_{v,Ed}$$







